

https://dspace.org/

The role of geological structures in the hydrogeology of the Upper Crocodile River Basin, South Africa

Nyebelele, Sipho

2020

https://hdl.handle.net/10539/30202

Nyebelele, Sipho (2019) The role of geological structures in the hydrogeology of the Upper Crocodile River Basin, South Africa, University of the Witwatersrand, Johannesburg, <http://hdl.handle.net/10539/30202>

Downloaded from a DSpace repository. https://dspace.org/

The role of geological structures in the hydrogeology of the Upper Crocodile River Basin, South Africa

GEOL7028
(MSc Research Report)

Sipho Nyebelele (776383)

Supervisor(s): Prof T.A. Abiye
Dr A. Tshibubudze

A Research Report submitted to the Faculty of Science, University of the Witwatersrand, in partial fulfilment of the requirements for the degree of Master of Science in Hydrogeology

School of Geosciences



WITS
UNIVERSITY

December 2019

DECLARATION

I declare that: THE ROLE OF GEOLOGICAL STRUCTURES ON THE HYDROGEOLOGY OF THE UPPER CROCODILE RIVER BASIN is my own work, that it has not been submitted for any degree or examination in any other university, and that all the sources I have used or quoted have been indicated and acknowledged by complete references.

I **Sipho Nyebelele** (Student number: **776383**) am a student registered for the degree of **Masters in Hydrogeology** in the academic year **2019**.

I hereby declare the following:

- I am aware that plagiarism (the use of someone else's work without their permission and/or without acknowledging the original source) is wrong.
- I confirm that the work submitted for assessment for the above degree is my own unaided work except where I have explicitly indicated otherwise.
- I have followed the required conventions in referencing the thoughts and ideas of others.
- I understand that the University of the Witwatersrand may take disciplinary action against me if there is a belief that this is not my own unaided work or that I have failed to acknowledge the source of the ideas or words in my writing.

Signature: _____ Date: _____

Abstract

The Upper Crocodile River Basin (UCRB) is made up of fractured crystalline rocks such as quartzites, granites, gabbro's and Bushveld Igneous Complex rocks that are intruded by dykes of varying ages and orientations. A study of the geological structures on the role they play on the hydrogeology of the UCRB was undertaken.

The use of ArcGIS for lineament analysis and magnetics data for the interpretation of lineaments in the study area revealed three main trends. A NNE-SSW, E-W and a NW-SE trend, where the NW-SE and NNE-SSW trends form conjugates of each other and the E-W lineaments forming extension release joints. The SW lineaments share their orientation with the southern Pilanesberg dyke swarm whereas the E-W have dykes that are doleritic in composition and are said to be post-Karoo intrusions. Rose diagrams revealed dominant orientations for these lineaments to be 135^{o}, 015^{o} and 085^{o} for the SE, NNE-SSW and E-W, respectively.

The drainage pattern is dominantly dendritic, which develops in low porosity rocks with the orientation of the streams following that of the lineaments. Additionally, dendritic pattern is caused by homogeneous material, and that is, geology of similar resistance. Trellis drainage patterns occur in two areas, one being subject to lineament control and the other affected by both the lithology and lineaments.

A total of four springs were used to estimate recession coefficients. Three of these were on dolomites and one on quartzites. The dolomitic springs share a similar recession coefficient, suggesting that regardless of their respective locations the dolomites share similar physical properties. The quartzite spring has a higher recession coefficient as such the physical properties are better suited for groundwater circulation than in the dolomites. The Maloney'-Eye has a bigger catchment, which resulted in higher discharge. The smallest spring catchment is observed for the Elandsfontein-Eye, however, it has a similar discharge to that of the quartzite spring.

The streams in the UCRB are predominantly gaining streams. However, one of the streams loses and gains depending on the seasons. The gain is facilitated by the fractures and the loss is possibly facilitated by the karsts on the dolomites.

The isotopic composition of the groundwater in the study area shows a depletion of heavy isotopes of δD and $\delta^{18}O$. The groundwater samples plotted along Meteoric Water Lines (MWL) shows an evolution pattern of water recharged directly from rainfall or rapid recharge through the fractures. Some samples are extremely depleted, which can be attributed to (1) recharge from high altitudes, (2) low humidity during condensation and/or (3) recharge during a colder climate. The average residence time of the groundwater based on tritium data is around 23 years.

Lineaments are very important for the hydrogeology of the UCRB on the basis that they affect the drainage patterns, stream orientation and play a fundamental role in the groundwater circulation. Although, the lineaments facilitate the groundwater flow, the residence time is still high on average and the recession coefficients are also high suggesting deep circulation. This dominance of lineaments and similarities in environmental isotopes shows that the possibility of compartmentalisation (on dolomites in particular) is very low.

Acknowledgements

First and foremost, I would like to thank my Supervisors Prof. T.A. Abiye and Dr. A. Tshibubudze for sharing their valuable knowledge with me. Moreover, Prof. T.A. Abiye for making research fund and bursary available to me. This was funded by the United States Agency for International Development (USAID) and the National Academies of Sciences, Engineering, and Medicine (NAS) through Partnership for Enhanced Engagement in Research (PEER) under cooperative agreement number AID-OAA-A-11-00012 Sub-Grant Number: 2000006304 and the Department of Science and Technology, South Africa (UID: 101594). I'll always be grateful for this opportunity.

Many thanks go to Dr. Khahliso Leketa for always availing himself when I need advice. I would also like to thank him for making the data available for me to use for this project. As well as, Mr Khuliso Masindi for lending me the groundwater occurrence and groundwater quality map.

To Katlego Matlou, Sicelo Ucucho, Carol Mohuba and Nomzamo Joy Sithole for the assistance in some aspects of the project such as proof reading, field work including the words of kindness and motivation went a long way when the going got tough.

I would like to extend my gratitude to the Birin family for the support they have shown me during the year, especially when I was feeling defeated and needed words of encouragement.

Lastly, I would like to thank my parents and family for being patient with me during this time, especially when I could not avail myself when they needed to see me.

Abbreviations

CGS - Council for Geoscience

DP - Drainage Patterns

EP - Enhanced Performance

IAEA - International Atomic Energy Agency

IGRF - International Geomagnetic field

JLMWL - Johannesburg Local meteoric water line

GMWL - Global meteoric water line

GNIP - Global Network of Isotopes

SMOW - Standard mean oceanic water

TU - Tritium Units

TTG - Tonalitic Gneisses –

UCRB - Upper Crocodile River Basin

Table of Contents

DECLARATION i
Abstract ii
Acknowledgements iv
Abbreviations v
List of Figures viii
List of tables xii
1. Introduction 1
1.1. Background 1
1.2. Overview of methods 2
1.3. Study area 3
1.3.1. Location 3
1.3.2. Geological setting 4
1.3.3. Hydrogeological setting 6
1.4. Aims 8
1.5. Literature review 8
2. Methodology 11
2.1. Geological mapping and structures 11
2.2. Borehole logs 11
2.3. Drainage Pattern 12
2.4. Discharge data collection for the recession constant determination 13
2.5. Isotopes 14
2.5.1. Stable isotopes 14
2.5.2. Tritium 14
3. Results and Discussion 16
3.1. Geological mapping and structures 16
3.1.1. Satellite imagery interpretation and lineament analysis 16
3.1.2. Magnetic lineament interpretation 23
3.2. Geological cross-sections 33
3.3. Borehole log analysis 37
3.4. Drainage Pattern 42
3.5. Spring recession curves 45
3.5.1. Albert's Farm spring 48
3.5.2. The Nouklip-Eye 51

3.5.3. The Maloney's-Eye 53
3.5.4. The Elandsfontein-Eye 56
3.6. Stream discharge analysis 60
3.6.1. Stream discharge at A2H005 and A2H009 stations 62
3.6.2. Stream discharge for the A2H050 and A2H051 stations 63
3.6.3. Stream discharge for the A2H044 and A2H023 64
3.7. Environmental Isotopes 65
3.7.1. Stable isotopes 67
3.7.2. Tritium 72
4. Conclusions 75
5. Reference list 77
Appendices A and B refer to USB 82

List of Figures

Figure 1. Map of the Crocodile catchment illustrating the location of the UCRB relative to the other neighbouring catchments like the Apies (Source: DWAF, 2012). The UCRB catchment is delineated in red. 4

Figure 2. Map of the UCRB highlighting the geology and drainage related to the study area. The Figure also shows the distribution of the sampled boreholes labelled as BH (#) and the dolomitic springs labelled as SP(#) (Map constructed by Mr. K Leketa). 6

Figure 3. The locations of the BH's used for the BH logs and their respective section lines. 12

Figure 4. (A) An image sourced from ESRI, it is a combination of different satellite images such as SPOT, LANDSAT and TerraColour imagery. The black box in 4A represents the portion of the study area described later in the report (B) Represents the lineaments extracted from A. 18

Figure 5. (A) An image sourced from ESRI, it is a combination of different satellite images such as SPOT, LANDSAT and TerraColour imagery. (B) Is an interpretation of all possible NNE-SSW trending lineaments in the study area extracted from (A). Rose diagrams isalso included in the image showing the dominant trend directions of the lineaments. 18

Figure 6. (A) An image sourced from ESRI, it is a combination of different satellite images such as SPOT, LANDSAT and TerraColour imagery. (B) Is an interpretation of all possible NW-SE trending lineaments in the study area. Rose diagrams is also included in the image showing the dominant trend directions of the lineaments. 19

Figure 7. (A) An image sourced from ESRI, it is a combination of different satellite images such as SPOT, LANDSAT and TerraColour imagery. (B) Is an interpretation of all possible E-W-trending lineaments in the study area. Rose diagrams is also included in the image showing the dominant trend directions of the lineaments. 20

Figure 8. (A) The localised analysis map of the area around the Hartbeespoort dam. This map highlights the fact that the lineaments show similar traits in regional and local scales. (B) The extracted lineaments with the fault movement directions as blue and orange arrows. The arrows represent the sense of direction on the associated block. 21

Figure 9. The stereonet representation of the lineaments interpreted in Figures 4, 5, 6, 7 and 8. The 015^{o} and 135^{o} are conjugates of each other, the angle in between the two lineaments is 60^{o} and the acute bisector is orientated at 165^{o}. The 085^{o} orientation is the rose diagram orientation for the E-W lineaments and 075^{o} is the calculated obtuse bisector, which in this case would represent the E-W orientation. 22

Figure 10. (A) Represents regional aero-magnetics data (the IGRF is not removed). The two black boxes show the Pilanesberg dyke swarms. (B) Represents an example of some of the regional

structures passing through the study as black lines trending in an E-W and NW-SE direction. The study area is located in the centre of the image. 23
Figure 11. The image represents the total magnetics intensity map of the study area. NW-SE and E-W dykes are represented by high magnetic intensity lines. Low intensity (possible fractures) is represented by low intensity dots arranged in a linear array. The blue/black dots represent the location of some of the boreholes used in this study. 24
Figure 12. (A) The regional aero-magnetics data showing the magnetic anomalies occurring throughout the study area. (B) represents an example of some of the regional structures passing in the study as black lines trending in an E-W direction..... 25
Figure 13. Dolerite dykes. (A) represents the dyke that also has vertical fracture within. (B) is a hand sample of the dyke viewed through a fresh surface. (C and D) are other views of the dyke with the fracture in question. The black arrow on C represents the north for A, C and D. 26
Figure 14. Orientations of fractures found on the E-W trending dolerite dyke, the average orientation is 119º/83º/E..... 27
Figure 15.(A) The regional aero-magnetics data showing the magnetic anomalies occurring throughout the study area. (B) Represents an example of some of the regional structures passing in the study as blue lines trending in an NW-SE direction with low magnetic anomalies. 28
Figure 16. Fracture orientations measured in the Albert's Farm (near Melville Koppies) the colours signify the fold limbs in which the lineaments were measured by Nyebelele (2017) and are not significant for this study..... 28
Figure 17. (A) The regional aero-magnetics data showing the magnetic anomalies occurring throughout the study area. (B) The Pilanesberg dykes are interpreted as yellow, showing their relative location based on borehole data and literature. 29
Figure 18. The 083º/88ºNE extensional fracture in the vicinity of the Roodekoppies Dam found on highly weathered Lebowa Granites. The white lines are an example of the fractures. The surface on the image is highly weathered, however, the fresh surface shows a pink to pale pink coarse-grained rock (granitic). The compass -clinometer represents the scale, the north arrow has deviated due to the uneven rock where the compass-clinometer is placed. 31
Figure 19. The 163º /67ºNE conjugate fracture in the vicinity of the Roodekoppies Dam found on the highly weathered Lebowa Granites. The surface on the image is highly weathered, however, the fresh surface shows a pink to pale pink coarse-grained rock (granitic). The compass-clinometer represents the scale; the north arrow has deviated due to the uneven rock where the compass-clinometer is placed. 32
Figure 20. Average orientations of the fractures found in the Roodekoppies area, the stereonet was constructed using 8 n values. 33

Figure 21. Simplified geological section of the UCRB, trending in the N-S direction. The possible compartments are numbered 1-7. The high points are associated with quartzites and other competent rock types and are possible recharge points. 35
Figure 22. Simplified geological section orientated in the E-W direction. The valleys are important points as far where the fractures and streams are located. The Pilanesberg dykes are marked here and can possibly form a compartment. 36
Figure 23. Borehole logs of the South West of the study area selected randomly, superimposed with the average water level in each borehole. From left to right the BH ID's are 37328, 37329,37808 and 38051. 39
Figure 24. Borehole logs from the West of the study area. The blue line denotes the average water level in each borehole. BH 37997 has syenite which is part of the Pilanesberg dyke swarm. 40
Figure 25. Borehole logs found on the eastern side of the study area. The blue line denotes the water level in each borehole. 41
Figure 26. The drainage of the UCRB, with the sampling points superimposed. The dendritic pattern dominates the entire study area. The black lines outline the limits of the dolomite units. 43
Figure 27. (A) The streams in the Lebowa Granites flowing in a NW-SE direction. (B) The streams in the Lebowa Granites flowing in the NE-SW direction. These streams are controlled by the two fracture directions. 44
Figure 28. The trellis pattern on the Silverton shales is highlighted by the NW-SE trending red lines and the NE-SW trending blue line. This is also consistent with the lineament direction. 45
Figure 29. Topographical map of the study area showing the estimated sizes of the catchment areas for the four springs used. 47
Figure 30. The recession curve for the Albert's Farm spring collected between 06 March 2017 to 06 January 2018. 49
Figure 31. The Location of the Albert's Farm spring, with the major lineaments passing in and around the spring. 50
Figure 32. The recession curve (times vs discharge) for the Nouklip-Eye (Data source: DWS hydrological site) 51
Figure 33. The Nouklip-Eye location, showing the lineaments that occur in and around the spring area that might result in the spring occurrence. 52
Figure 34, Cross-section of the Nouklip-Eye through a N-S section. The spring location is depicted with the star. The streams generally occur in valleys, as such, were not superimposed. 53
Figure 35. The recession curve (times vs discharge) for the Maloney's-Eye spring. The station ID measuring discharge is A2H010 (Data source: DWS hydrological site). 54
Figure 36. The Maloney's-Eye location with the associated lineaments in and around the spring area. 55

Figure 37. Conceptual model of the Maloney's-Eye, with the associated lineaments (Adapted from Meyer, 2014). 56
Figure 38. The recession curve (times vs discharge) for the Elandsfontein-Eye spring (Data source: DWS hydrological site). 57
Figure 39. The Elandsfontein-Eyeand the associated structures. 58
Figure 40. Conceptual model of the Elandsfontein-Eye showing that the spring occurs on a contact between shales and dolomites. 59
Figure 41. Google Earth image showing the gauging stations used. 61
Figure 42. Stream discharge hydrograph for the A2H009 and A2H005 gauging stations. The discharge measurements are monthly averages (Data source: DWS hydrological site). 62
Figure 43. Stream discharge hydrograph at the A2H009 and A2H005 stations (Data source: DWS hydrological site). The discharge measurements represent monthly averages. 63
Figure 44. Stream discharge hydrographs for the A2H044 and A2H023 gauging stations (Data source: DWS hydrological site). The discharge measurements are monthly averages. 64
Figure 45. The stable isotope plot for the groundwater samples in the UCRB, with respect to the GMWL, PMWL and JMWL. 70
Figure 46. Clusters of BH's are based on mean isotope similarity. The red-boxes represent these clusters and are numbered for reference purposes. 71
Figure 47. Average isotope values of the clusters. Plotted with the PMWL, GMWL and JMWL. 72
Figure 48. $\delta^{18}O$ versus tritium for the 9 boreholes with tritium measurements. Al, boreholes plot slightly below -2.00 ‰ and above -6.00 ‰. 74

List of tables

Table 1: The Pilanesberg dyke orientations and the locations. 30
Table 2. Summary of the recession coefficient data for the springs, including the coordinates, initial discharge and discharge at the end of recession. 60
Table 3: The stable isotopes data for boreholes , Albert's Farm spring (measured between June 2016 and May 2018) and Dolomitic springs. 65
Table 4. The average stable isotopic composition for the different clusters shown in Figure 46. 71
Table 5: showing the tritium data for the nine sampled boreholes. 73

1. Introduction

1.1. Background

Water is an important and vital natural resource, which is essential for the quality of life, food generation, hygiene, environment, industry, and power generation (DWAF, 2004). Therefore, it is crucial that good management of water resources is practiced in all types of water occurrences (DWAF, 2004). In 1994, the Department of Water Affairs stated that over 12 million people had no access to clean water and over 21 million people lacked appropriate sanitation. South Africa depends dominantly on surface water especially the major cities (Abiye, 2011). In most cases, surface water is sustained by the discharge of groundwater in the form of baseflow through stream beds and springs during dry seasons. Groundwater also serves as an important source of water in some communities (Abiye, 2011). As such, groundwater plays a crucial role, both in water supply and sustenance of streams. Hence, attempting to understand the role of geologic structures in the hydrogeology of a catchment is a crucial exercise.

The study area is dominated by crystalline bedrock, identified as metamorphic and igneous rocks like granites and quartzites. Intensive hydrogeological studies have been made on crystalline bedrock at global scale as opposed to sedimentary bedrock (Michalski and Britton, 1997). Crystalline bedrock has been intensively studied mostly to identify the best suited sites for nuclear waste disposal. A considerable amount of Earth surface is covered by crystalline rocks (igneous or metamorphic), that are in turn covered by unconsolidated sediment to some degree. In these rocks, groundwater is appreciably sparse and tends to be found in cracks and fissures. The importance of groundwater for water supply in crystalline bedrock has increased especially in the developing countries (Gustafson and Krasny, 1994). The main pathways in crystalline bedrock are inhomogeneous fracture networks that are distributed unevenly (Banks *et al.*, 2002).

Crystalline rocks are mainly characterised by fractures that control the occurrence of groundwater. In some cases, bedding fractures become enlarged by stress or relief, which causes the structures to facilitate groundwater flow (Michalski and Britton, 1997). An example of a fracture controlled hydrogeological process is in the Lambeng Fault in West Java (Indonesia), where fractures act as groundwater flow barrier. This fault has resulted in multiple springs along the fault line on the downthrown wall (Delinom, 2009). An example of structures controlling the hydrogeology of region in South Africa is in the Cape Fold Belt Mountains, where the streams exclusively flow along the fractures (Manjoro, 2015). Regional and localized faults are best studied through using remote sensing, in order to see the big scale picture.

In line with the complex hydrogeological problem related to geological structures. The purpose of this research is to understand how the geological structures or discontinuities including dykes, faults, fractures and bedding surfaces regulate the hydrogeology of the Upper Crocodile River Basin. Geological and structural mapping with the assistance of remote sensing was used to understand the study area, and environmental isotopes were used to understand hydrological and hydrogeological processes.

1.2. Overview of methods

Due to the structural complexities of crystalline rocks, several researchers have applied numerous methods for groundwater exploration. Remote sensing, as a method has been used to study geological structures, it has been used to conduct mineral exploration studies and to locate appropriate sites for toxic waste disposal (Kovalevsky *et al*, 2004). The Remote sensing method is an extremely powerful technique for earth resource exploration, which includes groundwater mapping and management (Kovalevsky *et al*., 2004; Singhal and Gupta, 2010). By the early 1980s remote sensing was used for routine analysis and interpretation of geology (Goetz and Rowan, 1981). In this study, visual interpretation of satellite imagery enhanced through GIS techniques was used as a tool to extract various structures. The satellite imagery analysis was performed besides ground- truthing in the field where possible.

Environmental isotopes have also been used in various parts of the world to study groundwater and surface water (Abiye, 2013). In an attempt to understand hydrogeological processes that are responsible for spring formation, groundwater discharge and recharge, environmental isotopes can be used amongst other tools, in order to understand hydrogeological processes in the catchment.

Oxygen-18 (^{18}O) and Deuterium (^{2}H) are generally used as environmental tracers and they are important for the good management of groundwater resources (Yeh *et al.*, 2014). The use of isotopes to study hydrogeological processes is well documented in Rose *et al.* (1996), where an array of isotopic tools were used to evaluate aquifer characteristics, residence time and flow paths. The use of environmental isotopes in conjunction with radiocarbon and tritium assists in the quantitative study of the origin, apparent age, and flow paths of groundwater at a regional scale (Rose *et al.* 1996).

Tritium (^{3}H) is the radioactive isotope of hydrogen. It is produced naturally primarily in the upper atmosphere through the interaction of cosmic-ray produced neutrons with nitrogen (Hiscock and Bense, 2014). ^{3}H then becomes part of the hydrological cycle after oxidation. ^{3}H shows a strong seasonal variation, where concentrations are less in winter than in summer due to the rain out effect (Hiscock and Bense, 2014). The use of carbon-14 (^{14}C) and ^{3}H for dating is particularly useful because dispersion rates are slow in most aquifers, hence, it represents groundwater residence time (Cook *et al.*, 2005).

Conversely, in fractured aquifers matrix diffusion, which is poorly understood, results in age discrepancies between apparent groundwater age and residence time, this will give a relatively larger age than expected (Cook *et al.*, 2005).

Discharge measurements from springs and streams can give information on the aquifer characteristics. This information can be assessed by the use of recession analysis from hydrographs (Amit *et al*., 2002). Spring hydrographs allow for the estimation of hydrological parameters like transmissivity and specific yield (Kresic and Bonacci, 2010). Moreover, it can assist with the understanding of porous media including fractured, jointed or karstic zones (Amit *et al*., 2002). The rate of depletion of the hydrograph can be associated with the hydraulic conductivity, if the curve shows rapid depletion then hydraulic conductivity is assumed to be high. The use of hydrographs depicts the entire aquifer response to hydrological processes like precipitation as opposed to the use of quantitative data obtained from the use of dyes and pumping tests (Padilla *et al*., 1994). Stream flow hydrographs can also be used to estimate gaining and loss from streams.

1.3. Study area

1.3.1. Location

The Crocodile (West) and Marico Water Management Area, is made up of multiple sub-catchments that includes the Crocodile River, which is a major tributary for the Limpopo River (DWAF, 2012). The Upper Crocodile River Basin (UCRB), makes up the upper portion of the Crocodile (West) catchment with an aerial extent of 4107 km^2 (Leketa *et al*., 2018) (Figure 1). This extends from Johannesburg in the south to just after Roodekoppies dam in the north (DWAF, 2012; Abiye *et al*., 2015). It ends after the Buffelspoort dam in the east, which is located on the south-east of the Hartbeespoort dam in the North-West Province (DWAF, 2005).

The UCRB is characterized by extreme urbanization and industrial activities, both anthropogenic factors require elevated water demands for industries and food production (Abiye *et al*., 2015). The main tributaries of the UCRB arise in the south around the Witwatersrand basin described as the rolling hills on the Highveld plateau (DWAF, 2012).

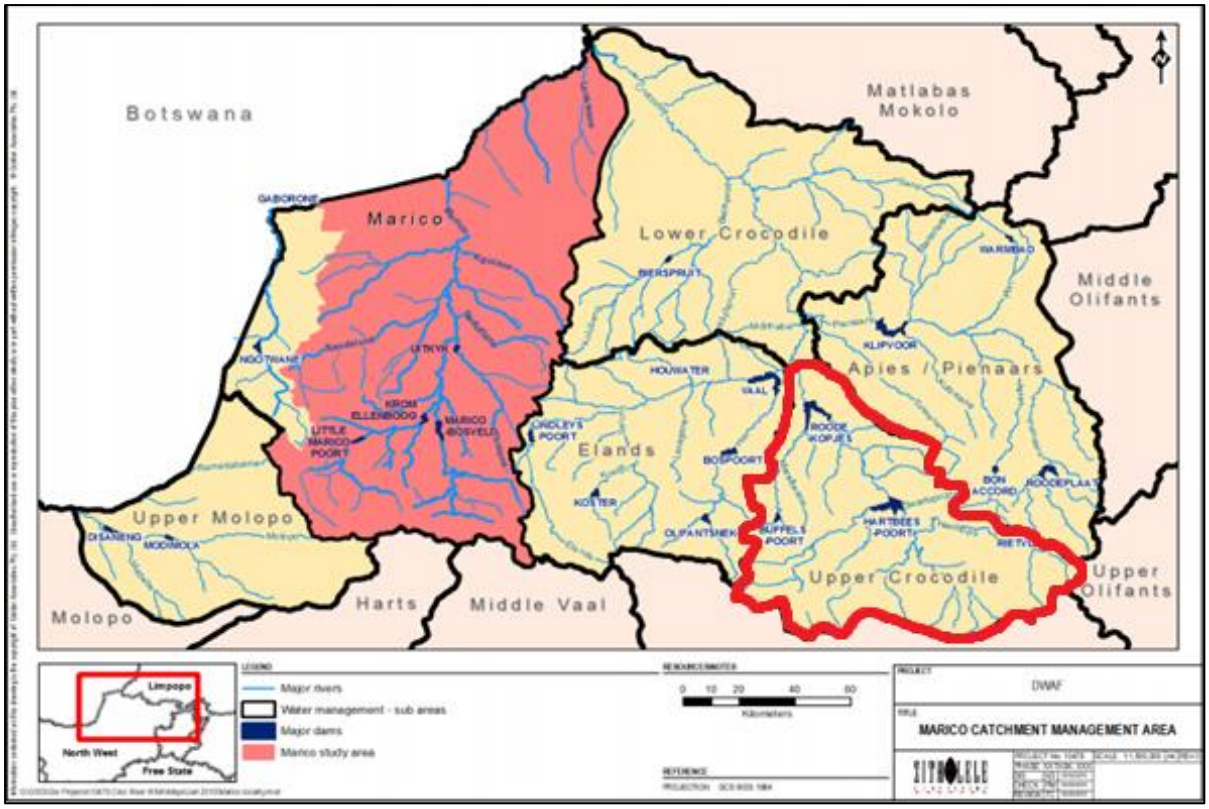


Figure 1. Map of the Crocodile catchment illustrating the location of the UCRB relative to the other neighbouring catchments like the Apies (Source: DWAF, 2012). The UCRB catchment is delineated in red.

The main pollutants affecting the basin are Acid Mine Drainage (AMD) from the West Rand region (Abiye *et al*., 2015), the agricultural sector in the form of fertilizers, pesticides and the wastewater from sewage treatment plants. The UCRB has 3 main dams; the Hartbeespoort dam, which is a hypertrophic man-made dam (Robarts and Zohary, 1984) with a capacity of 192800000 m^3 (Robarts *et al.*, 1982), the Roodekoppies dam in the northern region and the smaller Buffelspoort dam to the west of Roodekoppies dam.

The climatic setting of the catchment is semi-arid, with the average seasonal precipitation and potential evaporation of about 700 mm/year (Abiye, 2011).

1.3.2. Geological setting

The geological setting of the UCRB is particularly complex, considering the extent of the geological Formations as noted by SACS (1980). The Johannesburg Dome constitutes basement rocks that cover the eastern section, the central section is covered by the Transvaal Supergroup rocks of the Pretoria and Chunniespoort Groups. The northern region falls under the Bushveld Igneous Complex and the south-west is covered by the sedimentary rocks of the West Rand group of the Witwatersrand Supergroup.

The Johannesburg Dome, also known as the Johannesburg-Pretoria inlier (Anhaeusser, 1971) is a circular feature, as shown in Figure 2, which is made up of the Half-way House granite gneisses, Muldersdrif dunites and greenstones, it is bounded by the Witwatersrand Supergroup and Transvaal Supergroup rocks (Malmani dolomites and Pretoria Group rocks) (Poujol and Anhaeusser, 2001). The Dome is made up of a range of mafic and ultramafic rocks. The granitoid rocks that exist in the Dome are trondhjemitic and tonalitic gneisses (TTG's) and are intruded by tholeiitic dykes (Poujol and Anhaeusser, 2001), which could play an important role in the hydrogeology of the area. Archean greenstones also occur and are intruded by tonalite, granodiorite, granite, and migmatite, which are uncomformably overlain by the West Rand Group (SACS, 1980; Barton *et al.*, 1999; Poujol and Anhaeusser, 2001). The Johannesburg Dome is believed to have been emplaced at about 3.2 Ga (Poujol and Anhaeusser, 2001).

The West Rand Group is made up of 3 subgroups: The Hospital Hill at the bottom with alternating metasedimentary rocks such as magnetic mudstones and quartzites; the Government subgroup made up of alternating shales and quartzites, which are bound by iron formation at the top and bottom, and the Jeppestown subgroup with alternating magnetic mudstones and quartzites (Figure 2) (SACS, 1980; Smith *et al.*, 2013). The West Rand rocks were deposited between 2970 and 2914 Ma (Robb and Meyer, 1995).

The Chunniespoort Group is made up of dolomites, intercalated by cherts and local Penge banded iron formation (Kinnaird, 2005). The dolomites form an east-west band that has been associated with high storage capacities and the sinkholes form due to the dewatering of the dolomites (DWAF, 2004). The dolomites result in multiple structural problems around the basin in a form of sinkholes.

The Pretoria group is part of the Transvaal Supergroup, and is characterised by predominantly quartzites, shales and subordinate conglomerates, andesitic lavas, arkosic sandstones and diamictites (Figure 2) (Kinnaird, 2005; Erikson *et al*., 2009).

The Bushveld Igneous Complex rocks occur in the northern region of the study area (Figure 2). This is dominated by the Lebowa granites, and minimal gabbro's and norites (Hill *et al*., 1996).

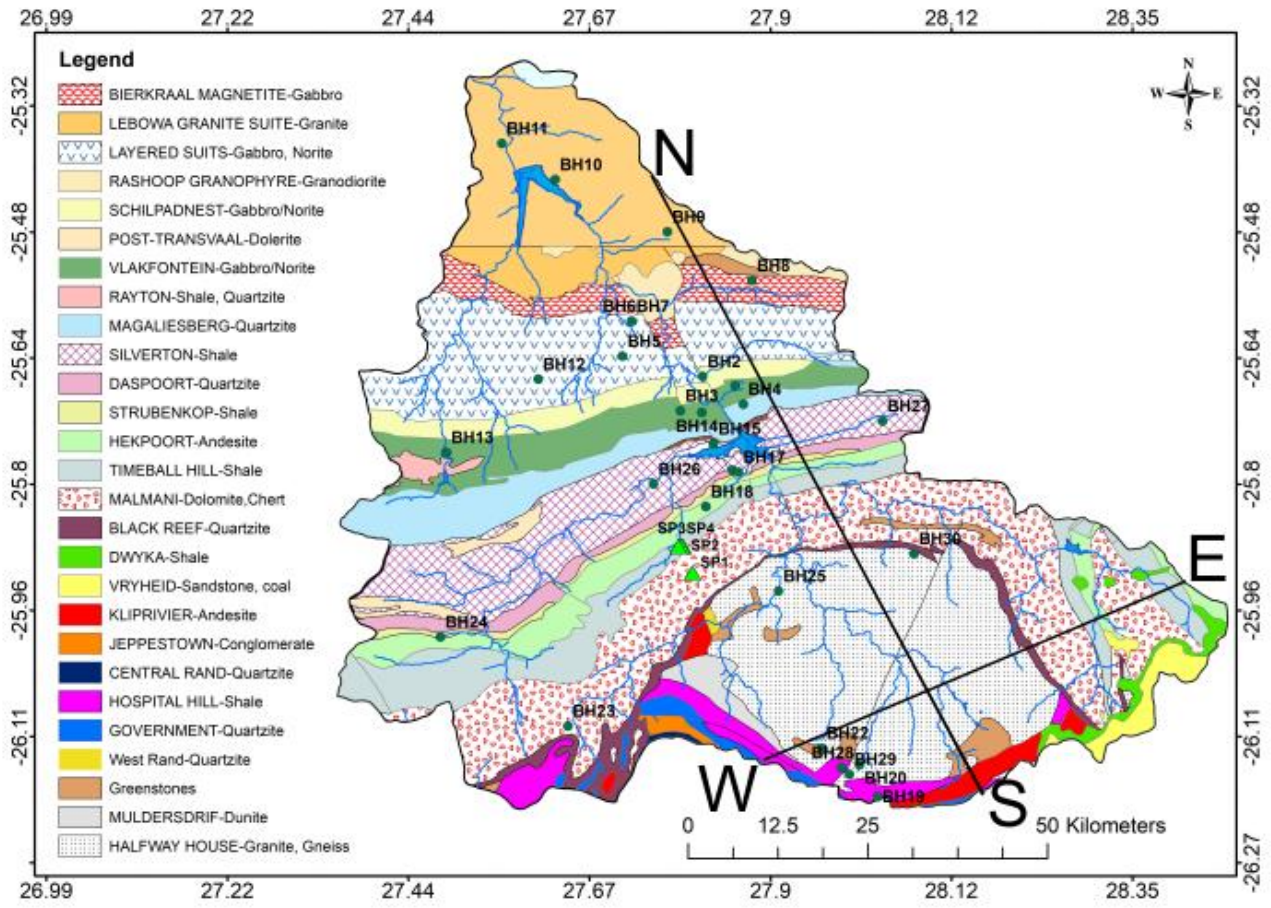


Figure 2. Map of the UCRB highlighting the geology and drainage related to the study area. The Figure also shows the distribution of the sampled boreholes labelled as BH (#) and the dolomitic springs labelled as SP(#) (Map constructed by Mr. K Leketa).

1.3.3. Hydrogeological setting

Crystalline or hard rocks in the hydrogeological context refer to aquifers with negligible matrix porosity and permeability, with water occurrences limited to fracture zones (Gustafason and Krasny, 1994). The crystalline nature of this basin resulted in fractured aquifers and as such shallow and extensive hydrogeological environment is expected (Abiye, 2011). The dolomites are the exception and boast high discharge rates and potential (Abiye, 2011). The West Rand aquifer has discharge rates ranging between 0.5 and 2.0 l/s, based on borehole data (Barnard et al., 1999).

The role of structures on the drainage pattern has been widely studied in several geological environments (Howard, 1967). Drainage pattern refers to a network, in which a group of streams form in an area (Howard, 1967). Howard (1967) noted eight different main drainage patterns as dendritic, parallel, trellis, rectangular, radial, annular, multi-basinal and contorted. In these patterns, it was further

stated that sub-patterns do exist due to the unpredictable trait of rocks (Howard, 1967). However, the role of geological structures on groundwater is still unclear in the study area.

The dykes in the dolomites act as a barrier, which divide the dolomite into compartments. Areas with fractures and chert layers are considered to be the best areas for groundwater exploration and elevated amounts of recharge (DWAF, 2006). Compartmentalisation in the dolomites was also observed by Trollip (2006) in the south of the study area. The compartmentalisation might not play a role in the crystalline rocks such as that of the Bushveld Igneous Complex.

The Bushveld Igneous Complex is a body of crystalline rocks like norites and pyroxenites with insignificant matrix porosity and permeability. Areas with faults, fractures, and joints are considered important for the occurrence of groundwater (Titus et al., 2009). Titus et al. (2009) classified the Bushveld aquifers into two groups, (a) a shallow weathered bedrock and alluvial aquifer and (b) highly and deeply fractured bedrock. The shallow aquifer is unconfined, characterized by saprolite to saprock zones. The thickness and occurrences of this zone are dependent on weathering processes (Titus et al., 2009). The deeper aquifer is unweathered and consists of fractures. This aquifer is semi-confined underlying the weathered zone. The hydraulic conductivity of the deep aquifer is dependent on the fractures and thus variable from place to place (Titus et al., 2009).

The drainage in the Johannesburg dome has been associated with the underlying structures as opposed to lithology. The structures trend in an N-S direction and the streams flow to the north (Vermaak, 2000). Vermaak (2000) identified three aquifer systems: (1) the shallow weathered aquifer, (2) deep secondary aquifer associated with fractures and joints and (3) a perched aquifer. The best yields occur along fractures, which tap the deep aquifers and the deep aquifers are recharged by the overlying shallow aquifer systems (Vermaak, 2000).

The understanding of the structures in the UCRB will feed into understanding whether the streams are losing or gaining, on the basis that fractures in crystalline rocks can serve as pathways for recharge or discharge. Fractures such as faults and joints are considered as areas of high permeability (Alfaro and Wallace, 1994).

1.4. Aims

The main aim of the research is to study the role of geological structures on the hydrogeological setting of the area including drainage patterns, stream discharge, and general groundwater occurrence. As well as, to gain an understanding of the role of geological structures on the occurrence, distribution, and yields of springs in the UCRB.

The specific objectives are:

- To locate regional faults, dykes and other structural features such as joints that cross-cut the UCRB using remote sensing, focusing on LANDSAT imagery data sets. Furthermore, to delineate the structures that might have a role in controlling the drainage patterns.
- To assess the connectivity of groundwater compartments by comparing environmental isotopes of δD, $\delta^{18}O$, and ^{3}H values.
- To assess the recession curve of the springs, in order to have an insight on aquifer properties.
- To assess the contribution of cross-cutting structures on stream discharge.

1.5. Literature review

Several published and unpublished reports and papers have been assessed on the topic of spring recession curves, for example, Amit *et al*. (2002) used data from two seasons (dry winter and wet summer) and data from an extremely dry year to produce spring hydrographs. A total of 5 springs were studied, that are located on carbonate rock formations. The dolomites were faulted, cracked and karstified. It was shown that the aquifer lithology and the shape of conduits affect recession curves and coefficients. In porous media characterized by slow flow, the recession coefficient is low. In fractured media the coefficient is expected to be high. The dolomites showed relatively high coefficients (Amit *et al*., 2002). The study of recession coefficients can be utilized in the UCRB in understanding the hydrogeological parameters of the study area, moreover, the area around the spring. Amit *et al.* (2002) analyzed nine carbonate springs located in Israel. The purpose of the study was to understand whether the springs discharge curves rely on precipitation or aquifer properties. The recession coefficients for the different years were found to be similar, based on these recession coefficients it was establish that these springs rely on aquifer properties as opposed to precipitation. Most springs in the UCRB occur at the contact between quartzites and shale besides in the dolomitic aquifer.

Compartmentalization in the dolomites was studied by DWAF (2006) and Meyer (2014). Meyer (2014) also described the compartments in the study area, on the basis of multiple dyke's cross-cutting the Malmani dolomites. In the Pretoria region, the dolomitic springs that have been supplying the city of Pretoria since 1855 are located on the east and west groundwater compartments (Naidoo, 2014). The compartments studied by Naidoo (2014) belong to the Chunniespoort Group These two compartments

that hosts high yielding springs are separated by the Pretoria syenite dyke and bounded in the north by the Pretoria Group rocks. Based on Naidoo (2014) the groundwater level between the two compartments differs by 8.5 m, with the west compartment being deeper. It was noted that the east and west compartments share a similar recharge point based on their similarities in isotope compositions.

The dolomite aquifer system belonging to the Malmani dolomites of the Chunniespoort Group owes its permeability due to secondary structures like faults, joints, bedding planes, dissolution cavities and fractures (DWAF, 2006). These structures have ensured deep weathering of the dolomites through karstification. A study conducted on the Vaal water management area through Landsat imagery showed that tensional fractures play a major role in facilitating the deep weathering of rocks (DWAF, 2006). Two conjugate lineaments (Witpoortjie and Bank) with small displacements and deep penetrations were found to be filled with residual material. They form the main conduits for groundwater percolation in the West Rand mines, these lineaments pose the greatest water hazard on underground mine workings (DWAF, 2006; Titus et al., 2009).

Faults are known to be a plumbing system for the crystalline aquifer and act as conduits for the migration of fluids (Berkowitz, 2002; Bense *et al.* 2013). However, the processes that accommodate strain in fault zones can lead to increased permeability and sometimes decreased permeability (Bense *et al.* (2013). The role of faults, fractures, folding and bedrock lithology in the Cape fold belts, for example, was studied by Manjoro (2015), where drainage followed the occurrence of geological structures. With the use of remote sensing and an intensive structural database, it was concluded that the streams aligned along lineaments and fold axis geometry (Manjoro, 2015).

Additionally, fault control on groundwater has been studied on metamorphic and igneous rocks of the Blue Ridge province, USA (Seaton and Burbey, 2005). Groundwater flow was controlled by thrust faults which act as both a conduit and a barrier. Many aquifers were noted, a shallow saprolitic aquifer, which could be equated with the Bushveld Igneous Complex and the Johannesburg Dome, on the premise that both areas have similar geological setting. The saprolitic aquifer is separated by a confining unit from the deep fractured high permeability aquifer (Seaton and Burbey, 2005).

The growth in the availability of multi-temporal satellite data has assisted with possibilities of studying large rivers from space (Smith, 1998). River basins have been studied by McCarthy *et al.* (2007) for tracking vegetation patches, and by Satyanarayana *et al.* (2013) to try and understand the morphology, sediment load and deposition of the Brahmaputra River, India. However, remote sensing has not been applied adequately to the studying of how drainage patterns relate to structural lineaments and lithological variations. Although, it is well known that drainage patterns are related to geological structures and lithology.

Dendritic drainage patterns are characterized by streams joining the mainstream at an angle, although, the angle tends to point downstream (Zernitz, 1932). Rectangular pattern differs from trellis in that it is more irregular (Zernitz, 1932). Zernitz (1932) argues that the dendritic pattern only occurs where the rocks offer uniform resistance in a horizontal direction, this is recognised mainly in crystalline rocks. The rectangular drainage patterns is characterized by right-angled bands in both the mainstream and its tributaries (Zernitz, 1932).

Stable and radioactive isotopes are known to be important indicators of hydrogeological processes and ecological patterns (West *et al.* 2014). Tritium analysis of streams during the winter season in the Kouris catchment (Cyprus), revealed that surface water tritium composition is similar to that of spring discharge (Boronina *et al*., 2005). This insinuates that groundwater and surface water are interconnected, by means of stream loss or gain. The Tritium from the ophiolitic complex indicated the presence of anthropogenic tritium. During the rainy season the springs were discharging elevated amounts of recent rainfall and as such the springs are endangered by the surface water pollution (Boronina *et al*., 2005). Abiye *et al*. (2015) used environmental isotopes to show that the fractured crystalline rocks and dolomitic aquifers are prone to pollution from surface water. The similarities in stable isotopes showed that there is an interaction between mine water flowing into streams and groundwater. Although, the groundwater circulation time was found to be slow based on tritium data analysis.

2. Methodology

2.1. Geological mapping and structures

Using a combination of single band images, all visible lineaments were extracted from the UCRB. The images included LANDSAT 8 OLI C1 level-1 (B1, B2, B3, B4) and LANDSAT 7 ETM+ C1 level-1 (B1, B2 and B3). The ArcGIS colour base-map was used to confirm the smaller lineaments whereas the black and white images from the different bands increased lineament visibility in the built-up areas.

Magnetic data were collected and compiled by the Council for Geoscience, and for the purpose of this study, the grid was not processed any further. The aim here was to identify any magnetic anomalies that can be identified as lineaments. The lineaments were then compared to groundwater isotopes in order to assess if the aquifer is compartmentalised or not and what the role of the structures could be. The lineaments were traced using ArcGIS.

Due to access problems, field mapping was limited along road sections. The purpose of this field investigation was to confirm the geology and mapped structures, and their relationship to drainage patterns, if at all. Consequently, the structural measurements were limited to only 8 stations. The measurements included orientations data for strike, dip and dip-directions of fractures. The resulting data were plotted on the Stereonet 10 software (version 10.2.0- 2018.10.30) program by Allmendinger. The data from the mapping was incorporated in the drainage data sets.

2.2. Borehole logs

The borehole logs were acquired from the DWS (Department of Water and Sanitation) administered National Groundwater Archive (http://www3.dwa.gov.za/NGANet). The data was obtained with coordinates, which ensured that they can be plotted on ArcGIS to see their respective proximities. From this, the study area was subdivided into four segments: the northern (predominantly Bushveld Igneous Complex), eastern, western and southern (Figure 3). Most of the boreholes were clustered on the western segment. To reduce the boreholes into a manageable number, boreholes were randomly selected perpendicular to the strike of the geology. The selected BH's were plotted in Figure 3, their sectional lines were also superimposed. Then from the selected boreholes, the lithological information was extracted and plotted using the Strater software (version 1.4.33, 2005). However, the borehole data was not very accurate and there were lots of discrepancies, this was established through quality control of the excel sheets containing the geological information. In the northern and southern segments, the boreholes did not have lithological information and were not plotted. The Johannesburg Dome does not have any borehole with lithological information, even though numerous private boreholes are operational in the area.

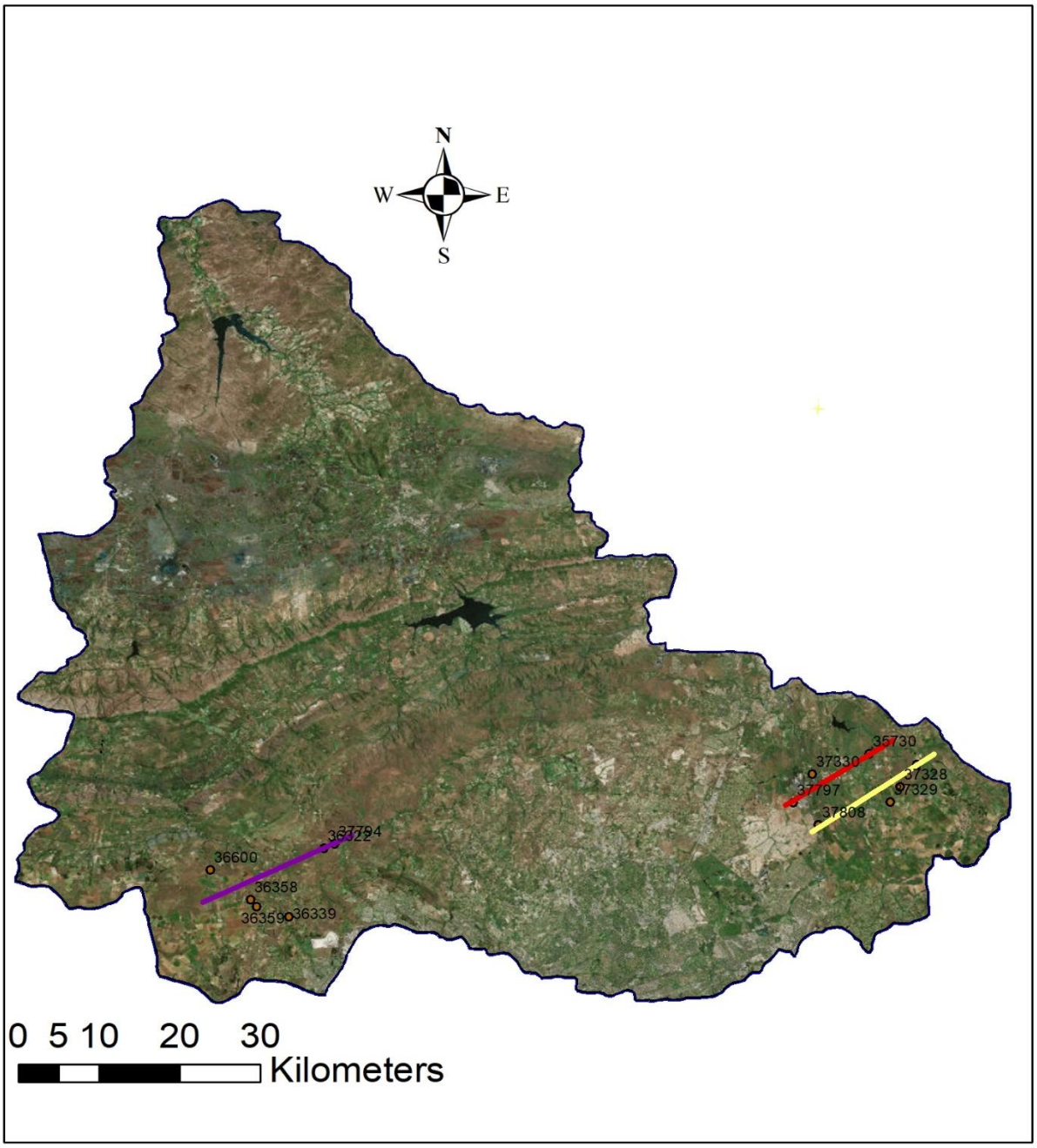


Figure 3. The locations of the BH's used for the BH logs and their respective section lines.

2.3. Drainage Pattern

In order to try and establish what the general drainage pattern looks like, the use of satellite imagery proved to be important. The satellite images were enhanced with the ArcGIS software. Streams were highlighted manually in order to see the general trends.

2.4. Discharge data collection for the recession constant determination

Spring discharge was measured using the float method adopted from www.hydromatch.com. It is very useful in canals and channels; however, it can also be used in streams and channels, with a decrease in accuracy. The float method of measuring velocity was done by observing the time it takes for the floater to traverse a section with a known length. A channel with equal width as possible was selected, and the length was selected based on whether it was going to limit bias as much as possible, normally kept below 2 m due to the size of the stream. The width of the channel was determined with a measuring tape. The time it takes for the 'floater' to move from the starting point X to the end point Y was recorded using a stop watch. Then velocity was calculated using the formula V=d/t, where V is velocity, d is distance (m) and t is time (in seconds). The velocity obtained was used to calculate discharge: Q=v*A, where Q is discharge in m^3/s, V is velocity in m/s and A is cross-sectional area in m^2.

The calculated discharge was then corrected by a factor of 0.25, which reduced the effects of velocity distortion. The factor of 0.25 was selected based on the fact that the stream is very shallow and rocky. Correction in such streams has poor accuracy as opposed to rectangular channels with smooth sides and bed. The floater was 1cm by 1cm by 1mm Styrofoam, this including the mass of the floater makes it less dense compared to the water; this is to ensure that it records the velocity of the water with as little distortion as possible. A 1m length (in some cases a 1.5 m and 2 m length) was chosen where the width dimension is relatively equal, this was because the area has a rocky channel and therefore it was challenging to find a section which is long enough to conduct the measurement. Measurements were taken 6 times in order to reduce error and the average of the data was recorded.

Additional discharge data were obtained from the DWS for the Maloney's-Eye dolomite spring and Nouklip-Eye and the Elandsfontein-Eye which were measured through automatic discharge gauge. A monthly average was taken for each spring.

The interpretation of this data was based on a hydrograph, the data obtained from this hydrograph was then used to calculate the recession coefficient.

Stream discharge data were collected from the DWS managed website (http://www.dwa.gov.za/Hydrology/). The selected stations had to be on the same stream, with as few tributaries as possible, and the distance had to be as short as possible. A number of stations that met the criteria lacked the data, as such they were discarded and only three combinations were used (A2H050:A2H051, A2H044:A2H023 and A2H005:A2H009).

2.5. Isotopes

2.5.1. Stable isotopes

The stable isotopes of $\delta^{18}O$ and $\delta^{2}H$ were analysed through the use of the Liquid Water Isotope Analyser-model 45-EP at the University of the Witwatersrand, South Africa. The instrument contains the laser analysis system and an internal computer, a liquid auto-sampler, a small membrane vacuum pump, and a room air intake line that passes air through a Drierite column for moisture removal. A Hamilton microliter syringe was used to inject 0.75 µL of the sample through a PTFE septum in the auto-sampler. The injection port of the auto-sampler is heated to 46°C to help vaporize the sample under vacuum immediately upon injection. The vapour then travels down the transfer line into the pre-evacuated mirrored chamber for analysis. A 1 ml aliquot of a sample was pipetted into a 2 ml auto-sampler glass vial and closed with PTFE septum caps. Five standards were used in the analysis procedure where the laser machine automatically calibrates itself and measures stable isotope values. The standards used area 5C: $\delta^{2}H$ -9.2 ±0.5, $\delta^{18}O$ -2.69±0.15, 4C: $\delta^{2}H$ -51.6 ±0.5, $\delta^{18}O$ -7.94±0.15, 3C: $\delta^{2}H$ -97.3 ±0.5, $\delta^{18}O$ -13.39±0.15, 2C: $\delta^{2}H$ -123.7 ±0.5, $\delta^{18}O$ -16.24±0.15, 1C: $\delta^{2}H$ -154±0.5, $\delta^{18}O$ -19.49±0.15. The laser machine is capable of providing accurate results with a precision of approximately 1 ‰ for $\delta^{2}H$ and 0.2 ‰ for $\delta^{18}O$ in liquid water samples of up to at least 1000 mg/L dissolved salt concentration.

The isotope data were interpreted using a Johannesburg Local Meteoric Water Line (JLMWL), Pretoria Local Meteoric Water Line (PLMWL) and Global Meteoric Water Line (GMWL). This will assist in explaining whether the samples went through evaporation or not before and post infiltration. It can possibly assist narrowing down the source of precipitation.

2.5.2. Tritium

Tritium samples were analysed at iThemba Labs, Johannesburg. A 500 ml of the samples were distilled with sodium hydroxide and then enriched by electrolysis. An electric current was applied, and the volume of water reduces to 20 ml. These samples were enriched by a factor of 20 and ready for liquid scintillation when half is mixed with 11 ml of Ultima Gold. The results were given in units of tritium units (TU). Each sample takes approximately 4 hours to analyse but months to prepare.

The tritium results were interpreted to estimate Mean Residence Time by using equation 1, the values that were calculated assisted in estimating circulation time. The background value used is 5.6 TU which was calculated by Abiye *et al.* (2015), using the Pretoria Global Network of Isotopes in Precipitation (GNIP) data set.

$$t = -17.93\ln\left(\frac{at^3H}{a0^3H}\right) \quad \ldots\ldots\ldots\

3. Results and Discussion

3.1. Geological mapping and structures

The mapping of geological structures in the study area was done through a combination of satellite imagery interpretation, aero-magnetics data interpretation and where possible, ground truthing of structures observed using the two methods. Fractures that trend in the NW-SE, NNE-SSW and E-W direction have been interpreted, with a combination of dykes that trend in an NW-SE and E-W direction. These structures have implications on the hydrogeology of the study area, playing a role on the groundwater and surface water dynamics.

3.1.1. Satellite imagery interpretation and lineament analysis

Using visual interpretation of the satellite imagery data, a combination of lineaments was observed. The combined use of SPOT, LANDSAT and Terra-Colour imagery is useful in identifying lineaments in the form of fractures and faults, however, with difficulty in built up areas. Figure 4A and 4B is an interpretation of all possible lineament trends in the study area. The box represents the localized analysis of lineaments studied. The study area has regional and localized structures that are somewhat related. The lineaments are orientated to the NW-SE, E-W and the NNE-SSW. The NNE-SSW lineaments have been presented in Figure 5, whereas, the NW-SE and E-W lineaments are displayed in Figure 6 and 7, respectively. The relationship of these lineaments is clearly visible in Figure 4, where the NW-SE and NNE-SSW regional and local lineaments form conjugate-sets with respect to each other. The relative occurrence of the NW-SE and NNE-SSW fractures is interpreted to be approximately at the same time. This is based on the fact that the lineaments do not displace each other. The NNE-SSW trending lineaments connect the SSW of the study area to the NNE (Figure 5). The NW-SE trending lineaments are less through going than the NNE-SSW trending lineaments, where the most dominant orientation from the rose diagrams is 135^{o}. The dominant orientation for the NNE-SSW trending lineaments is 015^{o}. Three quartzite layers are found in the study area, on the lineament analysis maps, the frequency of the fractures is higher on two of the three layers (Daspoort and Magaliesburg Quartzites). The frequency can be associated with the competency of the quartzites and their ability to undergo brittle failure. The lack of high intensity lineaments on the Witwatersrand Quartzite layers (such as the Orange Grove), can be associated with the difference in hardness in the different quartzite layers. The Daspoort and Magaliesberg Quartzites having higher competency than the Witwatersrand Quartzites. The high frequency associated with the quartzites is an example of lithologically controlled structure/lineament occurrence. The high frequency characteristics are not only observed on quartzites. In the northern part of the study area, the rocks of the Lebowa Granite Suite have an

increased frequency of the NW-SE lineaments (Figures 4 and 6). However, these high frequency lineaments are not thorough going in the entirety of the granites, this can be attributed to the local variations of the granite's characteristics. Based on Figure 4 and Figure 6, the NW-SE lineaments are characterised by local and regional lineaments that have implications on the groundwater circulation and stream flow direction. Considering that the NW-SE and NNE-SSW lineaments orientations are conjugates of each other with an expected palaeo-principal stress direction that has an N-S orientation, the E-W lineaments are possibly extensional stress release fractures as response to the N-S stress cessation. The E-W fractures are also associated with dyke occurrences which are further represented in Figures 8, 9 and 10. Whereas, the NW-SE fractures are associated with the occurrence of the Pilanesberg dykes. Although, the NW-SE and E-W lineaments are associated with dykes, NNE-SSW lineaments do not seem to have as much dyke-lineament association. Although, dykes trending in the NNE direction are present, the method used in this study could not pick up any of them. The relationship between fractures and dykes is that the fractures are areas of weakness where intrusions can occur. Unfractured or less fractured dykes could result in reducing groundwater circulation, of which would be otherwise high if the dykes were fractured (Bense *et al*., 2013). The relationship of the lineaments is shown on the stereonet presented in Figure 9. The orientation of the conjugates is at 015^{o} and 135^{o}, the calculated extensional pressure release fractures orientation is at 075^{o} and the measured is at 085^{o}. The occurrence of these fractures and lineaments in the study area could affect possible compartmentalisation of groundwater particularly in the dolomites. The plot in Figure 9 allows for the estimation of the stress direction (σ_1) to be orientated at 165^{o}, which is the orientation of the Brits Graben. The data used to plot the rose diagrams can be found on appendix A.

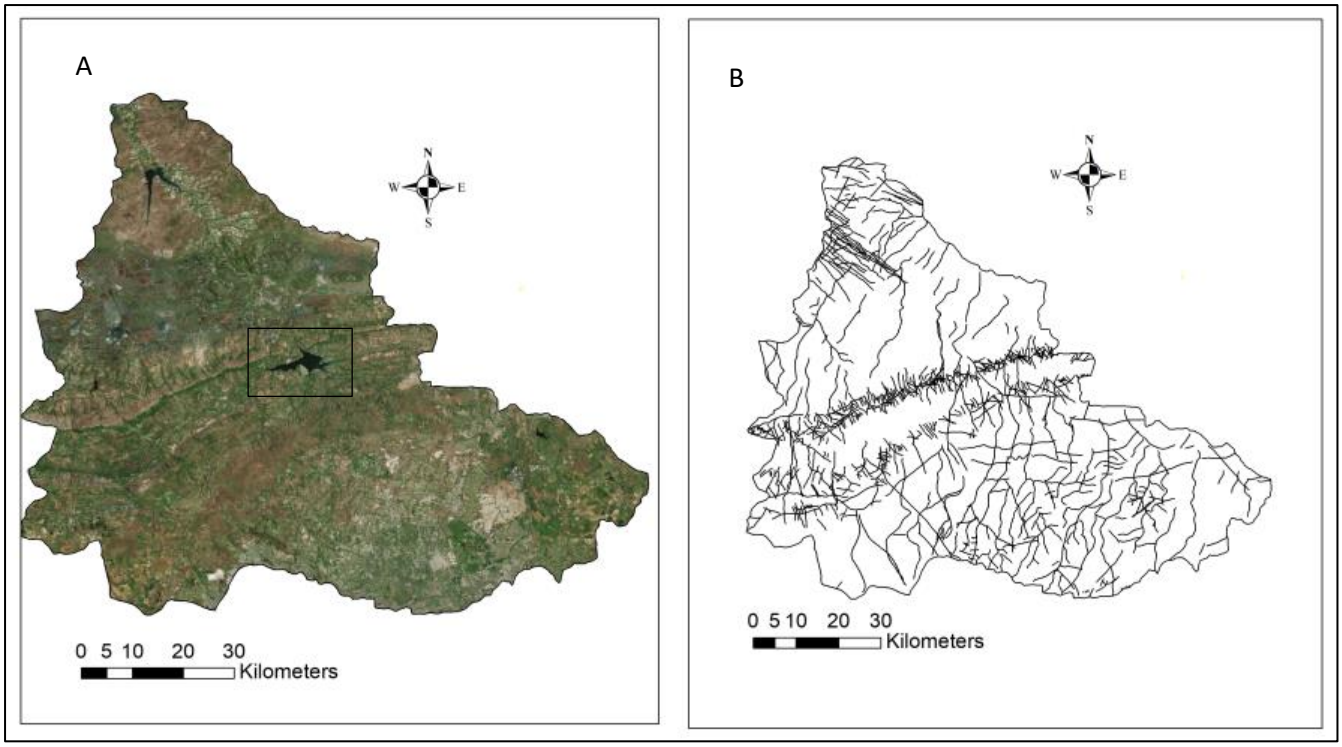


Figure 4. (A) An image sourced from ESRI, it is a combination of different satellite images such as SPOT, LANDSAT and TerraColour imagery. The black box in 4A represents the portion of the study area described later in the report (B) Represents the lineaments extracted from A.

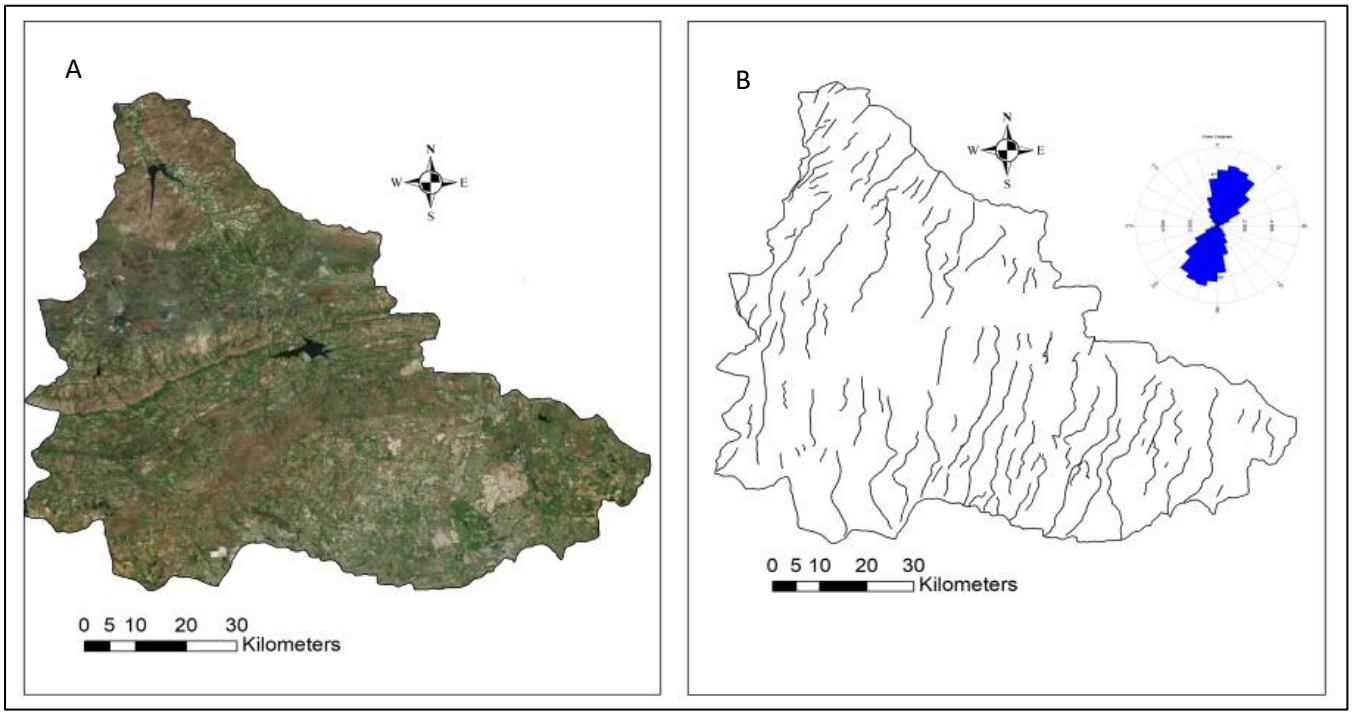


Figure 5. (A) An image sourced from ESRI, it is a combination of different satellite images such as SPOT, LANDSAT and TerraColour imagery. (B) Is an interpretation of all possible NNE-SSW trending

lineaments in the study area extracted from (A). Rose diagrams is also included in the image showing the dominant trend directions of the lineaments.

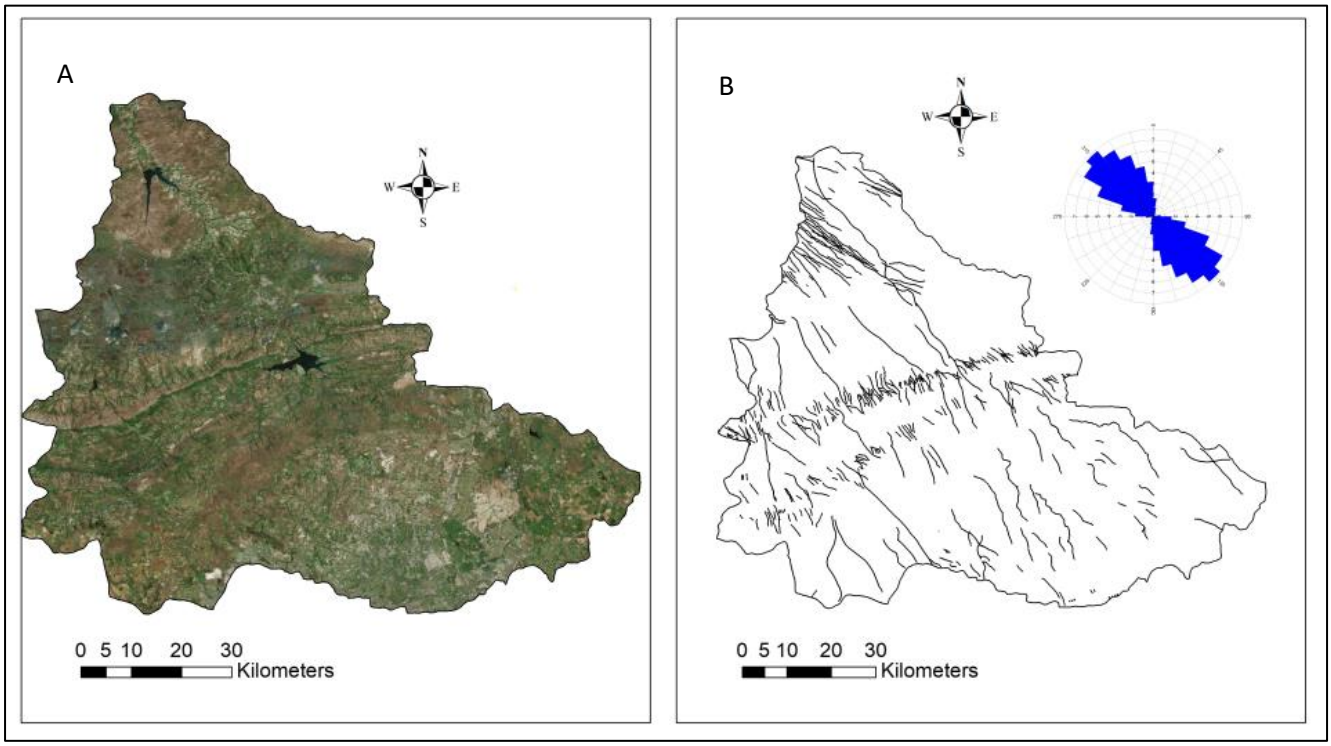


Figure 6. (A) An image sourced from ESRI, it is a combination of different satellite images such as SPOT, LANDSAT and TerraColour imagery. (B) Is an interpretation of all possible NW-SE trending lineaments in the study area. Rose diagrams is also included in the image showing the dominant trend directions of the lineaments.

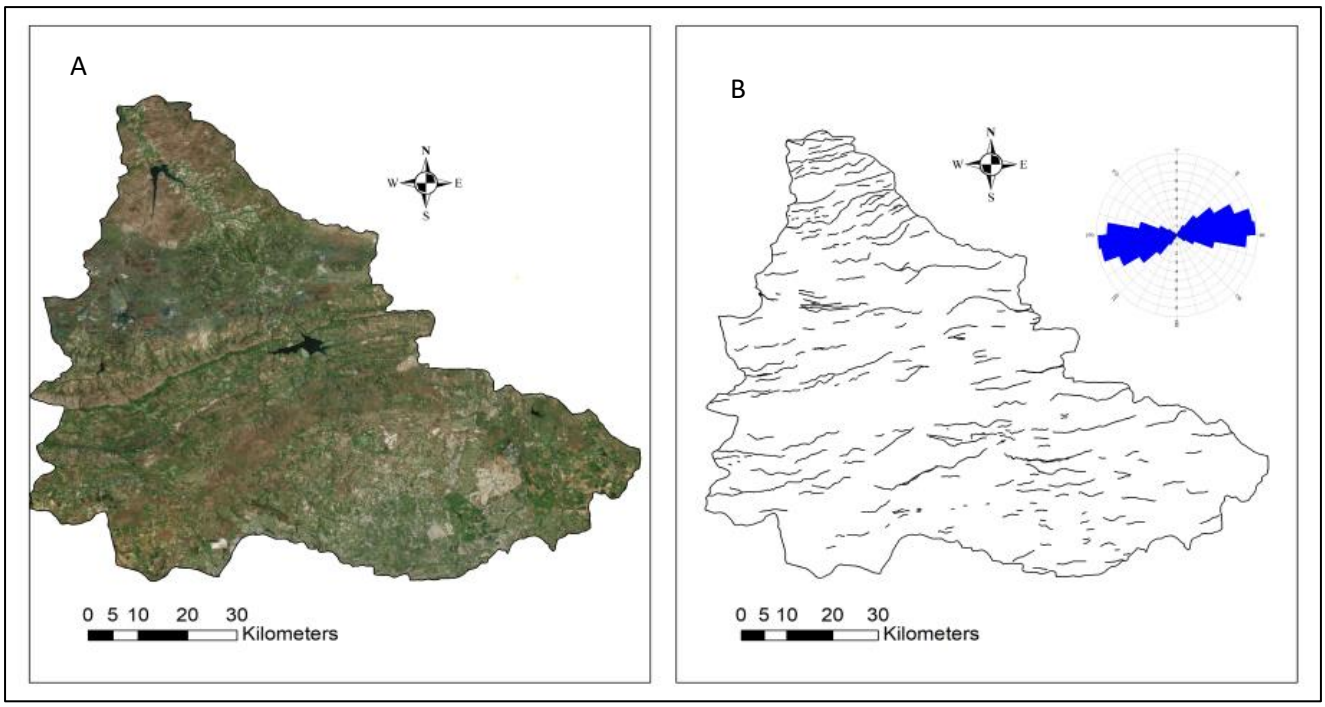


Figure 7. (A) An image sourced from ESRI, it is a combination of different satellite images such as SPOT, LANDSAT and TerraColour imagery. (B) Is an interpretation of all possible E-W-trending lineaments in the study area. Rose diagrams is also included in the image showing the dominant trend directions of the lineaments.

The Hartbeespoort Dam is known for the Brits Graben that intersects the dam and displaces the Magaliesburg quartzite ridges (Figure 2). As such it is a perfect area to have localized study of the lineaments. The associated block movement along the faults in the Hartbeespoort Dam area are presented in Figure 8. The movement of the quartzite ridges have been associated with the Brits Graben. It plays a role of allowing groundwater seepage from the Hartbeespoort Dam through a network of synthetic faults (associated with the Brits Graben). The role of the Brits graben on groundwater flow was documented by Titus *et al.* (2009), where pumped boreholes showed quick recovery of which can be attributed to the synthetic faults associated to the Brits graben. Furthermore, the Brits Graben associated faults resulted in an increase in mine groundwater seepage, through the fractures. The fault movements are consistent with what would be expected in conjugate-sets, in that there are right-handed offset (blue arrows) and left-handed offset (orange arrows) movements (Figure 8B).

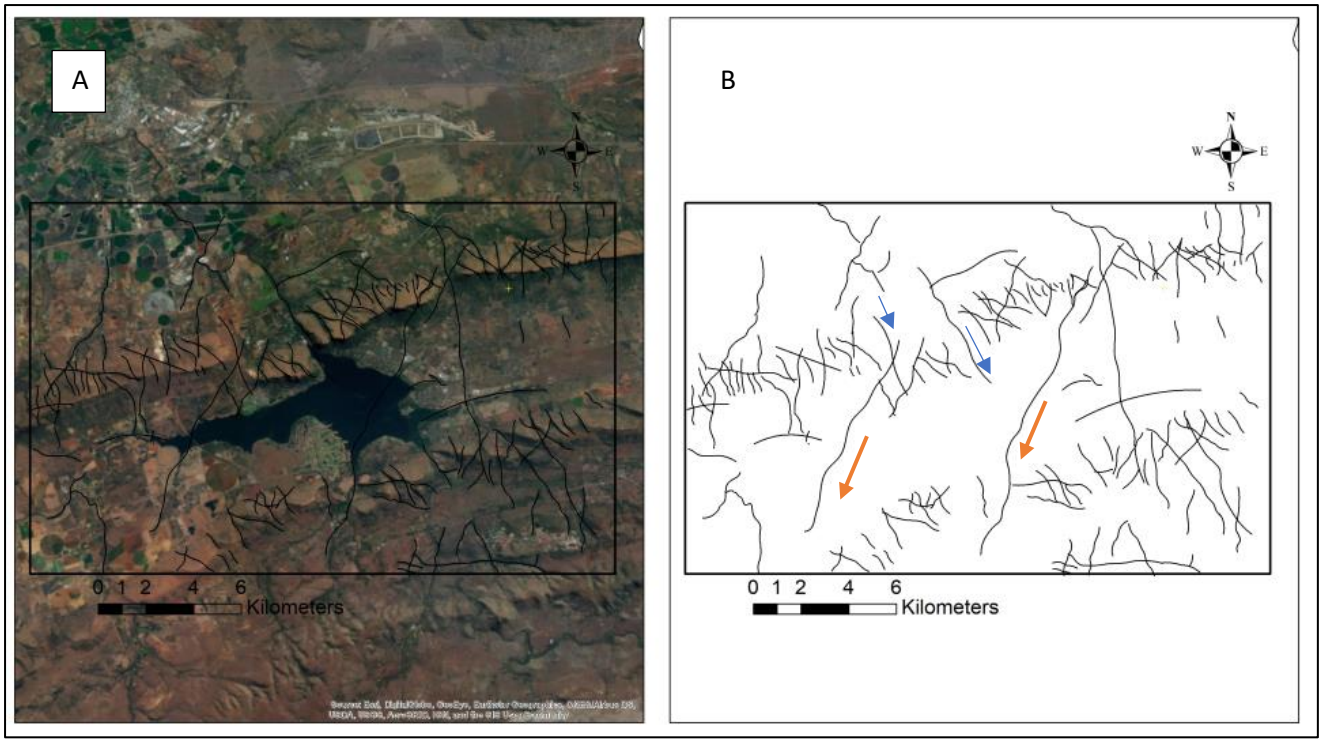


Figure 8. (A) The localised analysis map of the area around the Hartbeespoort dam. This map highlights the fact that the lineaments show similar traits in regional and local scales. (B) The extracted lineaments with the fault movement directions as blue and orange arrows. The arrows represent the sense of direction on the associated block.

Stereonet interpretations can be useful for the analysis of lineaments. For the purpose of this study the dominant orientations were taken from the rose diagrams, the dips were assumed to be 90^{o} and this because most of the lineaments dealt with ranged from 80^{o} and 90^{o}. Orientations of the two conjugates are 015^{o} and 135^{o}. The acute angle calculated from the conjugates is 60^{o} (as expected for conjugates), the acute bisector orientation is 165^{o}.

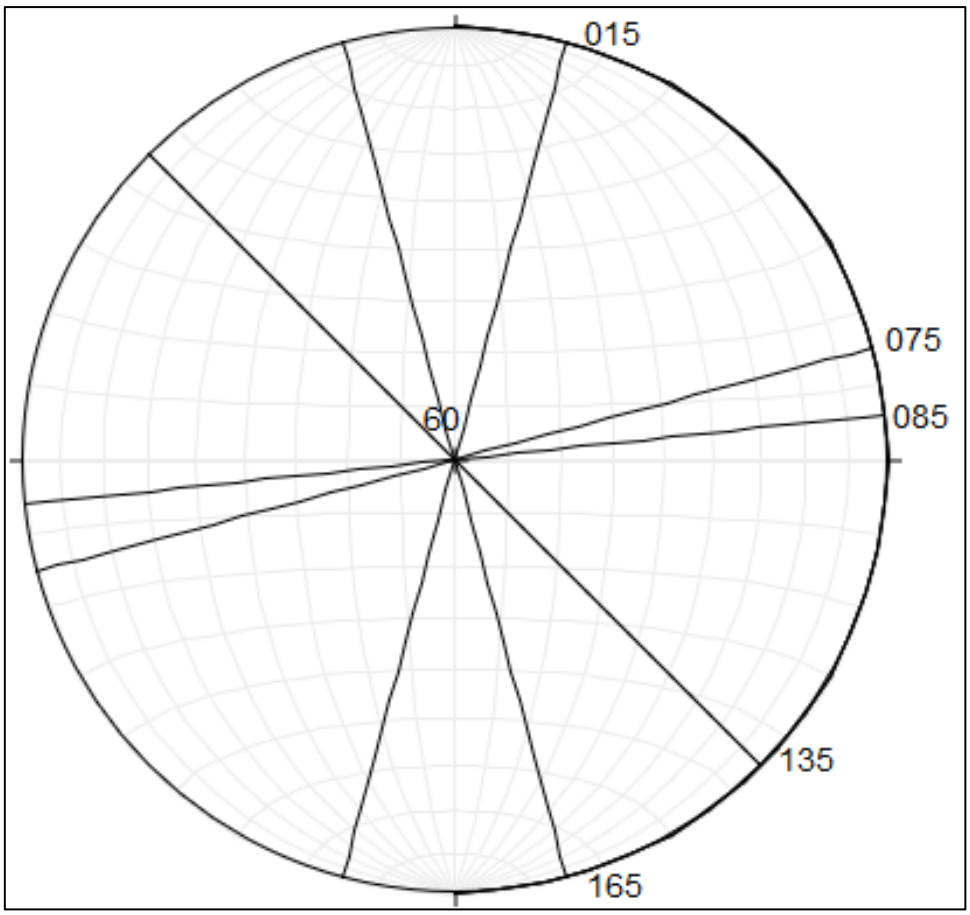


Figure 9. The stereonet representation of the lineaments interpreted in Figures 4, 5, 6, 7 and 8. The 015° and 135° are conjugates of each other, the angle in between the two lineaments is 60° and the acute bisector is orientated at 165°. The 085° orientation is the rose diagram orientation for the E-W lineaments and 075° is the calculated obtuse bisector, which in this case would represent the E-W orientation.

3.1.2. Magnetic lineament interpretation

Fractures are useful for groundwater storage and circulation. They can serve as a groundwater barrier, conduit and sometimes as both (Meyer, 2014). Using the magnetic grid of South Africa supplied by the Council for Geoscience, the study area was found to be dominated by regional structures (Figure 10A and 10B). Figure 11 shows a close up of the study area. The magnetic data were collected between the 1980s and 1990s with flight lines that were orientated in an N-S direction (Stettler *et al*., 1999). These regional structures are highlighted by different signatures on the South African landmass in general, and the study area in particular. Regional structures can be seen intersecting the study area in Figure 10 as example. The north and south Pilanesberg dyke swarms are marked using the two black boxes in Figure 10.

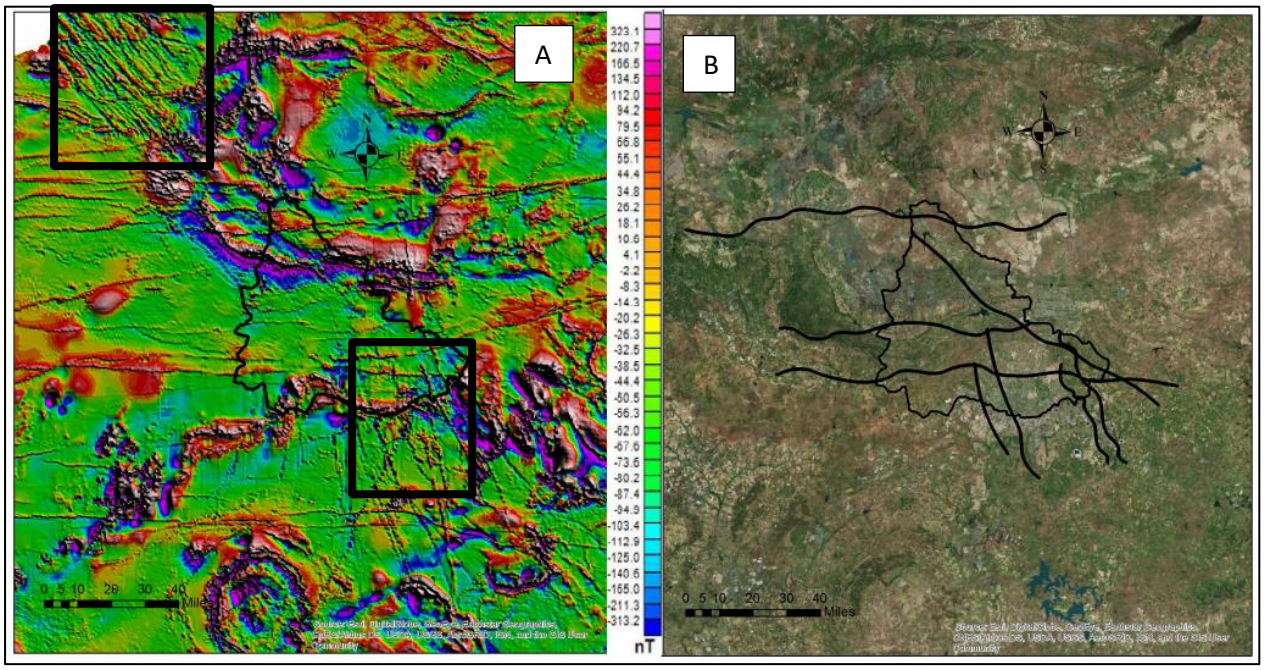


Figure 10. (A) Represents regional aero-magnetics data (the IGRF is not removed). The two black boxes show the Pilanesberg dyke swarms. (B) Represents an example of some of the regional structures passing through the study as black lines trending in an E-W and NW-SE direction. The study area is located in the centre of the image.

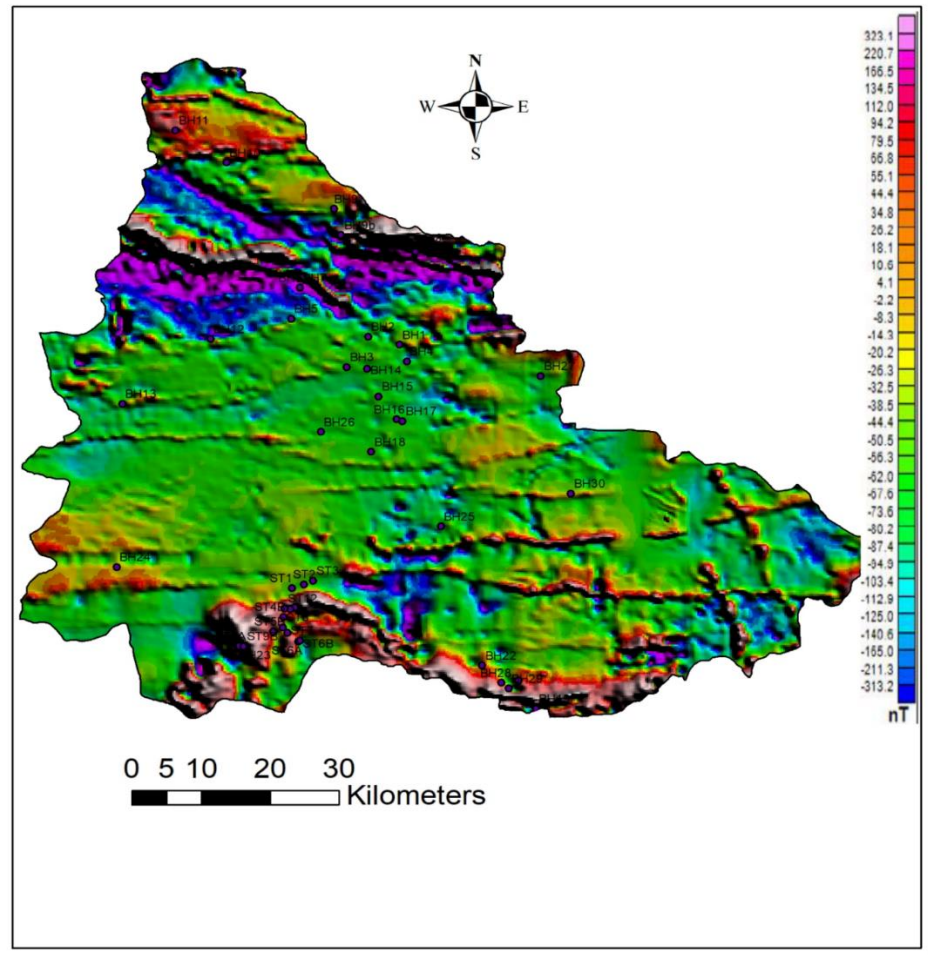


Figure 11. The image represents the total magnetics intensity map of the study area. NW-SE and E-W dykes are represented by high magnetic intensity lines. Low intensity (possible fractures) is represented by low intensity dots arranged in a linear array. The blue/black dots represent the location of some of the boreholes used in this study.

In Figure 12, there are E-W trending structures with high magnetic intensities that are greater than 18.1 nT. Some authors such as Hilliard and McCourt (1995) described E-W striking, south-dipping, thrust sense, shear zones in the granitoids of the Johannesburg Dome. However, for shear zones low magnetic intensities would be expected and based on the magnetics image no significant E-W low magnetic intensity structures are visible, particularly in the Johannesburg Dome rocks. Furthermore, the occurrence of these shear zones were later confirmed by Gibson *et al*. (1999). Gibson *et al.* (1999) associated the shear zones with the Vredefort impact event. The regional extent of these shear zones is not discussed by both Hilliard and McCourt (1995) and Gibson *et al*. (1999), as such further field investigations would need to be made to understand what these specific structures are.

Through ground truthing, the E-W lineaments are represented by the dolerite dykes that trend in an E-W direction. Figure 13 represents a collage of the dyke images; the width of the dykes is about 79.61

meters. The fact that these dykes have fractures could facilitate groundwater recharge, allowing for increased groundwater circulation without any impact of compartmentalisation. Figure 13a displays vertical fracture that occurs on the dykes. Whereas Figure 13b represents a close-up view of a medium grained mafic rock on the fresh surface. All the images were taken facing west, on a stream section, in Kramerville, Sandton. The fracture orientations on the dykes are shown on Figure 10 (n=5 due to the small section) with an average orientation of 119º/83º/E. These are vertical fractures that could have occurred during the cooling stage. These dykes are said to be Post-Karoo aged dykes (~ 182 Ma) (Meyer, 2014). These dykes are believed to be forming compartments by Meyer (2014). However, this argument does not take into account the occurrence of the intense fractures throughout the study area. Although Meyer (2014) focused solely on the dolomites, the author conceded that the dolomites were fractured, however, did not consider that it was a possibility that the fractures could also occurred on the dykes themselves leading to interconnected compartments. This is due to the fact that the lineaments/fractures might result in groundwater from different compartments mixing. It is important to note that the dykes have only been verified in the field in the southern part, as such the occurrence of the dykes close to the Roodekoptjies Dam is based on the similarity in signatures.

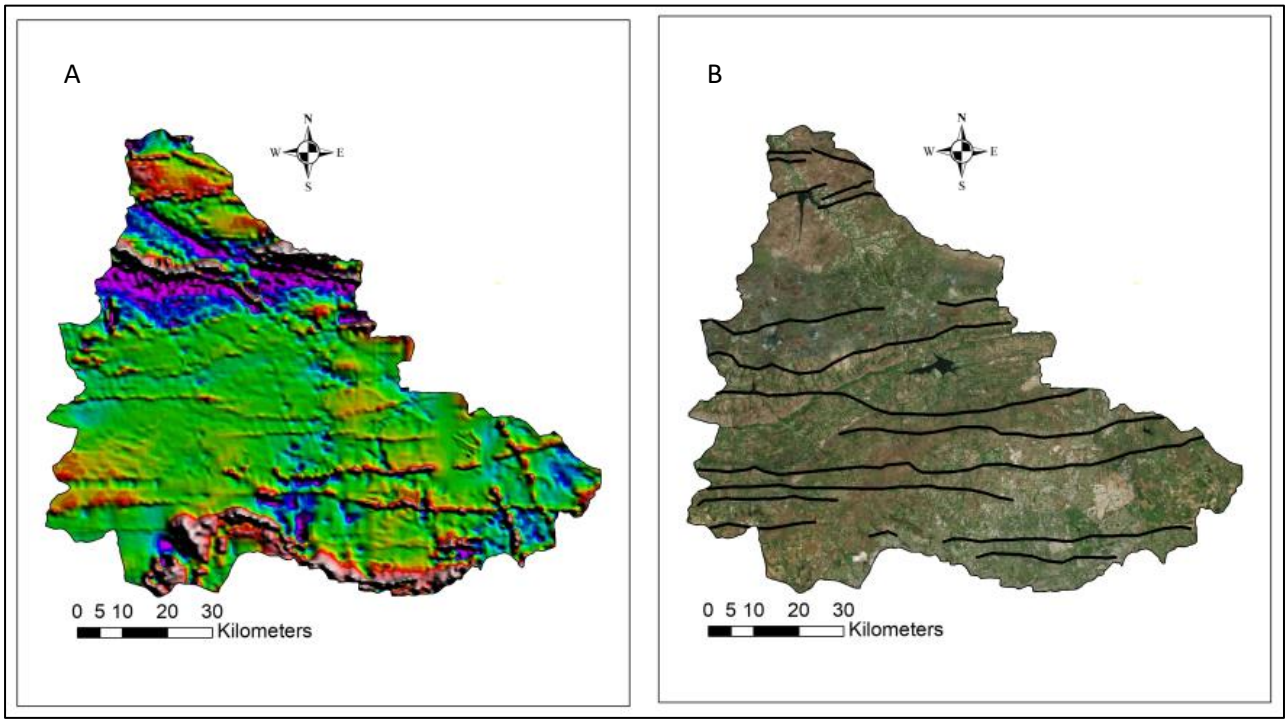


Figure 12. (A) The regional aero-magnetics data showing the magnetic anomalies occurring throughout the study area. (B) represents an example of some of the regional structures passing in the study as black lines trending in an E-W direction.

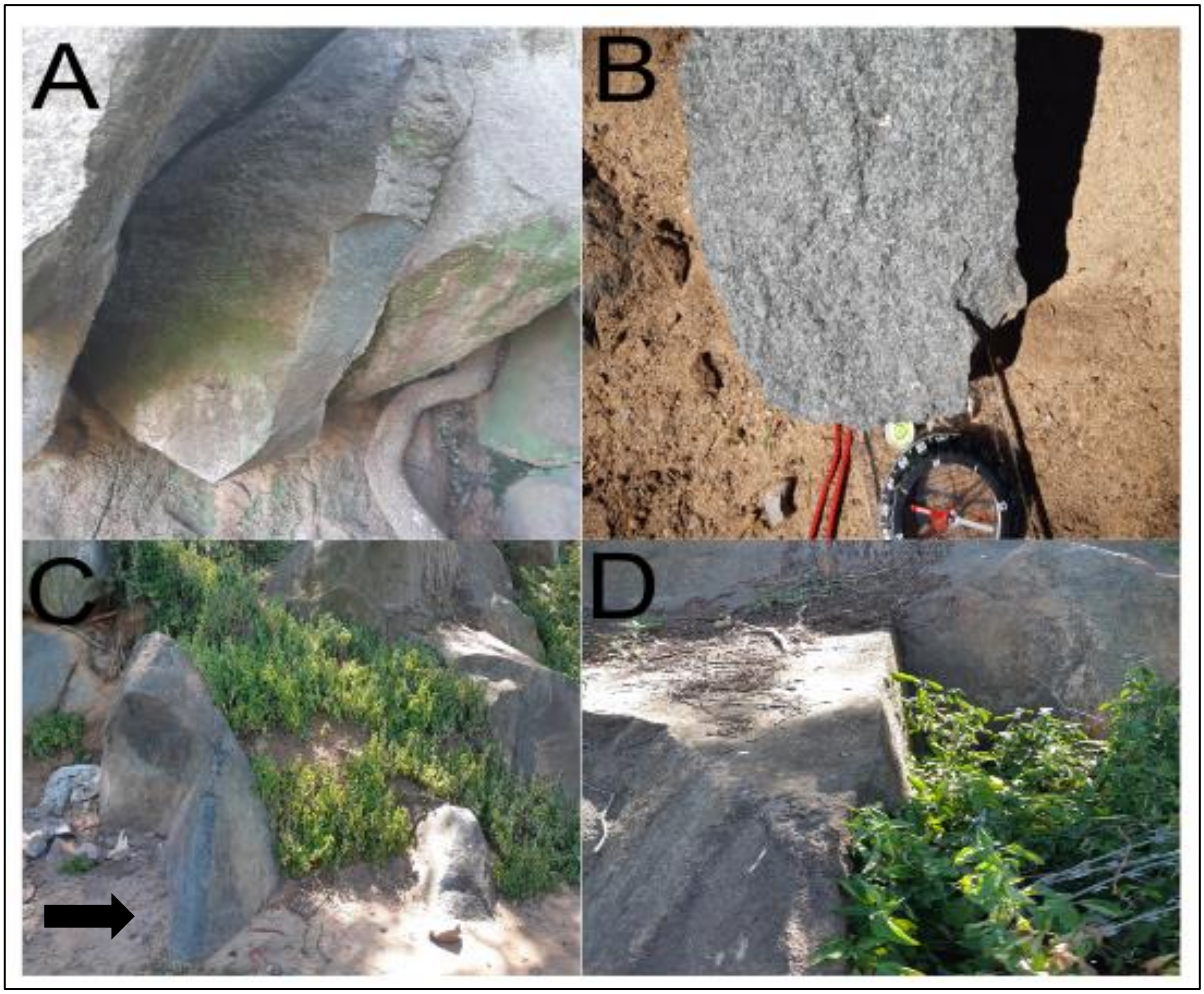


Figure 13. Dolerite dykes. (A) represents the dyke that also has vertical fracture within. (B) is a hand sample of the dyke viewed through a fresh surface. (C and D) are other views of the dyke with the fracture in question. The black arrow on C represents the north for A, C and D.

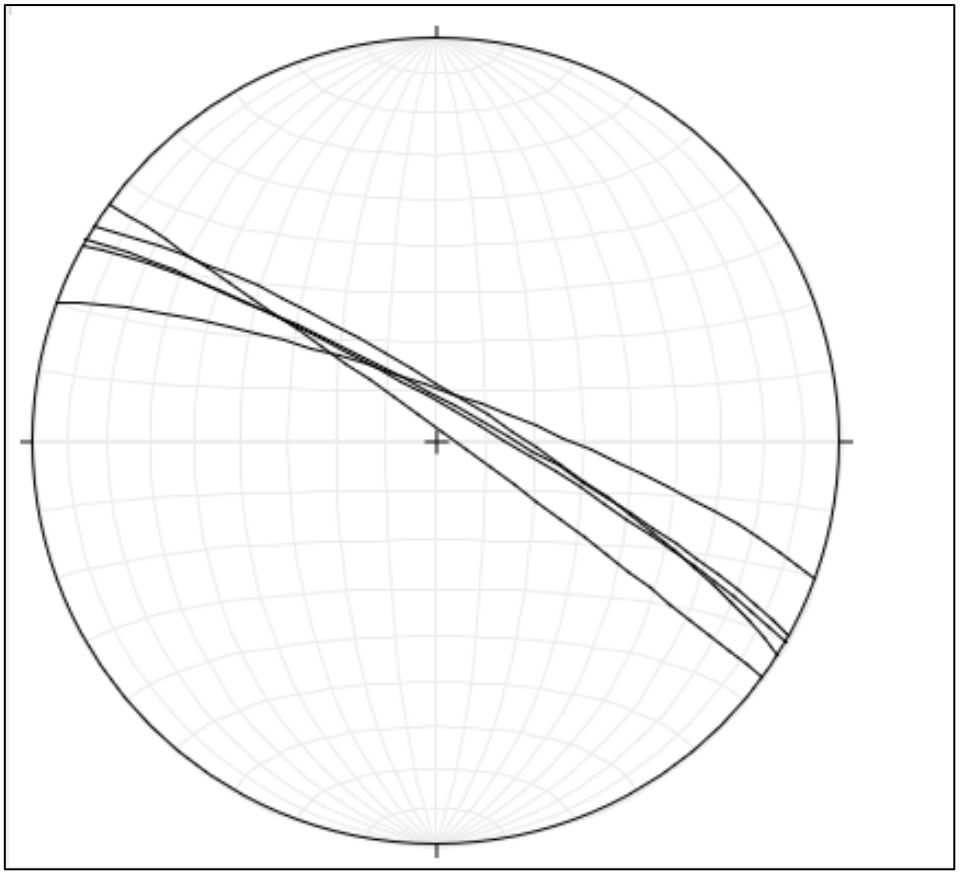


Figure 14. Orientations of fractures found on the E-W trending dolerite dyke, the average orientation is 119º/83º/E.

NW-SE trending lineaments visible in both the magnetic data and LANDSAT imagery are shown in Figure 15. In the magnetic data, they show up as negative anomalies with average magnetic intensities of -213 nT and in the LANDSAT imagery as streams that trend in a NW-SE direction. The low magnetic intensity is a trait associated with fractures and faults. One of these fractures displaces the east and west cliffs at the Melville Koppies Nature Reserve (located at -26.167569; 28.009917). Some of the fractures were described by Nyebelele (2017), where the average fracture orientation is 139º/88º/W. These NW-SE trending fractures along with the shear zone described by Hilliard and McCourt (1995) played a major role in the occurrence of the Albert's Farm spring. All the measured fracture orientations were plotted on a stereonet using the Allmandinger software by Nyebelele (2017) (Figure 16). Although the streams do show some deviation, the general trend where these structures are highlighted is in a north westerly direction. These fractures play a major role in the circulation of groundwater in the south of the Hartbeespoort Dam.

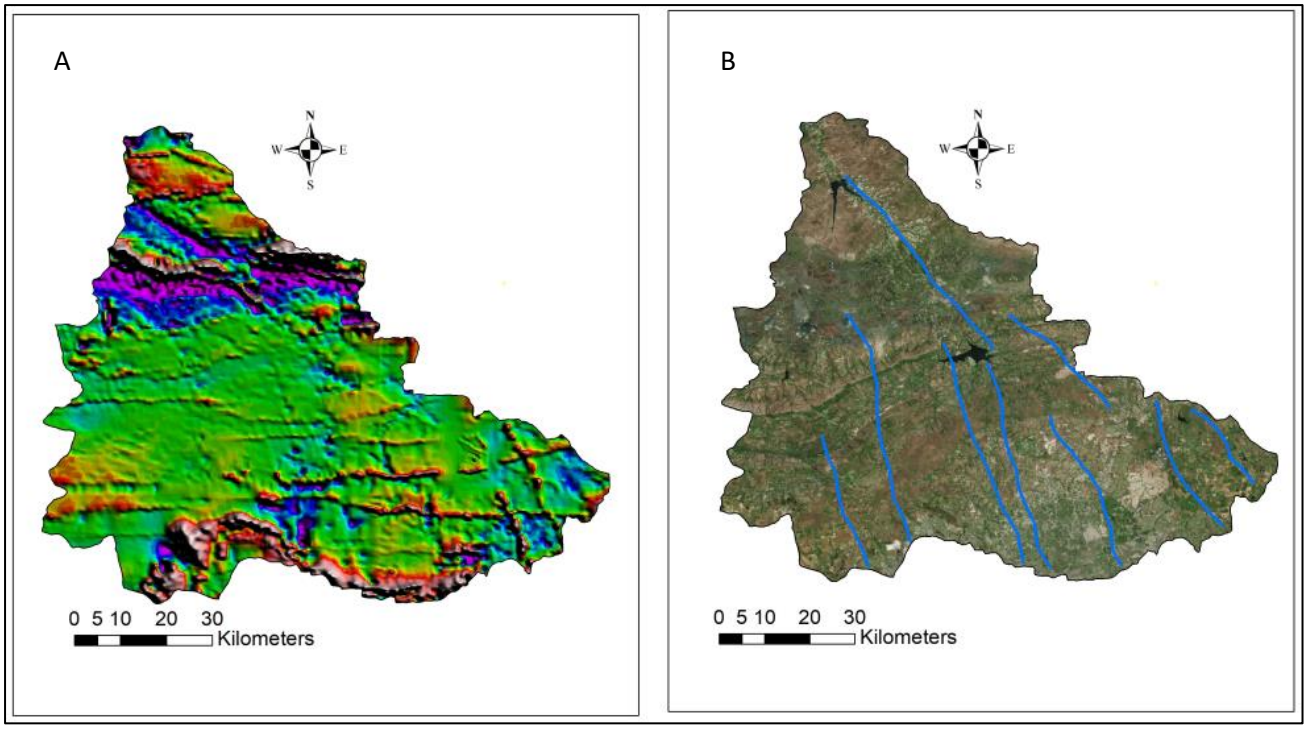


Figure 15.(A) The regional aero-magnetics data showing the magnetic anomalies occurring throughout the study area. (B) Represents an example of some of the regional structures passing in the study as blue lines trending in an NW-SE direction with low magnetic anomalies.

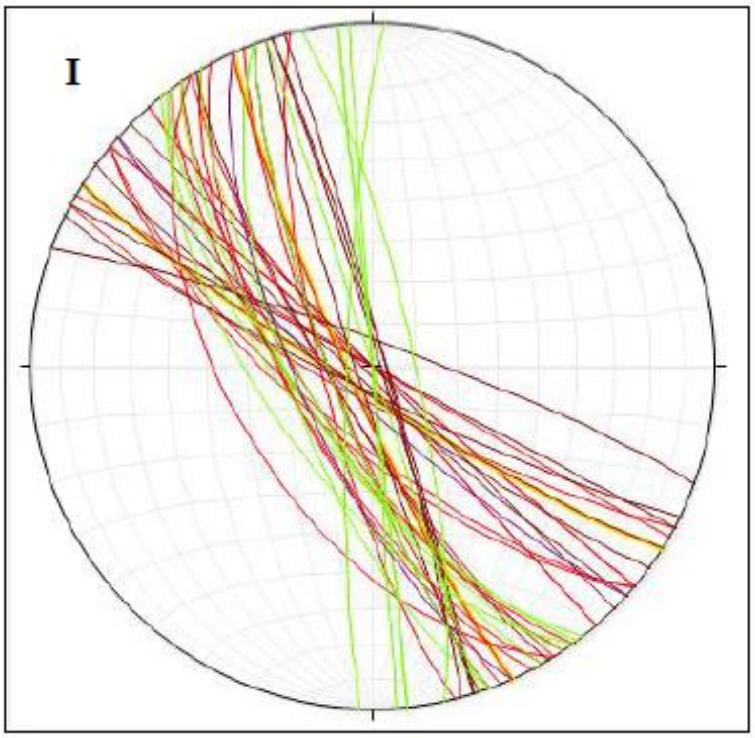


Figure 16. Fracture orientations measured in the Albert's Farm (near Melville Koppies) the colours signify the fold limbs in which the lineaments were measured by Nyebelele (2017) and are not significant for this study.

The Pilanesberg dykes (Figure 17) are literature documented structures trending in a NW-SE direction, following the lineaments in Figure 6 which are also trending in the same direction. Figure 17B has 3 lineaments annotated based on figure 17A anomalies (on the east of the image). The two smaller lineaments on the west are not visible on the magnetics data, however, were mapped by Lee (2015) and their orientations have been presented in Table 1. The northern dyke is a grey syenite dyke and south to it on the right is a red syenite dyke. The general composition of the dykes is tholeiitic with dolerite syenite variations (Emerman, 1991; Cawthorn *et al.*, 2012). In the event that the IGRF from the magnetic data in Figures 4 and 5 was removed, the dykes show a strong negative anomaly of about-352 nT (Lee *et al*., 2013; Lee, 2015). The Pilanesberg Dykes are important in the occurrence of the Fountains Springs, near Pretoria, forming barriers that subsequently result in the occurrence of the springs (Naidoo, 2014; Meyer, 2014).

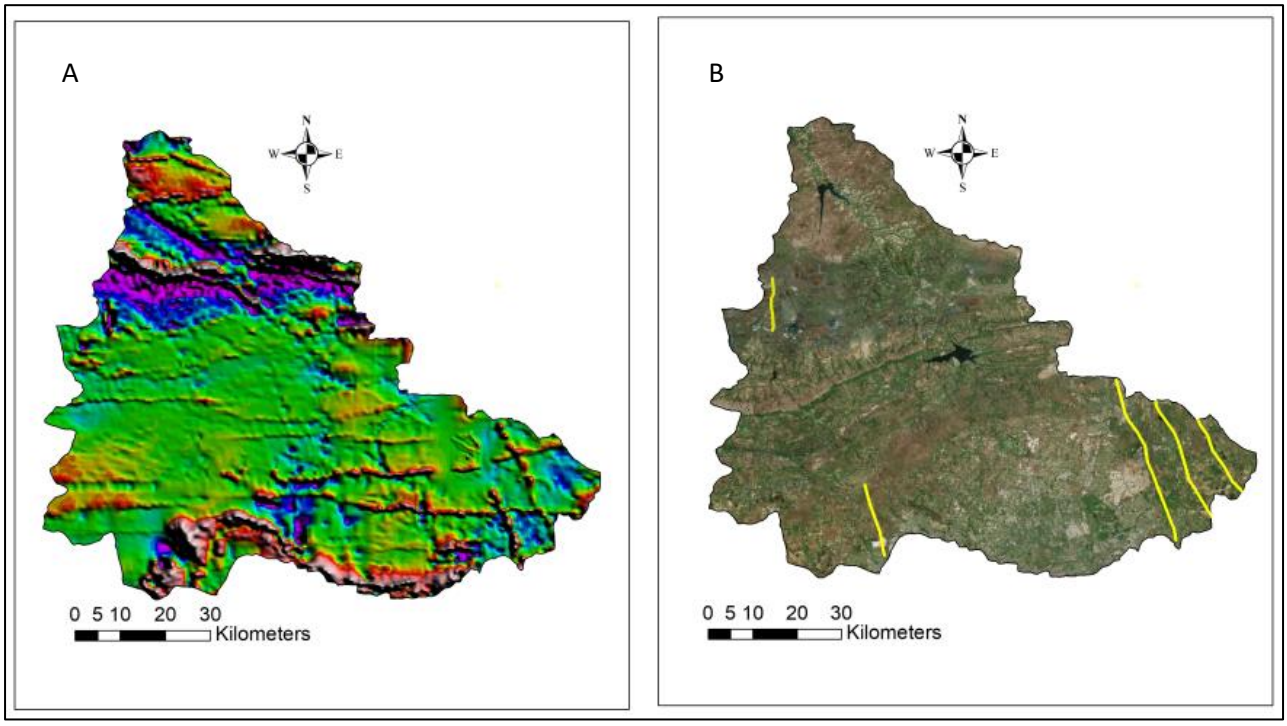


Figure 17. (A) The regional aero-magnetics data showing the magnetic anomalies occurring throughout the study area. (B) The Pilanesberg dykes are interpreted as yellow, showing their relative location based on borehole data and literature.

Table 1: The Pilanesberg dyke orientations and the locations.

ID	Lat	Long	Orientation
Dyke 1	-25.9004	27.45178	285º/80ºN
Dyke 2	-25.9005	27.45183	196º/65ºW
Dyke 3	-25.8861	27.44968	266º/5ºNW
Dyke 4	-25.886	27.45776	203º/52ºW
Dyke 5	-25.8851	27.45727	023º/5ºE

Field measurements of fracture orientations in the study area were made around the Roodekoppies Dam. Due to lack of permission to access some of the farms the fracture measurements were limited to 8 n values. One of the conjugate fractures with average orientations of 163º/67ºNE (Figure 18), this is consistent with the rose diagram orientations and the measurements made by Nyebelele (2017) suggesting that the bulk of the study area is characterised by similar lineament relationships. The 083º/88ºNNW (Figure 19) is consistent with the E-W trending lineament, also consistent with the rose diagram orientations. The fractures in Figure 18 are the most dominant and are interpreted as part of lineaments in Figure 5 and 6. These fractures could be very important for the groundwater circulation, groundwater recharge or discharge on the crystalline rocks of the Bushveld Igneous Complex. The streams that form on these dominant fractures were dry because it was during winter, as such they are non-perennial or possibly losing streams.

The NW-SE trending fractures are important for groundwater circulation and ensuring a sustained spring discharge in the Albert's Farm spring. An average orientation for the Albert's Farm spring fractures, related to the NW-SE lineaments orientation is 139º/88ºW. These fractures could be a response to regional stresses that affected the Kaapvaal Craton, such as the emplacement of the Bushveld Igneous Complex and or the Vredefort impact structure. The fractures responsible for the occurrence of the Albert's Farm spring and sustained discharge for the spring, are possibly connected and have a dense network that allows for significant amounts of groundwater recharging from different locations to reach the spring.



Figure 18. The 083º/88ºNE extensional fracture in the vicinity of the Roodekoppies Dam found on highly weathered Lebowa Granites. The white lines are an example of the fractures. The surface on the image is highly weathered, however, the fresh surface shows a pink to pale pink coarse-grained rock (granitic). The compass -clinometer represents the scale, the north arrow has deviated due to the uneven rock where the compass-clinometer is placed.



Figure 19. The 163º /67ºNE conjugate fracture in the vicinity of the Roodekoppies Dam found on the highly weathered Lebowa Granites. The surface on the image is highly weathered, however, the fresh surface shows a pink to pale pink coarse-grained rock (granitic). The compass-clinometer represents the scale; the north arrow has deviated due to the uneven rock where the compass-clinometer is placed.

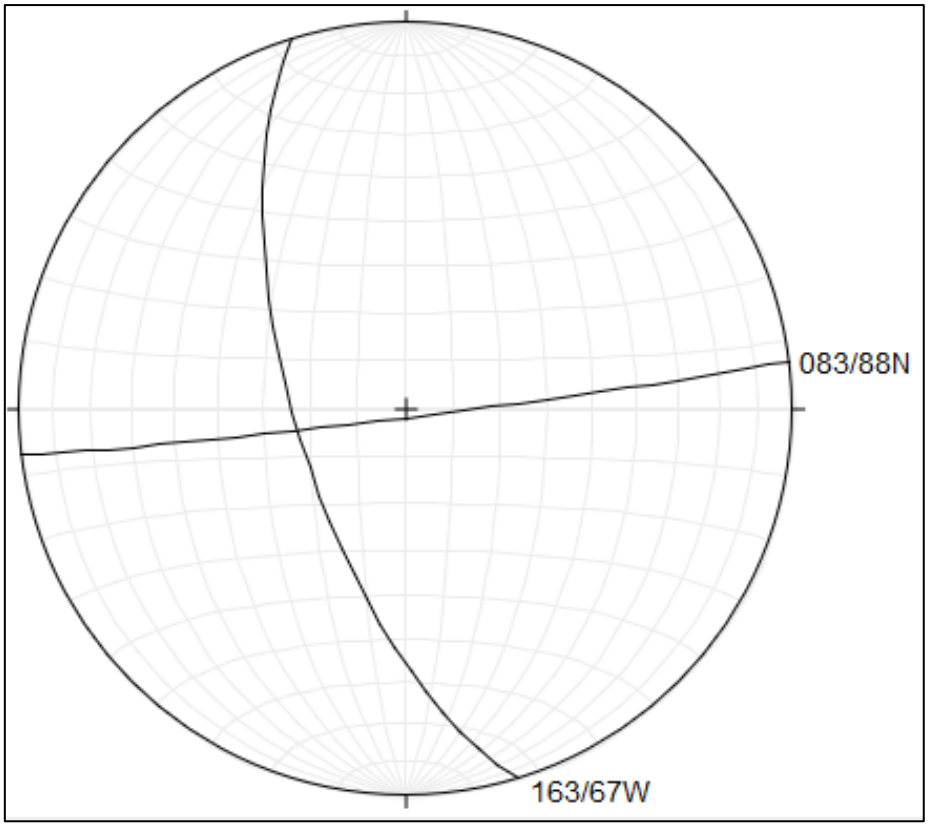


Figure 20. Average orientations of the fractures found in the Roodekoppies area, the stereonet was constructed using 8 n values.

The geological mapping conducted through remote sensing method (satellite image interpretation and magnetics) revealed three main lineament orientations. These lineaments are interpreted as NW-SE, NNE-SSW and E-W trending. The NW-SE and NNE-SSW lineaments form conjugates of each other with the E-W trending lineaments being extensional joints. The lineaments are associated with dyke occurrences in the form of the Pilanesberg dyke swarms and the unnamed E-W trending dykes. The fractures suggest that the possibility of compartmentalisation of groundwater might not be possible, due to the connections of different parts of the study areas groundwater made possible by fractures.

3.2. Geological cross-sections

Geological cross-sections are important in trying to conceptualise the geology of the study area. Figure 21 has the N-S section (slightly NW-SE but simplified to N-S), which passes perpendicular to the E-W trending lineaments. The possible compartments are numbered 1-7. Figure 22 is an E-W section of the study area, it has faults/fractures that adopted from the magnetics data. The NW-SE trending lineaments form valleys and allow for streams to flow in preferential orientations matching the fracture orientations. The average orientation of the fractures is 139º/88ºW. These fractures are important for

groundwater circulation (Nyebelele, 2017). The occurrence of fractures in the study area might result in the mixing of groundwater from different compartments. As such, if compartmentalisation occurred, a lot of mixing would not have to be expected, unless interconnected by fractures. The dykes would be important in creating groundwater barriers, however, the fractures would cut across the dykes allowing for groundwater movement. The fractures are also important for the recharge especially on the quartzite ridges, where water can easily seep and join the groundwater system. The fractures are also important for the discharge as already mentioned where the Albert's Farm spring (hosted by quartzites) is fracture controlled. The geological contacts can also play a role in the seepage and recharge of groundwater.

According to Barnard (2000) and Abiye et al. (2011), the Witwatersrand Supergroup rocks have a borehole yield of between 0.5-2 l/s. The Johannesburg Dome has a yield of 0.5-2 l/s and is classified as an intergranular and fractured aquifer type. The Malmani dolomites have a yield of > 5 l/s (representing the highest productivity). This high yield can be attributed to the occurrence of faults and cavities, which are good recharge zones (Abiye *et al*., 2011). The rest of the rocks post the Malmani dolomites have a yield of 0.5-2 l/s, with exceptions of some rocks found near Crocodile River.

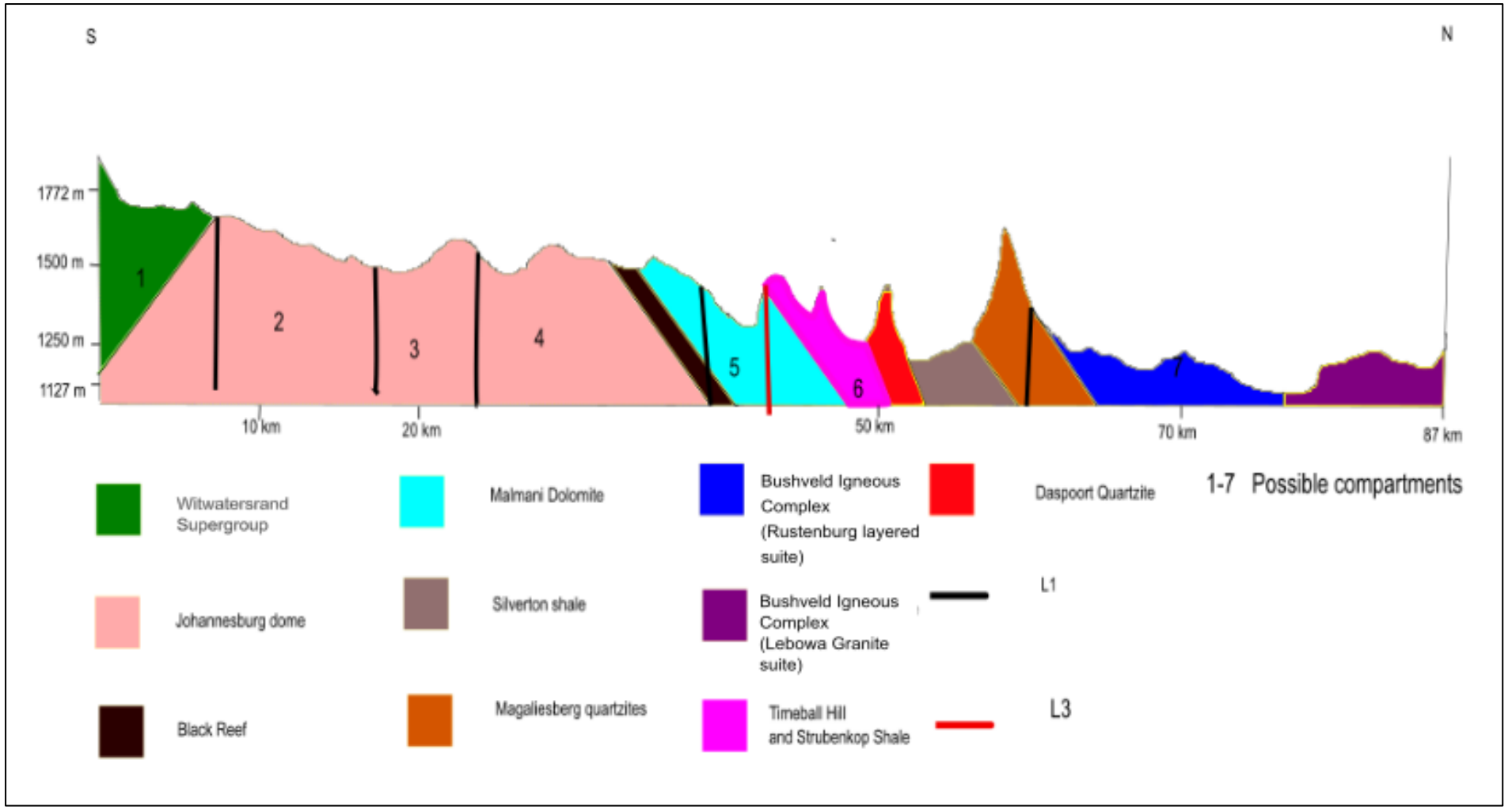


Figure 21. Simplified geological section of the UCRB, trending in the N-S direction. The possible compartments are numbered 1-7. The high points are associated with quartzites and other competent rock types and are possible recharge points.

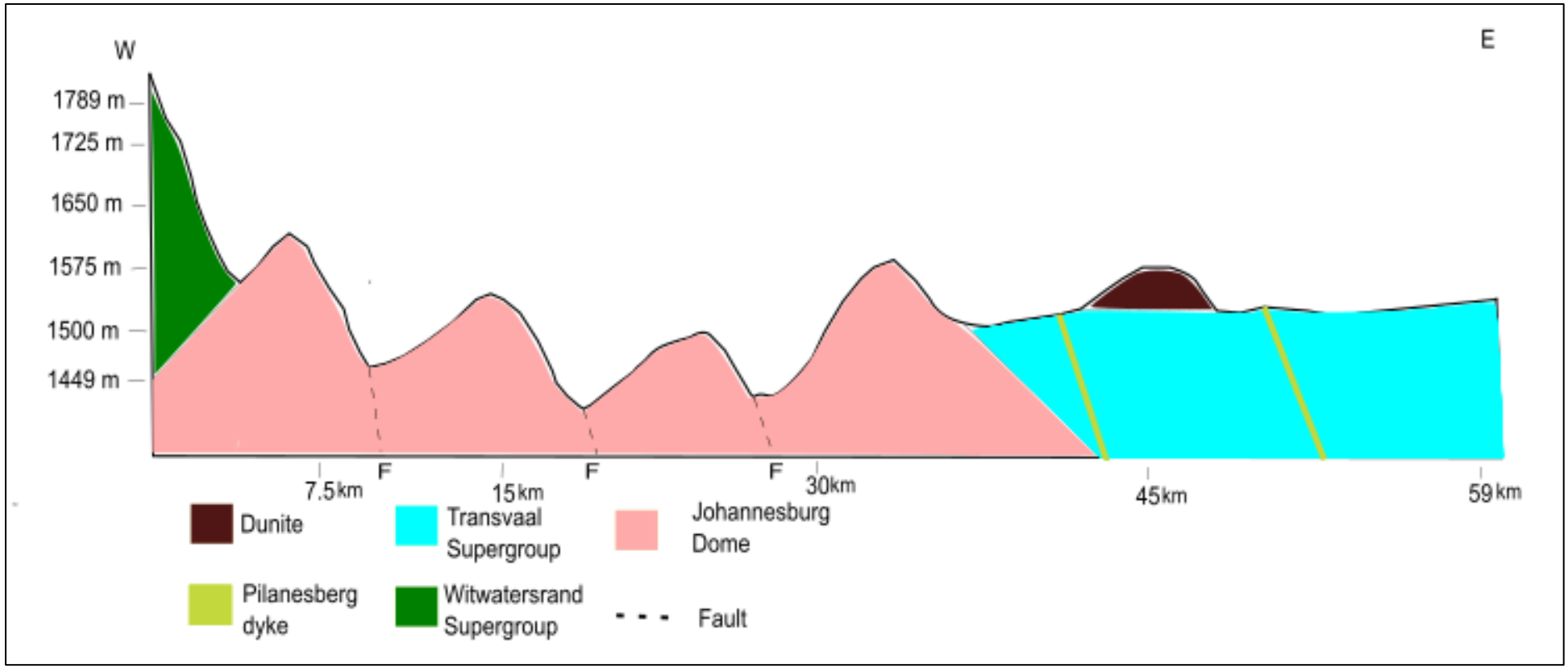


Figure 22. Simplified geological section orientated in the E-W direction. The valleys are important points as far where the fractures and streams are located. The Pilanesberg dykes are marked here and can possibly form a compartment.

3.3. Borehole log analysis

Borehole logs are important for providing information on the subsurface condition. Three parts of the study area (Figure 3) with BH's that have lithological information were selected, and the selected BH's are shown in Figure 23, 24 and 25. The BH spatial distribution is presented in figure 3. Figure 23 represents borehole logs from the eastern segment. Borehole ID's are 37808, 37329, 37328 and 38051, from left to right. Their respective distance apart is 8.6 km between 37808 and 37329, 2.23 km between 37329 and 37328, and 3.42 km between 37328 and 38051. The total length of the section is 14.25 km. The blue line denotes the average static water level from the time of BH completion to the last most recent measurement (which varies from BH to BH). It is important to note that in fractured aquifers the piezometric water level varies significantly depending on the fracture network. BH 37808 is separated from BH's 37329, 37328 and 38051 by the two Pilanesberg dykes presented in Figure 17. The water level is higher in 37808 and 37329 compared to the water levels in 37328 and 38051. The abrupt drop in water level between 37329 and 37328 can be associated with the occurrence of the Pilanesberg dyke that passes in between the two BH's. It is unclear, based on the limited information available as to whether the BH's that have dykes (37808) have higher water levels due to the dyke occurrence or not. The dolomites presented in Figure 23 are classed as C5 BH by Barnard (2000), this represents groundwater yield of >5 l/s.

Figure 24 has more BH's that are still in the western segment of the study area. The ID's are 37997, 37330 and 35730, from left to right. The respective distance between 37797 and 37380 is 4.21 km and between 37350 and 35730 is 6.71 km. The total distance covered by the section is 10.92 km. The water level change observed between 37797 and 37330 can be associated with the fact that 37997 occurs directly on the Pilanesberg dyke, whereas 37330 seems to be occurring on a discontinuity formed by the NW-SE fracture.

The boreholes in the western segment have on average a deeper static water level of 65.62 mbgl. The eastern segment has an average static water level of 38.4 mbgl. The geology is fairly similar, however, rocks such as quartzites and shales that were not found in the east can be found here.

The western segment (Figure 25) BH's highlighted more lineaments that were not picked up during the visual interpretation. These fractures are and can be associated with the NW-SE trending lineaments from Figure 6 and 15. BH's 36600, 36358 and 36359 are on the left side of the lineament whereas 36339, 36322 and 37794 are on the right. The total length of the section is 21.68 km. The BH's on the right of the lineament show higher groundwater levels than those on the left. The BH logs plotted here are in no account representative of the entire study area. However, we can draw to a conclusion that in both east and west segments of the study area, ground water levels are shallow and are controlled by the occurrence of lineaments. The crystalline nature of the UCRB rocks result in groundwater controlled

by secondary features such as fractures and weathering. Bushveld Igneous Complex BH's that were sourced from the DWS lacked lithological data, however, it would be expected of these BH's to have similar features as the BH's in Figures 15, 16 and 17.

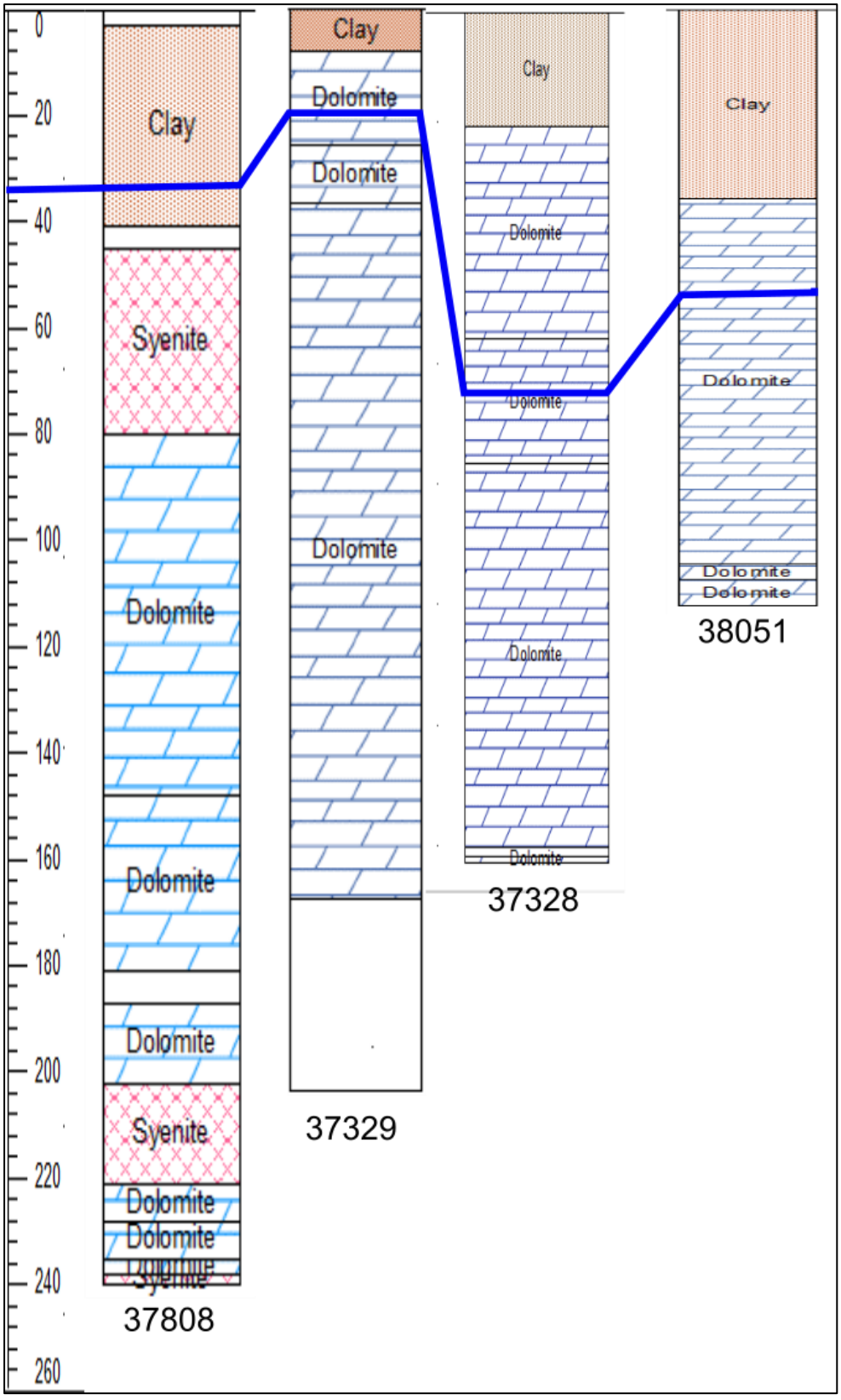


Figure 23. Borehole logs of the South West of the study area selected randomly, superimposed with the average water level in each borehole. From left to right the BH ID's are 37328, 37329,37808 and 38051.

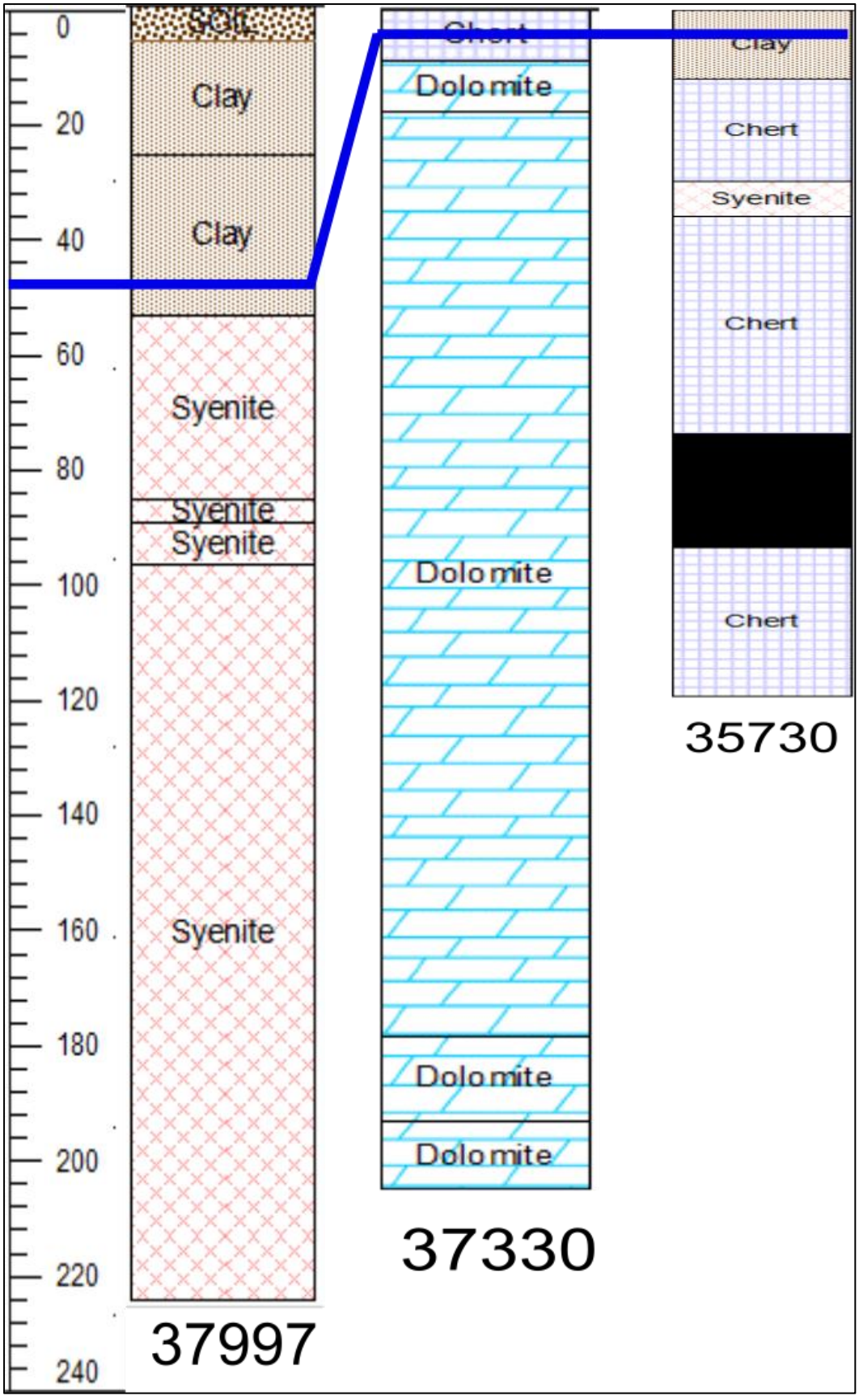


Figure 24. Borehole logs from the West of the study area. The blue line denotes the average water level in each borehole. BH 37997 has syenite which is part of the Pilanesberg dyke swarm.

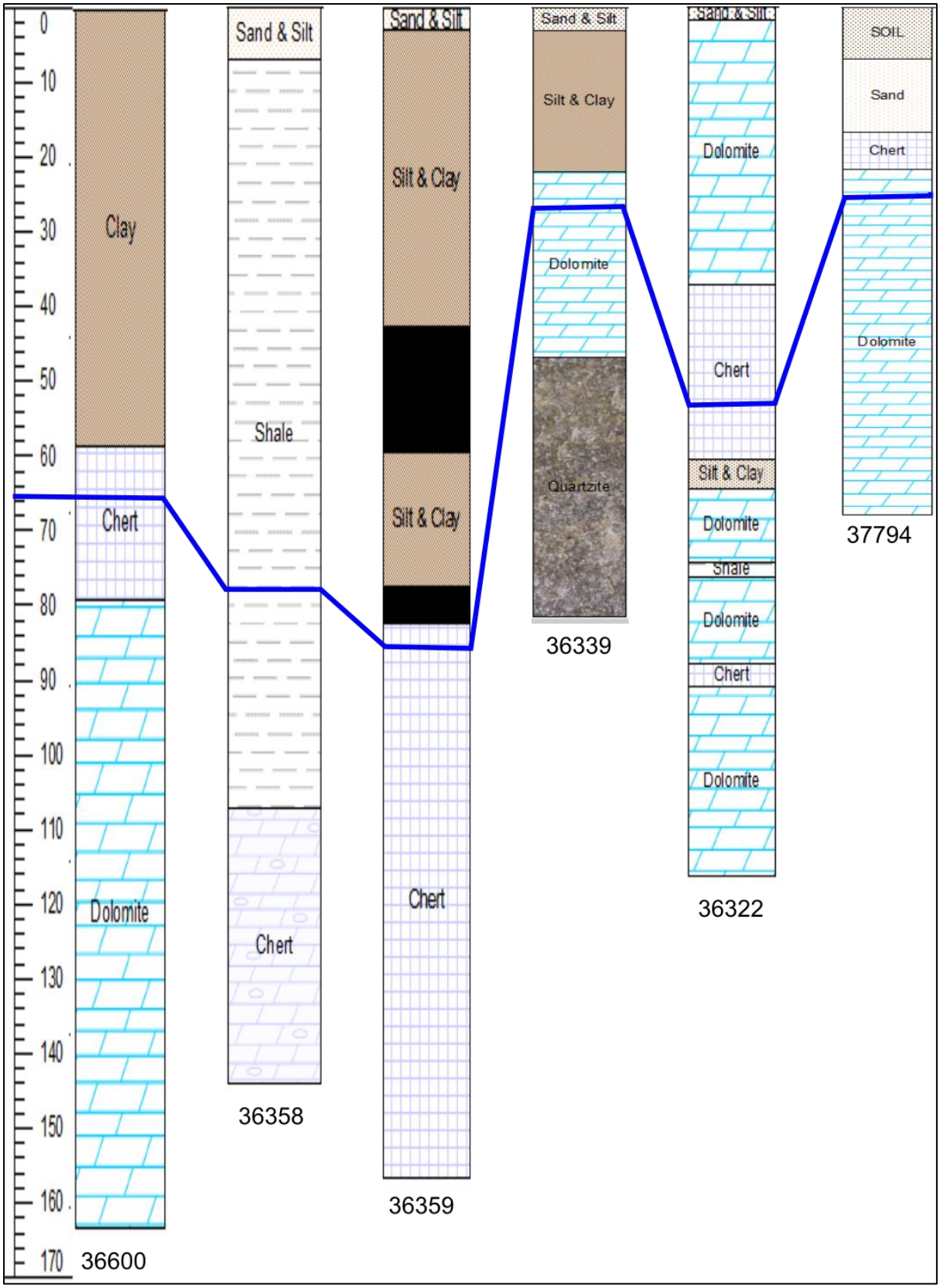


Figure 25. Borehole logs found on the eastern side of the study area. The blue line denotes the water level in each borehole.

3.4. Drainage Pattern

The drainage patterns of any region are affected by the lithology and structures (Howard, 1967; Manjoro, 2015) (Figure 2). Drainage analysis is also an important tool in trying to understand the structural fingerprints of an area using aerial photograph (Howard, 1967). The analysis of drainage density can also assist in the understanding of the permeability of an area. Since the geological setting is represented by crystalline rocks, the visible pattern is dominantly dendritic with overall major stream directions of NW-SE stream direction (Figure 26). However, the tributaries of the main streams tend to flow in the same direction as along the NNE trending fractures. The dendritic drainage pattern can be associated with low permeability rocks (Howard, 1967). In two regions of the study area, a trellis pattern has been detected. One site is located in the Bushveld Igneous Complex on the Lebowa Granite suite (Figure 27A and 27B). Figure 27A displays streams flowing to the NW-SE direction, which is associated with the conjugate fracture in Figures 5, 6 and 9. The other stream direction in Figure 27B represents the NE trending fracture shown in Figure 5. The other lineament-controlled drainage pattern is on the Silverton shales of the Pretoria group, where the overall stream direction changes from N-S to a more E-W direction (Figure 28). The trellis pattern located on the left limb of the Roodekoppies Dam in the North West (Figure 27A and 27B) is controlled by the conjugate structures as shown in Figures 4, 5, 6 and 7. The trellis pattern is lithologically controlled. This is based on the fact that the shales are bounded to the N and S by much harder rocks in the form of quartzites, which form ridges that are impermeable. This dictates the streams preferably to flow towards the Hartbeespoort Dam, in order to continue flowing north. In essence the study areas' drainage is controlled by the lithology and structures. The dendritic pattern is due to the lithology; however, the preferred flow orientation is caused by the lineaments. The trellis patterns also suggest both lithological and structural controls. The dolomites are estimated to be within the two black lines (Figure 26), the streams on the eastern side of the study area are dense whereas on the west they are less dense. This difference in density on dolomites has implications on the porosity. The streams on the left could be losing and the east could be gaining.

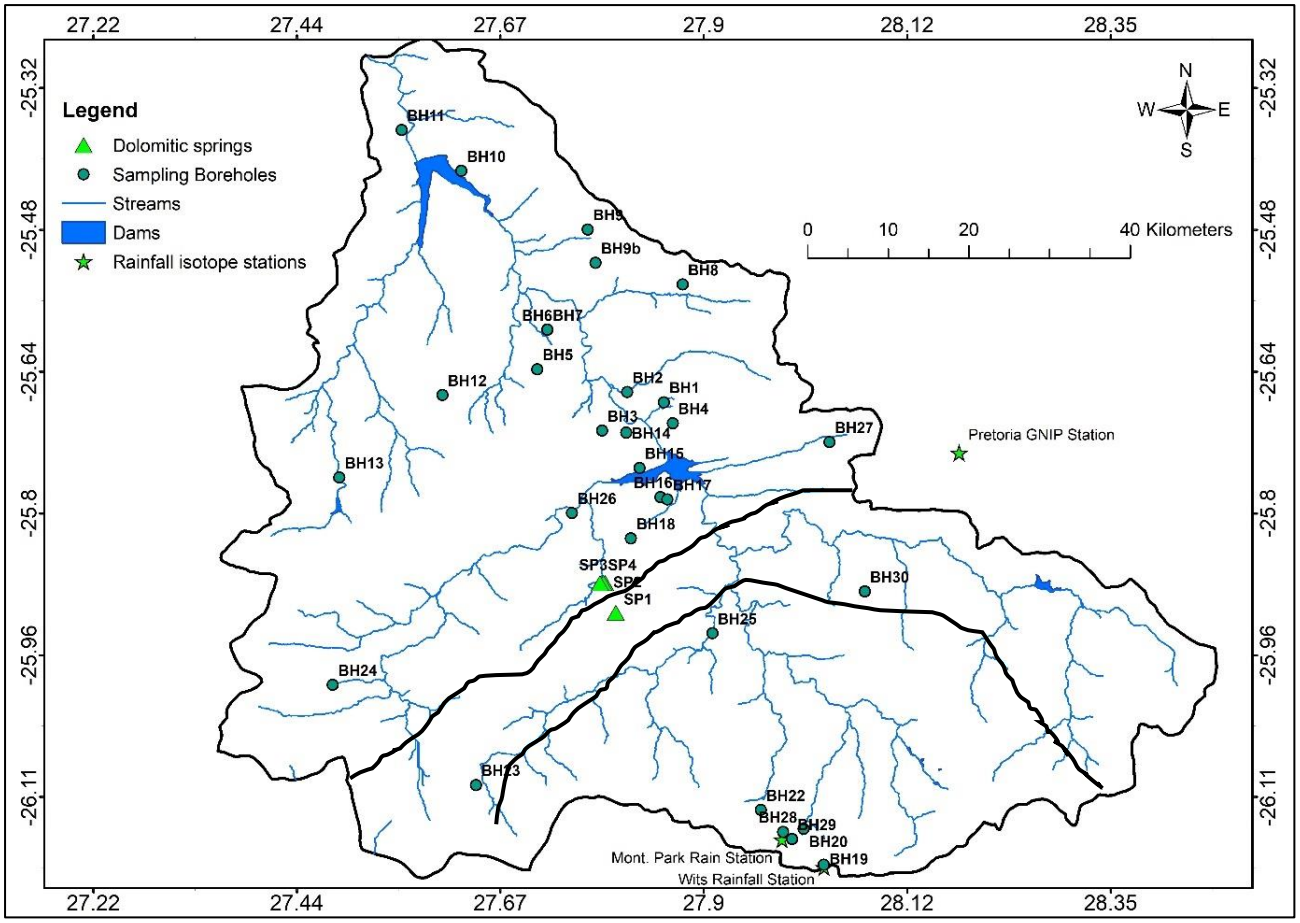


Figure 26. The drainage of the UCRB, with the sampling points superimposed. The dendritic pattern dominates the entire study area. The black lines outline the limits of the dolomite units.

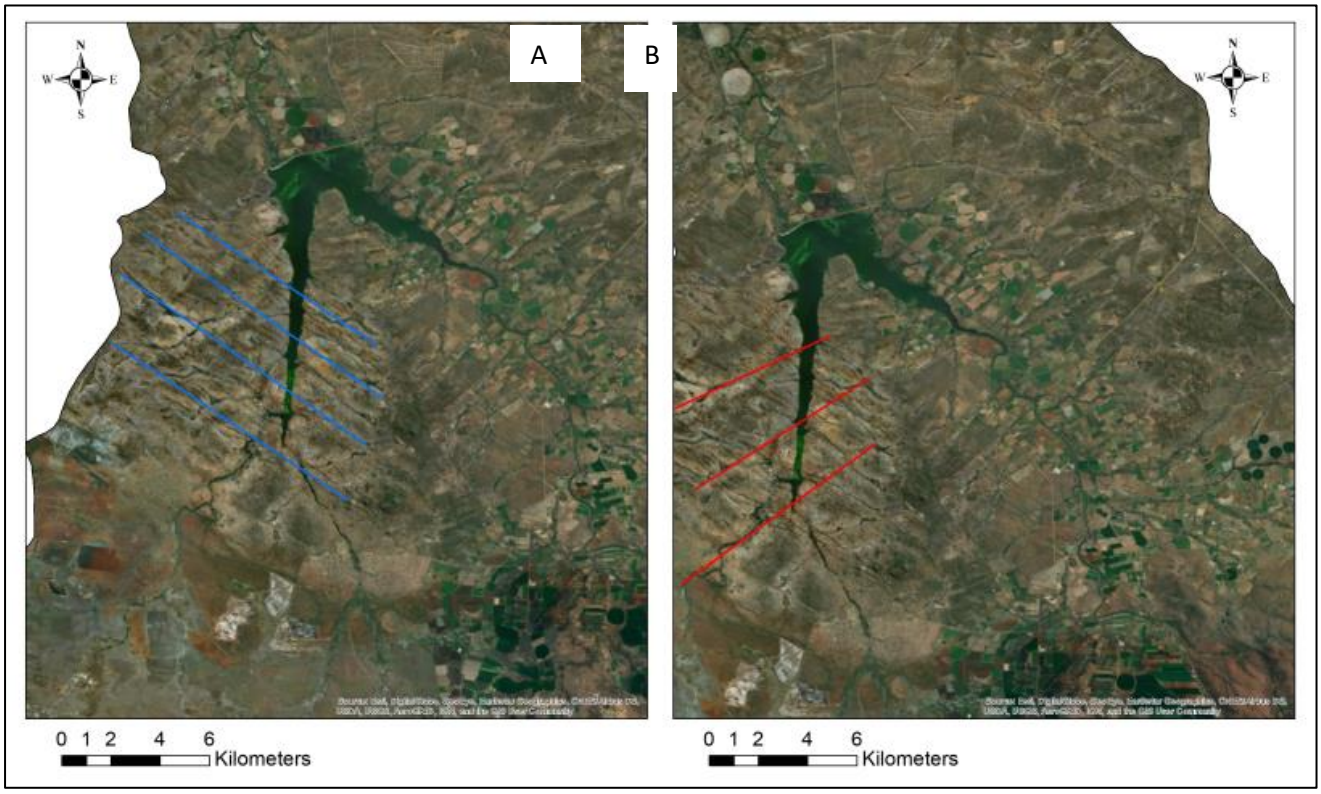


Figure 27. (A) The streams in the Lebowa Granites flowing in a NW-SE direction. (B) The streams in the Lebowa Granites flowing in the NE-SW direction. These streams are controlled by the two fracture directions.

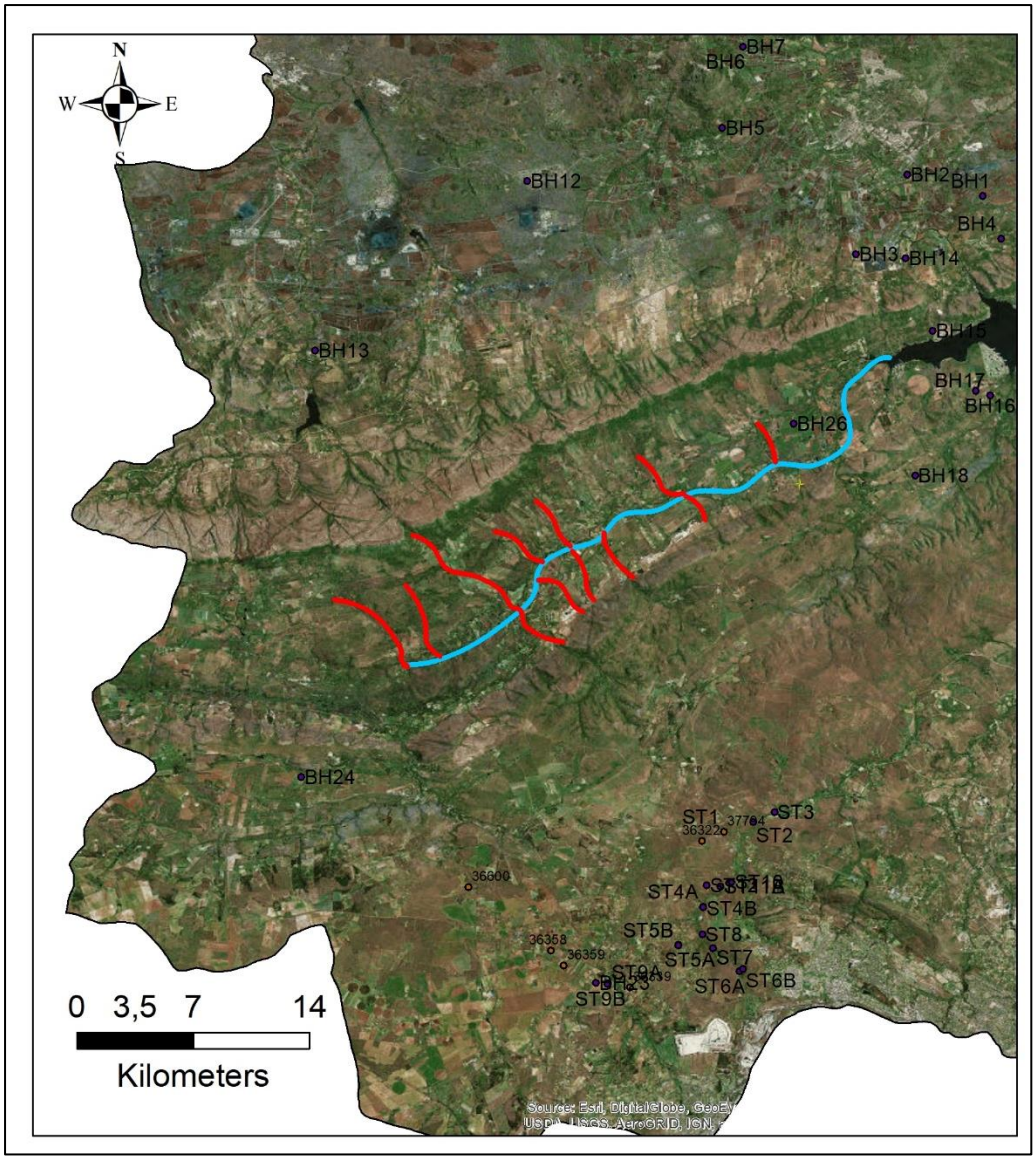


Figure 28. The trellis pattern on the Silverton shales is highlighted by the NW-SE trending red lines and the NE-SW trending blue line. This is also consistent with the lineament direction.

3.5. Spring recession curves

A spring discharge hydrograph is essentially a summary of numerous processes that govern the transformation of precipitation and other water inputs in the spring drainage area into a single output at the spring (Kreissic and Bonacci, 2010). Karsts and fractured aquifers react in a similar manner to water inputs. The analysis of the recession limb can give an insight into aquifer traits such as porosity and storage capacities, transmissivity, specific yield and the catchment geometry (Korkmaz, 1990; Amit *et al.*, 2002; Kreissic and Bonacci, 2010). The most commonly used equation is the Maillet equation (2) below adapted from Maillet (1905) in Civita (2008). Equation 2 can also be expressed as equation 3 to calculate the recession coefficient:

$$\boldsymbol{Qt = Q0e^{-\alpha(t-t0)}}\textbf{.....(2)}$$

Where: Q_t: Discharge at a specified time after recession;

Q_0: Discharge at the start of recession;

t: time since recession began

α: recession coefficient

The Maillet equation can also be expressed as equation (3) below:

$$\boldsymbol{\alpha = \ln(\frac{Qo}{Qt})/t}\textbf{.....(3)}$$

The locations and possible catchment areas for the four springs are plotted in Figure 29. The catchments were outlined using a combination of river head locations and elevation. The spring with the highest catchment is the Maloney's-Eye at about 246.23 km^2, followed by 187.47 km^2, 29.16 km^2 and 17.78 km^2 of the Nouklip-Eye, Albert's Farm spring and the Elandsfontein-Eye, respectively. The catchment size plays a role on the amount of discharge from the spring itself. The discharge amount follows the size of the catchment for these springs, and that is, the larger the catchment, the higher the discharge. The data available for the springs spans to over 100 years for the dolomitic springs and just over two years for the Albert's Farm spring, as such, included in appendix B. Meyer (2014) estimated the catchment for the Maloney'-Eye to be around 177 km^2. Where the shales would act as groundwater retardants. This would be true if the groundwater was not dominated by fractures.

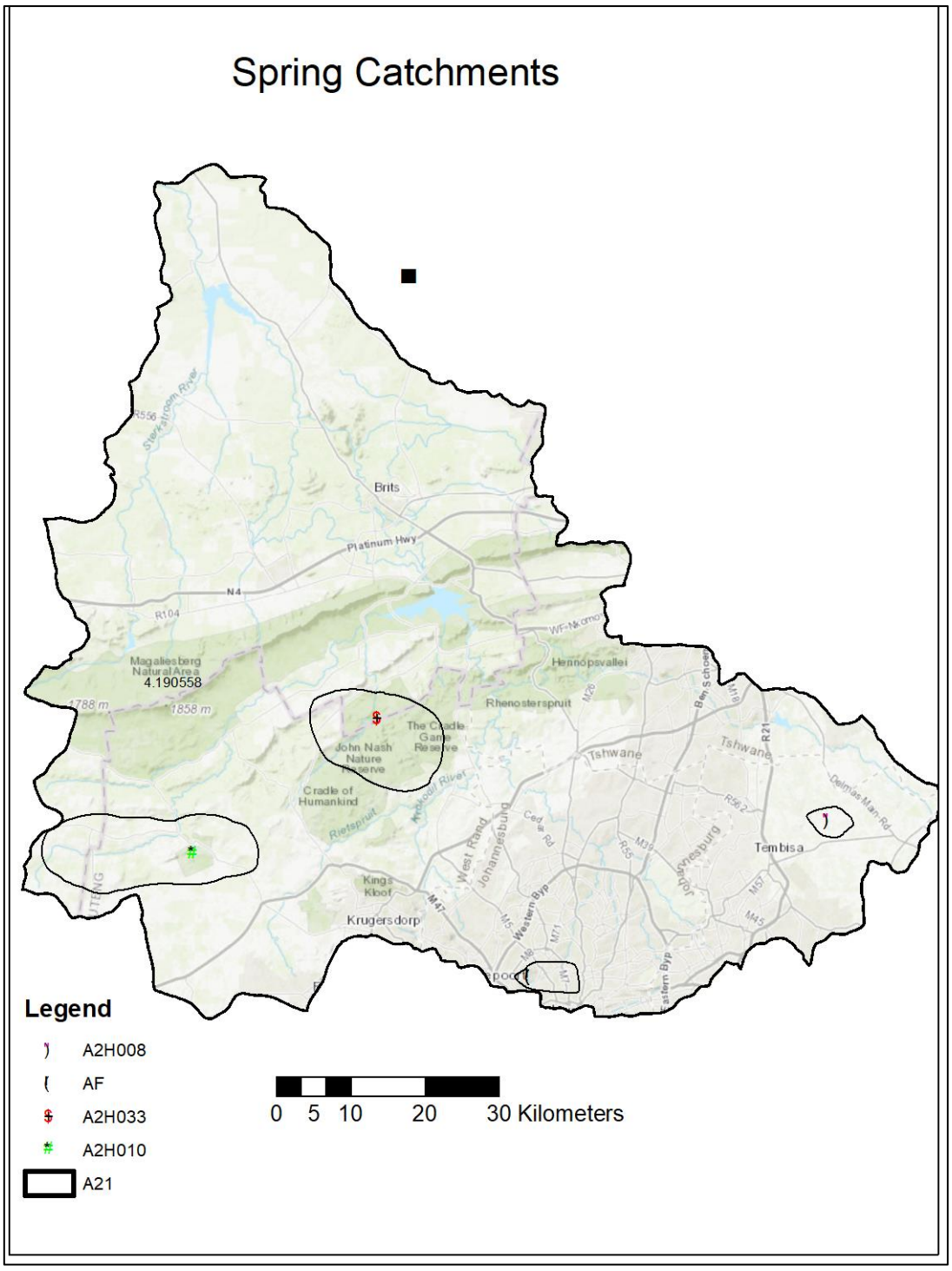


Figure 29. Topographical map of the study area showing the estimated sizes of the catchment areas for the four springs used.

3.5.1. Albert's Farm spring

The Albert's Farm spring feeds a small recreational dam for birds. Unlike the other springs it does not have a gauging station as such manual and improvised measurements were employed. The spring is located in the Northcliff area of Johannesburg. It has multiple structural complexities that have resulted in the spring occurrence. It is the only spring that is not connected to dolomites directly by either being on or being directly on a fracture that is closely connected to dolomites.

In the case of the Albert's Farm spring the hydrograph is displayed in Figure 30 showing Q_0 to be 1300.82 m^3/day. The time since recession began is 246 days. The chosen Q_t = 229.09 m^3/day. The recession coefficient is calculated as shown below.

$$\alpha = \ln\left(\frac{1300.82}{229.09}\right)/246$$

$$= 0.007059$$

The high recession coefficient observed for the AF spring can be attributed to fast flow through fractures, whereas if it was lower it would be reflecting slow circulation through porous media (Amit *et al*., 2002). The recession coefficient depends on the aquifer transmissivity and storativity. This is in line with the expected results for a fracture-controlled spring. The occurrence of multiple peaks in Figure 30 can be associated with different recharge events. Between April and June there is a recession of some sort, however, this is attributed to erroneous manual sampling method. It is important to also note that the Albert's Farm spring has recharge sources that are both local and regional where the local sources are probably more important in the wet season than the regional which would serve as baseflow. The first part of the falling limb (between 1300.82 m^3/day and 473.81 m^3/day) is particularly steep on the AF spring, suggesting that the unsaturated zone contributes a lot to the spring discharge (Civita, 2008). The second part of the falling slope represents the contribution by the saturated zone (Civita, 2008). And for the Albert's Farm spring the gradient of the falling limb is shallow (between 473.81 m^3/day to 229.09 m^3/day) which suggests that the travel time within the saturated zone is low. This contrasts with what we gather from the recession coefficient suggesting fast flow.

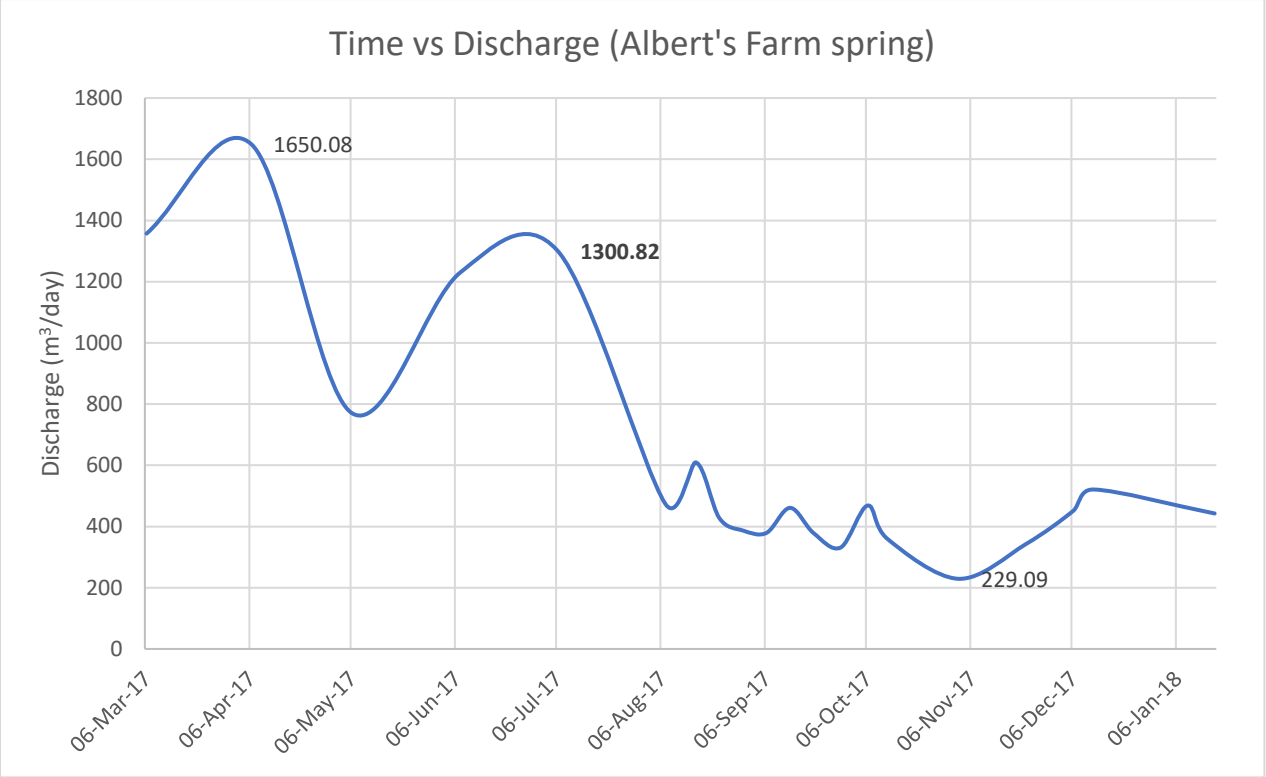


Figure 30. The recession curve for the Albert's Farm spring collected between 06 March 2017 to 06 January 2018.

The visible fractures that result in the occurrence of the Albert's Farm spring are shown in Figure 31. The occurrence of these fractures so close to the spring, could be the reason why we see the smaller peaks between Aug and Sep, Sep and Oct and in Oct, resulting in a rapid response from the spring. Albert's Farm spring is a fracture-controlled spring, mainly by the NW-SE trending fractures, however, the NE-SW trending fractures could be important as regional groundwater circulation that leads water to the spring.

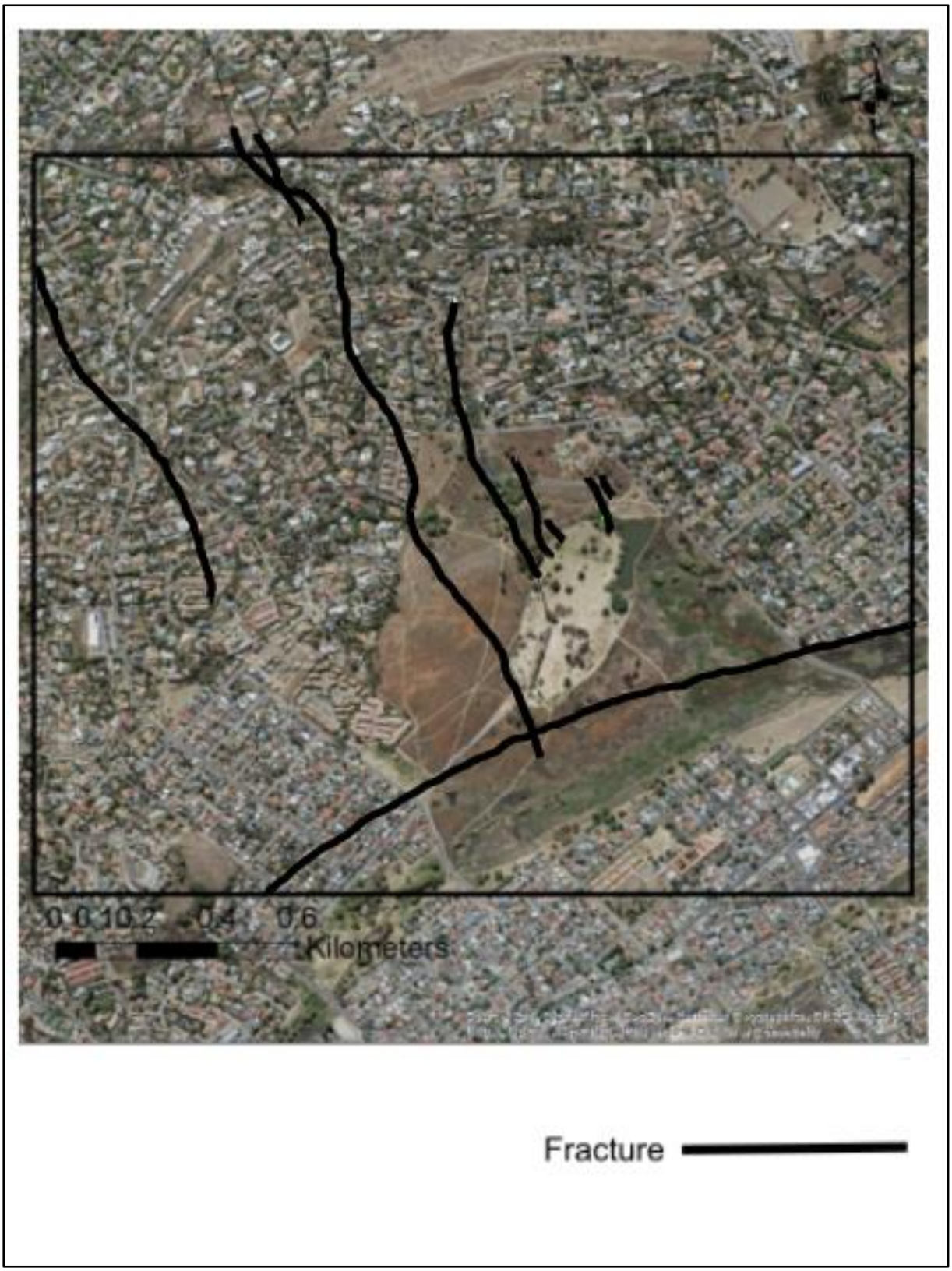


Figure 31. The Location of the Albert's Farm spring, with the major lineaments passing in and around the spring.

3.5.2. The Nouklip-Eye

The Nouklip-Eye (A2H033) is located at the Hartebeeshoek area. The spring discharges from the Malmani dolomites of the Chunniespoort Group. It is relatively higher than the Albert's Farm spring, which showed a peak of 1650 m^3/day. The Q_0 = 6786.58 and Q_t = 5443.2 m^3/day. The time it took from the beginning of recession to the end of recession is 61 days. The calculated α is 0.003616 (Figure 32). The short recession time could be associated with the connectivity of the karst and fracture networks, suggesting that the Nouklip-Eye is subjected to high hydraulic conductivity. At the end of recession, which is subsequently related to the end of the rainy season in autumn the base flow takes precedence. This is suggestive of the fact that the spring depends mainly on baseflow, nevertheless, during the rainy seasons, the karst system and fracture networks allow for quick flow within the aquifer. The Nouklip-Eye is located in the dolomite, and it is surrounded by classic undulating terrain of the karst system. Although the valleys are classic karst type, they follow the NW-SE trending lineament suggesting that the occurrence and orientation of these valleys and the subsequent spring is largely controlled by the lineaments. The steep rise and fall of the limbs can be associated with catchment size, in the case of Nouklip-Eye, the catchment size is small compared to other springs. The other possible reason for this trait could be the presence of shallow groundwater circulation, which would result in a quicker response to rainfall by the spring. The Nouklip-Eye has a slope with a similar gradient throughout, suggesting that the saturated and the unsaturated zone are contributing similar amounts of water to the spring.

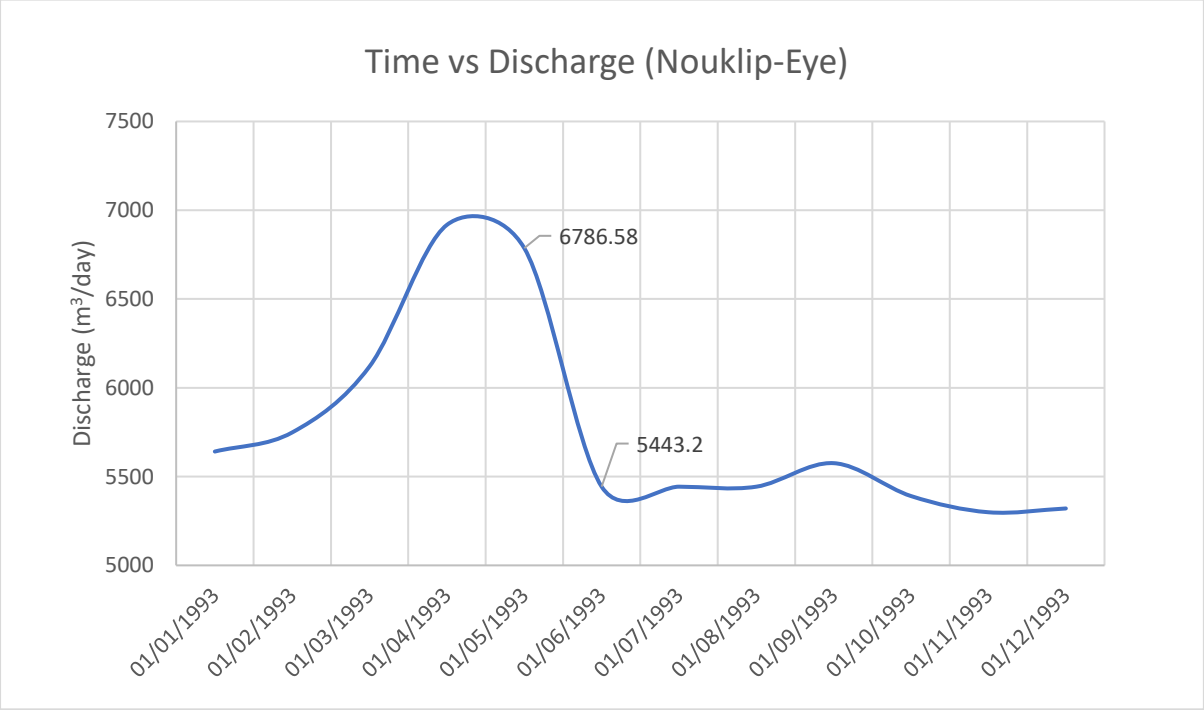


Figure 32. The recession curve (times vs discharge) for the Nouklip-Eye (Data source: DWS hydrological site)

Figure 33 shows the lineaments associated with the occurrence of the Nouklip-Eye. It has two dykes in the north and south, and a combination of the NW-SE and NE trending lineaments. The low yield can be associated with groundwater flow being blocked by the dykes or that the fracture does no intersect ta well-developed dolomite conduit or void.

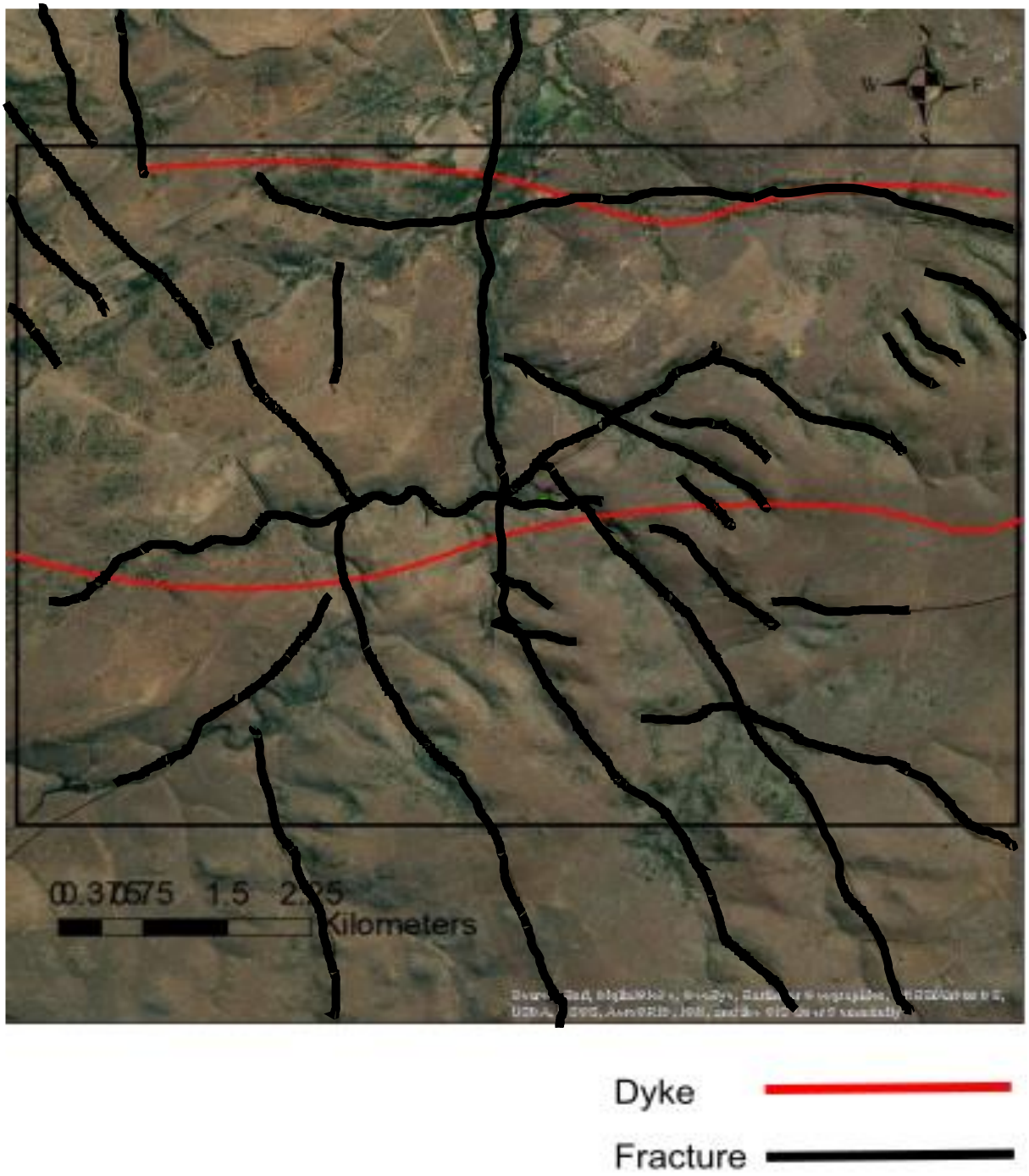


Figure 33. The Nouklip-Eye location, showing the lineaments that occur in and around the spring area that might result in the spring occurrence.

The cross-section in Figure 34 shows where the Nouklip-Eye occurs relative to the lithologies. The spring is at a contact between chert-rich Malmani dolomites and Strubenkop FM shales and quartzites. Due to the low permeability of the shale unit, it has the potential to be a barrier for the north-south circulation of groundwater. Consequently, the spring emerges through either the NW-SE or E-W trending lineament to the surface. Therefore, this spring could have been both lithological and structurally controlled. The dyke on the south of the spring regulates the amount of groundwater that reaches the spring, this explains the low discharge of a spring is associated with high groundwater potential.

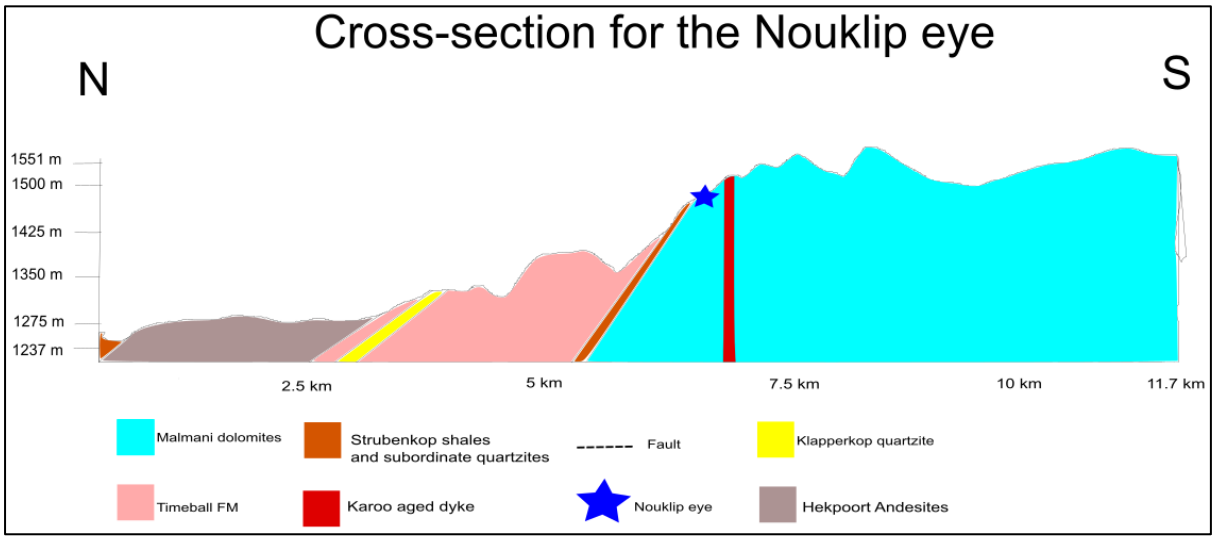


Figure 34, Cross-section of the Nouklip-Eye through a N-S section. The spring location is depicted with the star. The streams generally occur in valleys, as such, were not superimposed.

3.5.3. The Maloney's-Eye

The Maloney's-Eye is located on the top of the Magalies River catchment (A21F), in Steenekoppies. It is underlain by the Malmani dolomites of the Chunniespoort Group (Wiegmans *et al.*, 2013). It is important to note that the Maloney's-Eye comprises of a family of springs clustered together in one area. Wiegmans *et al*. (2013) suggests that the low density of streams in and around the springs assists with increasing the recharge potential. The α for the Maloney's-Eye is 0.004398, calculated from Q_t which is 23414.4 and the Q_0 of 13691.52. The recession period is about 122 days. The time it took from the beginning of recession to the end of recession was twice that of the Nouklip-Eye (Figure 32). The similarities in recession coefficients for the two springs can be associated with the similarities in aquifer properties. The first part of the falling limb (between 23414 m^3/day to 18 000 m^3/day) represents the input from the unsaturated zone during and after the precipitation (Civita, 2008) which could be in the form of interflow. The second part for the falling limb (ranging between 18 000 m^3/day to 14 000 m^3/day) represents the saturated zone of the aquifer, the steeper it is the quicker the time of travel

(Civita, 2008). The time it takes from the end of the previous recession (Figure 35) to the end of the recession is longer for this spring and that can be associated with the elevated recharge that takes place in and around the spring due to the well-developed sinkholes and fractures in the catchment area (Van Schoor, 2002; Oosthuizen and van Rooy, 2015). The discharge point of the Maloney's-Eye is on the lower contact of the quartzites the main source of the spring is from the Malmani dolomites. The spring occurrence seems to be affected by both the NW-SE and the NE-SW trending lineaments, however, the NW-SE trending lineament seems to be playing a major role. This is on the basis that just 5 km north of the spring, a clear displacement of the quartzite ridge is visible, and the stream flows in that direction as part of the Magalies River. The Maloney's-Eye based on the shallow rise and fall implies a large catchment.

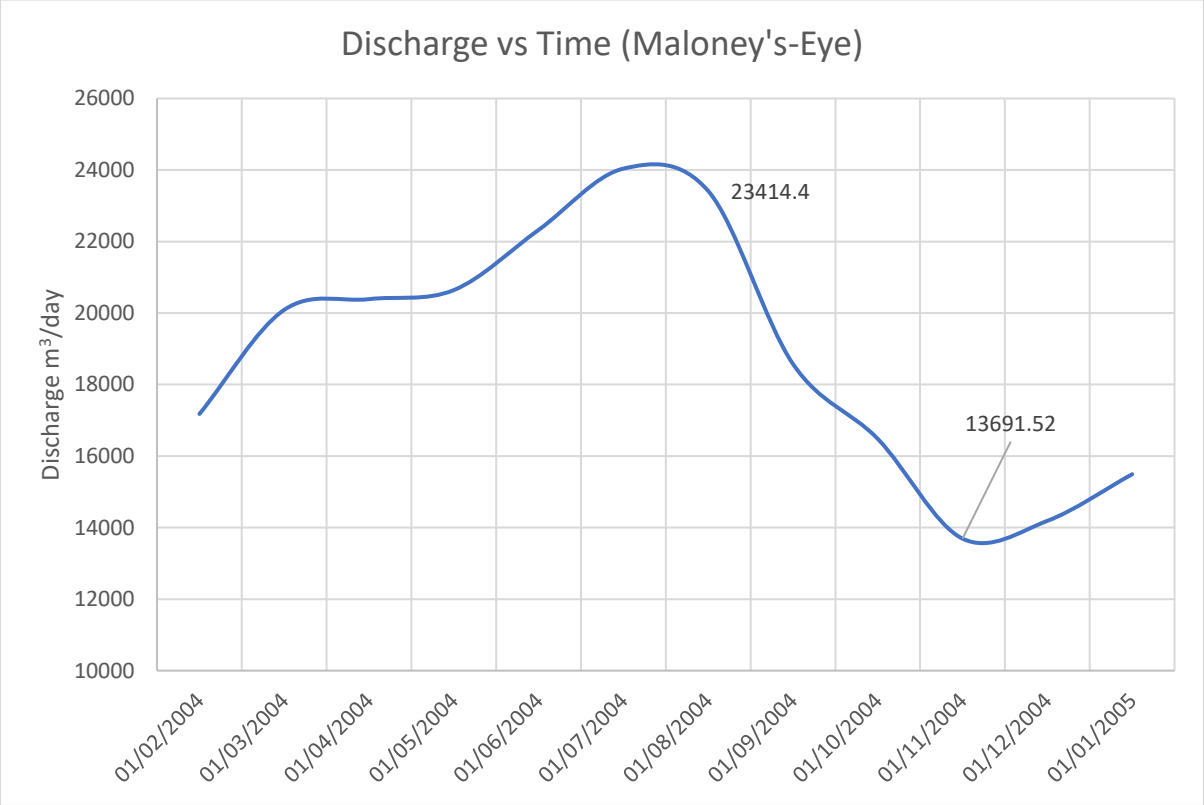


Figure 35. The recession curve (times vs discharge) for the Maloney's-Eye spring. The station ID measuring discharge is A2H010 (Data source: DWS hydrological site).

The Maloney's-Eye represent a group of springs that occur close to each other. The spring discharge could be facilitated due to an E-W Karoo dyke that is responsible for blocking the north flowing groundwater, as such the groundwater is forced to flow up in a series of fractures in and around the area.

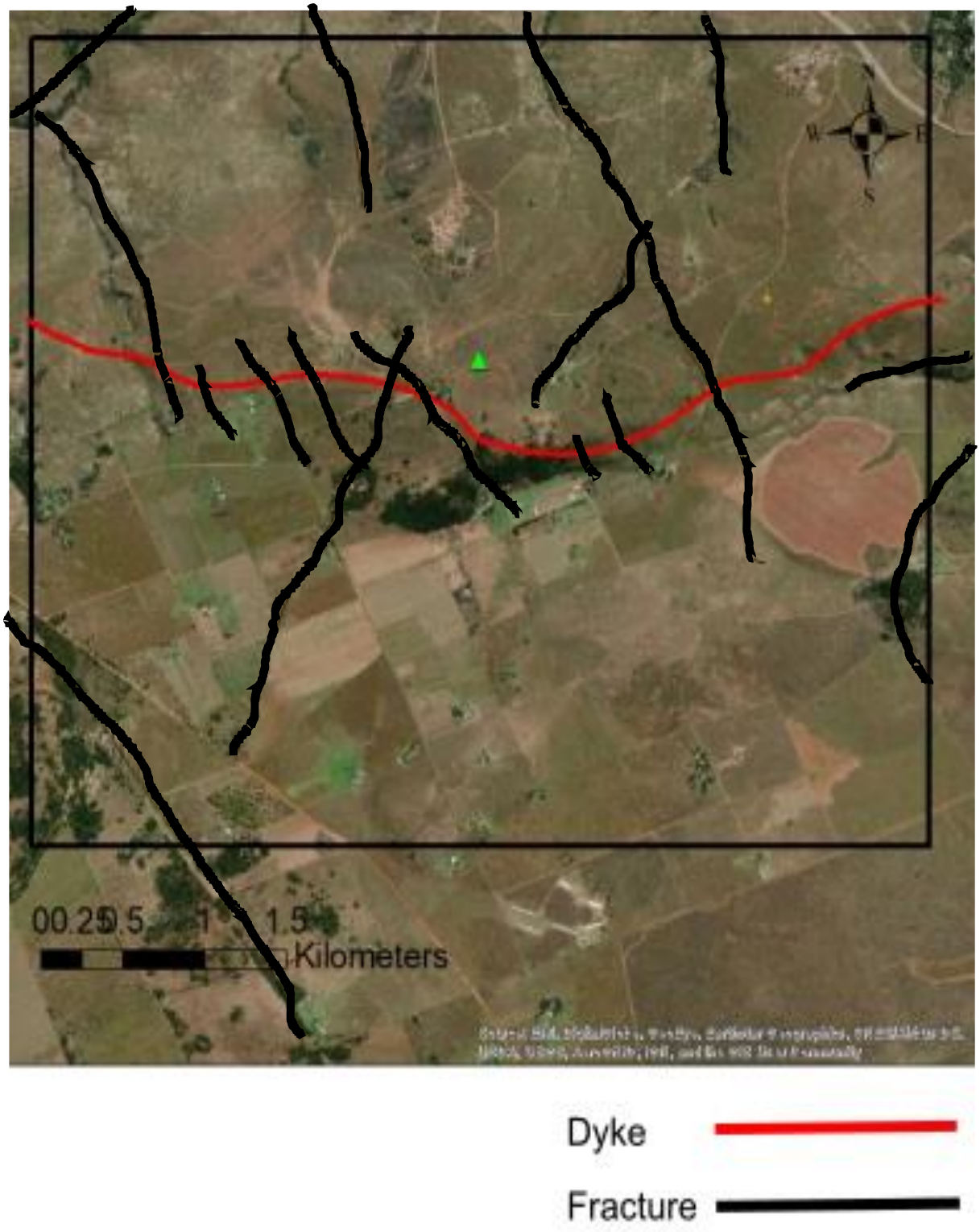


Figure 36. The Maloney's-Eye location with the associated lineaments in and around the spring area.

The conceptual model in Figure 37 adopted from Meyer (2014) shows that the Maloney's-Eye occurs close to the dolomite-quartzite contact. However, the occurrence of a fault that trends in an E-W direction acts as a conduit that subsequently forms the springs. The discharge of the Maloney's-Eye is

due to the large catchment size and the absence of groundwater delays between the recharge points and the spring point.

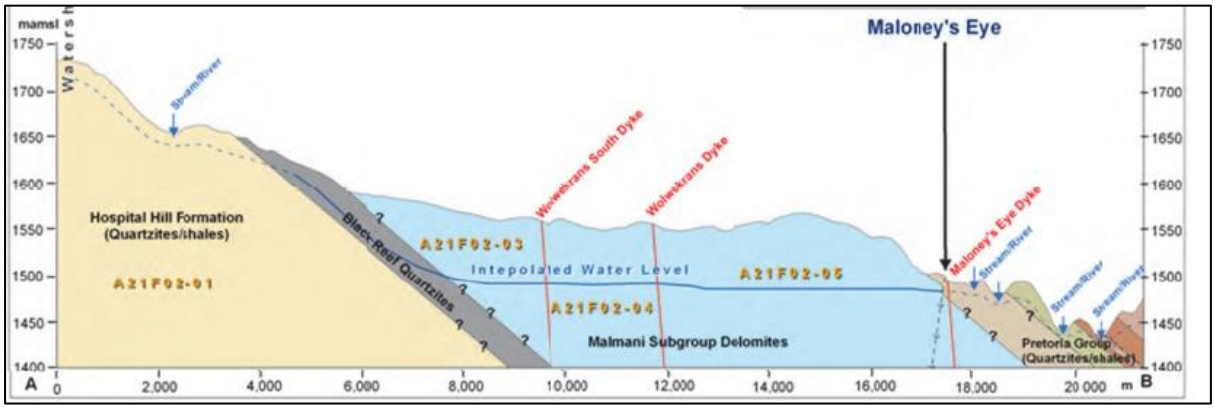


Figure 37. Conceptual model of the Maloney's-Eye, with the associated lineaments (Adapted from Meyer, 2014).

3.5.4. The Elandsfontein-Eye

The Elandsfontein spring is located in the eastern side of the study area, about 8.4 km east of Tembisa. It forms the headwater of small stream. Based on the remote sensing observation, it is immediately clear that the discharge is not significantly high even though the spring is located on the Malmani dolomites of the Chunniespoort group. This low yield is also observed on the recession curve in Figure 38. This low discharge as compared to the Maloney's-Eye high discharge, which is on the same lithology, shows how variable karst aquifers are. The availability of high recharge, more interconnected fracture sets, and caves or lack thereof, can play a huge role in the groundwater circulation. The Q_t for this spring is 1630.08, Q_o is 604.8 and the calculated recession coefficient is 0.004633. It is important to note that the recession coefficients for the dolomite springs are more or less the same, due to the similarity in aquifer characteristics. It took longer for the Elandsfontein-Eye to go from beginning to the end of recession, which is 214 days.

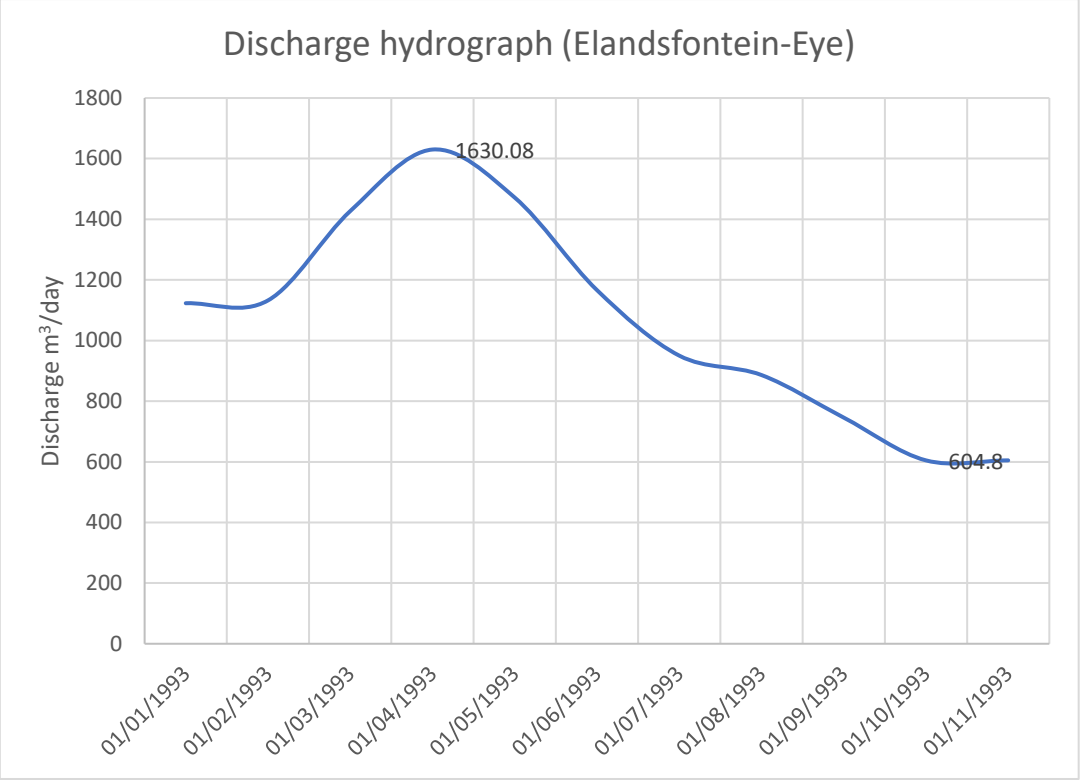


Figure 38. The recession curve (times vs discharge) for the Elandsfontein-Eye spring (Data source: DWS hydrological site).

The Elandsfontein-Eye has the most dykes in its close proximity (Figure 39) compared to the other springs. The dykes are limiting the size of the catchment within the dyke's proximity, unless the fractures allow for groundwater to pass through the dykes. The possibility of fractures allowing for the transfer of groundwater outside the dykes is highly unlikely considering the low groundwater discharge observed in Figure 38.



Figure 39. The Elandsfontein-Eyeand the associated structures.

The schematic cross-section of the geology around the Elandsfontein-Eye is shown in Figure 40. Figure 40 further emphasizes the dominance of dykes in the Elandsfontein-Eye. The spring occurs at a contact between shales and dolomites. This spring can be classified as a contact spring. The dyke on the NE of

the spring ensures that the groundwater flow of the dolomite aquifer is reduced and limited to the portion shown in Figure 40. As such this explains why the Elandsfontein-Eye has such a low discharge compared to the other dolomite springs and the Albert's Farm spring.

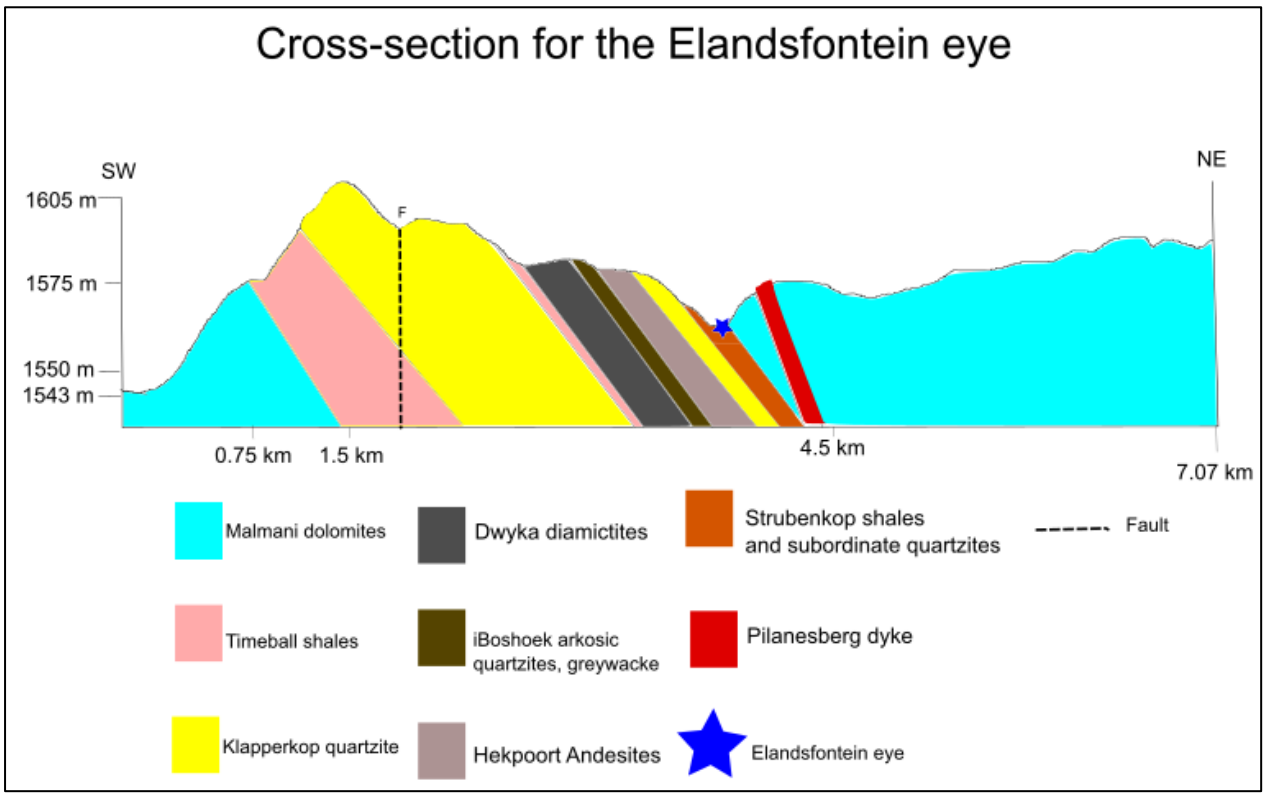


Figure 40. Conceptual model of the Elandsfontein-Eye showing that the spring occurs on a contact between shales and dolomites.

In conclusion the spring data has been presented in the form discharge hydrographs. The hydrographs were then used to get the recession curves and subsequently the recession coefficients. In the dolomitic springs although the discharge is significantly different, the recession coefficient is similar. However, all the dolomitic springs recession coefficients are much lower than that of the Albert's Farm spring. The fractures on the quartzite allow for increased quick flow as opposed to the dolomitic springs, suggesting that the dolomites have less developed fractures and karsts as far as groundwater flow is concerned. This could be a result of the chert layers acting as barriers. The cross-sections show that the spring occurrence is influenced by both the lithologies and structures.

Table 2. Summary of the recession coefficient data for the springs, including the coordinates, initial discharge and discharge at the end of recession.

Spring Name	**Spring ID**	**Lat**	**Long**	**Qt**	**Q0**	**T (days)**	**α**
Albert's Farm	AF	-26.155315	27.970258	1300.08	229.09	246	0.007059
Nouklip-Eye	A2H033	-25.87523814	27.78583542	6786.58	5443.2	61	0.003616
Maloney's-Eye	A2H010	-26.02236	27.56336	23414.4	13691.52	122	0.004398
Elandsfontein-Eye	A2H008	-25.98583	28.33111	1630.08	604.8	214	0.004633

3.6. Stream discharge analysis

Stream discharge data can assist in understanding whether streams loose to groundwater or are sustained by baseflow from groundwater, particularly if fractures/lineaments are cross-cut by the streams. Three combinations of discharge stations have been used with variable distances between the discharge stations (Figure 41). A total of 19 stations were used which had varying distances from each other. The combinations are A2H005 and A2H009; A2H050 and A2H051 and A2H044 and A2H023. Although the entire year has been depicted on the graphs, the most important section is the winter period (June to August) when the rainfall input is low or absent. It is important to note that in between the gauging stations, there are no known waste water discharge points.

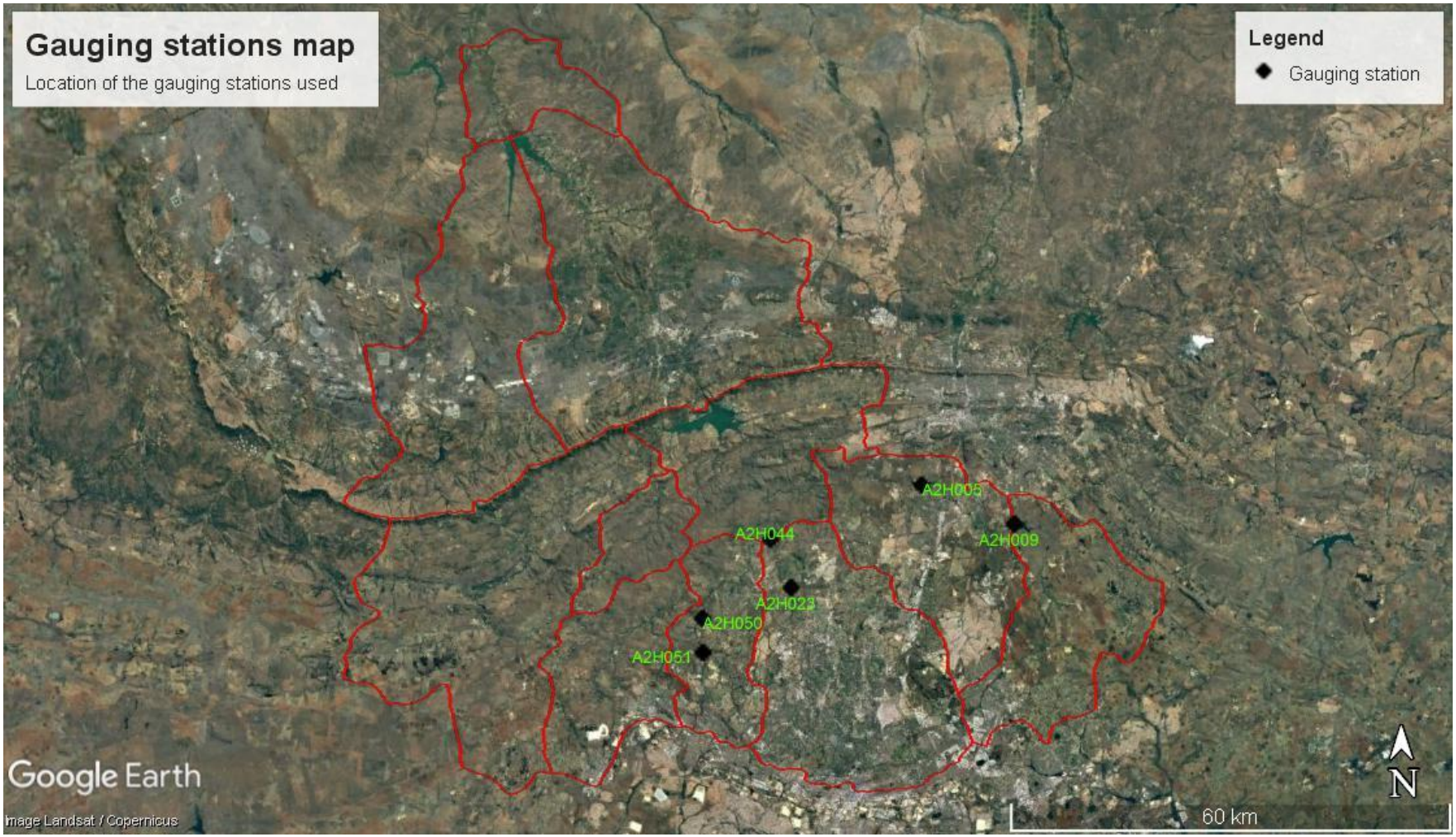


Figure 41. Google Earth image showing the gauging stations used.

3.6.1. Stream discharge at A2H005 and A2H009 stations

Figure 42 shows stream discharge measurements for the A2H005 and A2H009 stations. The measurements at the A2H009 gauging station shows more or less consistent discharge rate that is because the station is located on a dam mouth with controlled discharge rate. However, the A2H005 gauging station has a higher discharge throughout the year, but it significantly rises between mid-June and the beginning of August suggesting a strong contribution of baseflow in that period. The drop-in discharge during September is opening room for the speculation that the groundwater and surface water interactions between these two stations changes from time to time, and that is, at some points the stream loses to the groundwater whereas at some instances the groundwater feeds the streams. Another possible reason for this drop could be that the farmers in and around the stream stop depending on the groundwater in the rainy season and use the stream accounting for the significant downstream water loss. The A2H005 gauging station is underlain by dolomites whereas the A2H009 gauging station is underlain by shales. The variation in the discharge for the A2H005 gauging station could be associated with the degree of fracturing of the dolomites.

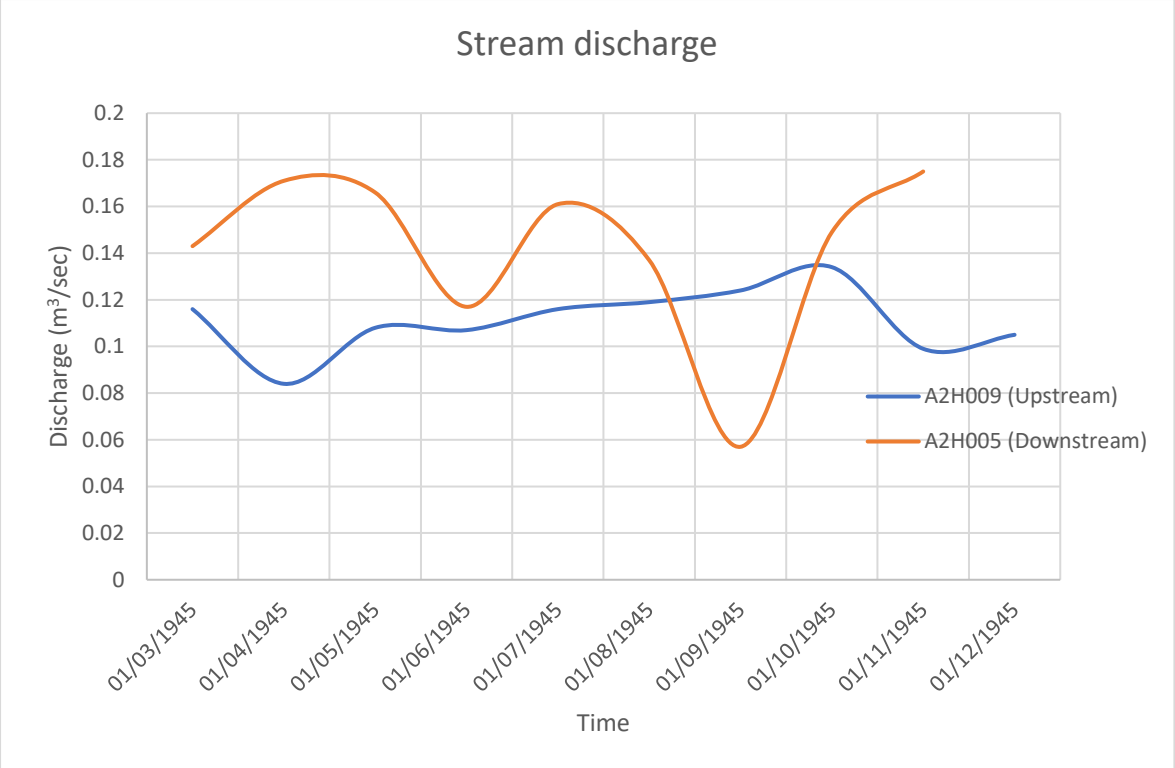


Figure 42. Stream discharge hydrograph for the A2H009 and A2H005 gauging stations. The discharge measurements are monthly averages (Data source: DWS hydrological site).

3.6.2. Stream discharge for the A2H050 and A2H051 stations

Figure 43 has stream discharge measurements for the combinations of A2H050 and A2H051 gauging stations. The graphs look exactly the same except that the downstream (A2H050) has more discharge than the upstream station (A2H051). The beginning and the end of the hydrological year is depicted by the drop-in discharge in mid-April and the rise in discharge mid-September. The section between mid-April and in mid-September was sustained by groundwater in the form of baseflow. This section allows for the stream to be classified as a gaining stream. The tributaries joining this mainstream are not large, and they would be expected to be dry or would have low discharge during the winter months. As such it is assumed that the increase in discharge is be due to the baseflow contribution. However, the structures resulting in the baseflow are not consistent throughout, therefore, different parts of the section could be gaining, and some sections could also be losing.

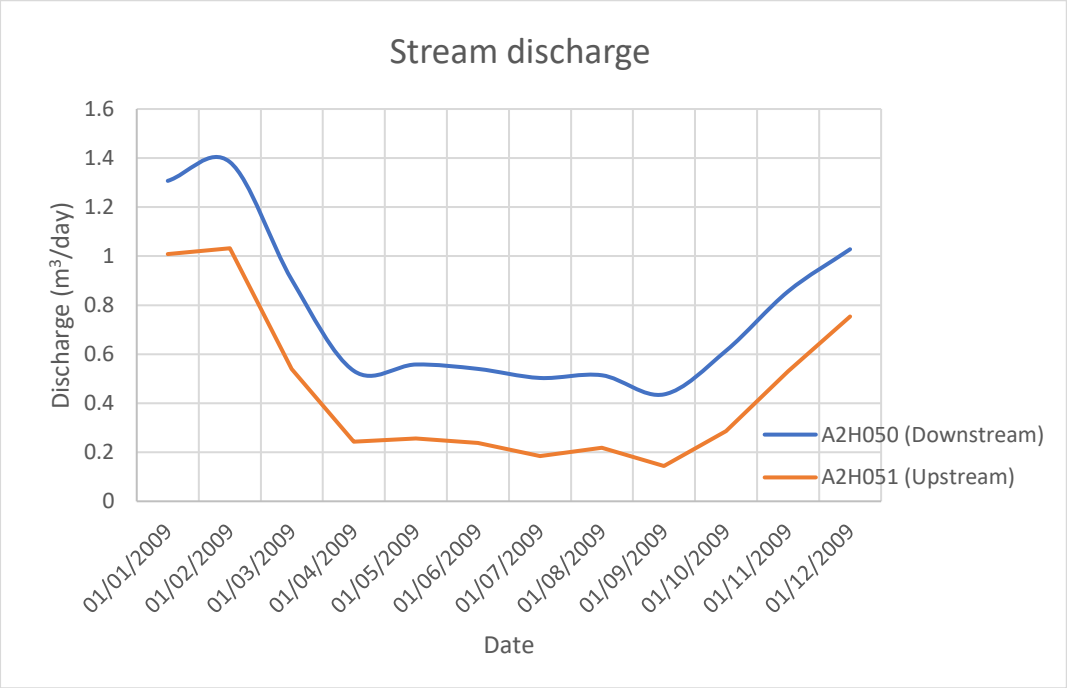


Figure 43. Stream discharge hydrograph at the A2H009 and A2H005 stations (Data source: DWS hydrological site). The discharge measurements represent monthly averages.

3.6.3. Stream discharge for the A2H044 and A2H023

Figure 44 displays stream discharge measurements at the A2H044 and A2H023 gauging stations. The plot looks relatively the same with A2H044 having more kinks than A2H023. The difference in discharge at any given point for the 2015 year was more $8m^3/s$. The two streams show consistent discharge through out the rainy and dry seasons. A2H044 has shallow peaks that happened in different times, including July. The July kink could be a representation of delayed flow of groundwater into the stream in the form of baseflow. All together this stream depicts a loosing system, since the upstream station shows higher discharge than the downstream station.

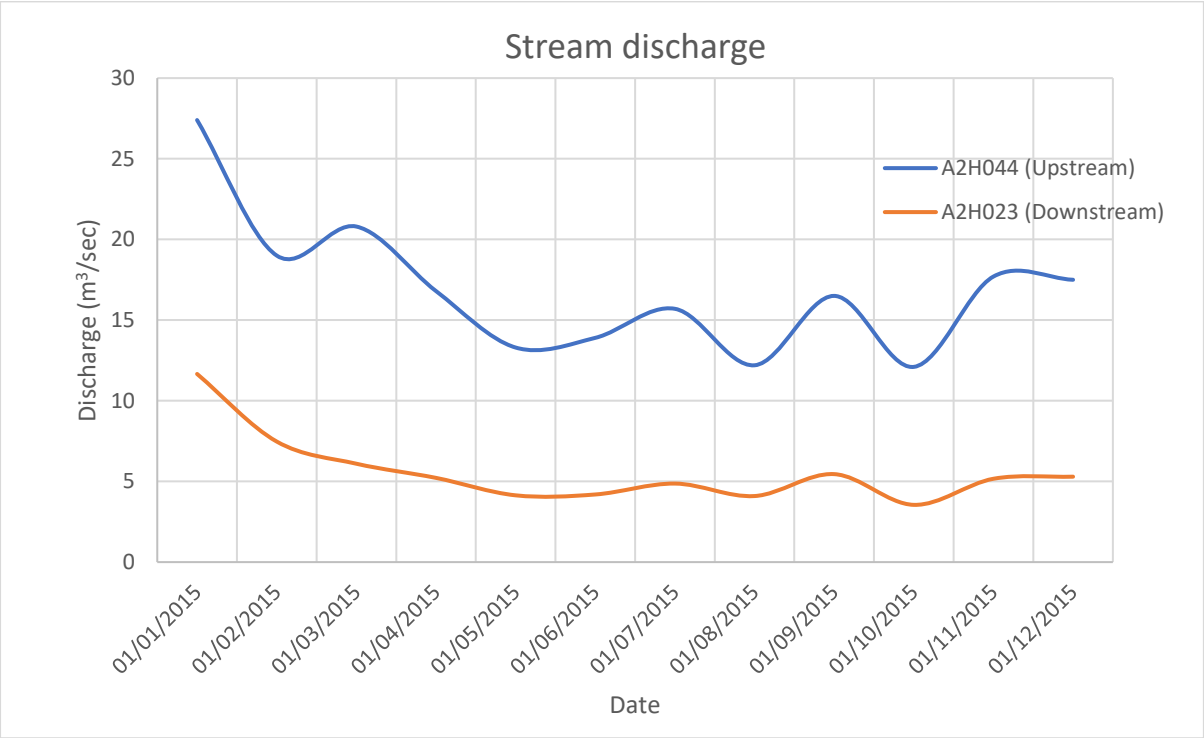


Figure 44. Stream discharge hydrographs for the A2H044 and A2H023 gauging stations (Data source: DWS hydrological site). The discharge measurements are monthly averages.

The stream discharge data for three combinations helps in concluding that baseflow is important for sustaining rivers in the study area. Although, there could be discharge loss on the western dolomites, the other streams depend highly on groundwater. The groundwater dependence is shown on the multiple springs that occur on multiple parts of the study area, predominantly on the dolomites.

3.7. Environmental Isotopes

The stable isotopes of Oxygen and Hydrogen are plotted below as the PMWL (IAEA GNIP), JMWL, GMWL (Figure 45) the complete data set can be found in Table 3 for the BH data, for the Albert's Farm spring isotopes, Dolomite springs (not the springs cited above) and for the DWS provided isotope information. The tritium data is shown in table 4. Using stable isotopes and radioactive dating can help in determining the origin, residence time and the flow path of groundwater (Rose *et al.* 1996). Yeh *et al.* (2014) suggest that Oxygen-18 and Deuterium are important as tracers of hydrogeological processes such as recharge, ground-surface water interactions and basin hydrology. The data presented includes boreholes and springs.

Table 3: The stable isotopes data for boreholes, Albert's Farm spring (measured between June 2016 and May 2018) and Dolomitic springs.

BH No	**δD ‰**	**δD StDev ‰**	**δ ^{18}O ‰**	**^{18}O StDev ‰**
BH1	-6.5	0.62	-1.39	0.13
BH2	-6.8	0.97	-1.11	0.18
BH3	-19.4	1.06	-4.09	0.08
BH4	-18.1	1.63	-3.96	0.18
BH5	-9.9	0.55	-1.94	0.11
BH6	-0.9	1.49	-0.35	0.19
BH7	-5.0	0.59	-0.89	0.15
BH8	-9.6	0.54	-2.01	0.26
BH9	-17.8	0.85	-3.05	0.15
BH9b	-11.3	0.64	-2.32	0.06
BH10	-17.1	1.44	-3.00	0.24
BH11	-10.1	2.28	-1.71	0.28
BH12	-14.4	0.61	-3.12	0.10
BH13	-12.9	0.26	-2.14	0.09
BH14	-26.5	0.12	-4.79	0.04
BH15	-6.9	0.34	1.58	0.03
BH16	-39.3	0.40	-12.65	0.10
BH17	-38.9	0.12	-13.47	0.03
BH18	-32.8	0.07	-9.76	0.04
BH19	-12.3	0.29	-2.23	0.05
BH20	-12.41	0.00	-3.52	0.00
BH22	-15.8	0.66	-3.55	0.05

BH23	-12.5	3.47	-2.62	0.27
BH24	-22.5	0.50	-5.08	0.36
BH25	-21.6	0.36	-4.32	0.05
BH26	-16.8	0.30	-3.27	0.08
BH27	-15.1	0.68	-3.18	0.08
BH28	-17.3	1.00	-3.83	0.11
BH29	-18.2	1.46	-3.83	0.17
BH30	-25.3	0.35	-5.15	0.03
Albert's Farm spring (Data collected over a year)				
	-19.3	0.23	-5.27	0.10
	-21.6	0.28	-6.01	0.09
	-19.1	0.14	-4.30	0.05
	-14.5	0.00	-2.86	0.00
	-13.7	1.28	-3.79	0.13
	-15.9	0.28	-3.78	0.12
	-14.3	0.06	-3.57	0.10
	-12.5	0.53	-3.09	0.03
	-15.0	0.85	-3.43	0.05
	-16.4	0.56	-3.67	0.09
	-15.2	0.71	-4.13	0.20
	-12.3	0.53	-3.11	0.11
	-14.9	0.37	-3.46	0.04
	-16.3	1.21	-3.92	0.23
	-15.2	0.33	-3.05	0.05
	-18.3	0.35	-3.72	0.08
	-20.3	0.35	-4.12	0.08
	-12.0	0.44	-2.28	0.08
	-11.7	1.50	-2.81	0.15
	-10.5	2.21	-2.79	0.25
	-14.2	0.45	-2.86	0.12
	-15.9	1.32	-3.45	0.14
	-12.9	0.85	-3.10	0.11
	-12.3	2.76	-3.13	0.39
Dolomitic springs				
SP1	-27.6	0.360	-4.97	0.09

SP2	-27.5	0.499	-5.11	0.10
SP3	-29.6	0.381	-5.28	0.07
SP4	-27.8	0.427	-4.77	0.06
SITE 1	-15.8	0.522	-3.24	0.09
SITE 2	-15.8	1.509	-3.21	0.27
SITE 3	-16.4	0.429	-2.65	0.11
SITE 4A	-17.8	0.329	-3.45	0.16
SITE4B	-14.5	0.574	-2.11	0.08
SITE 5A	-25.1	2.999	-3.52	0.27
SITE5B	-23.2	1.098	-3.87	0.18
SITE 6A	-19.3	2.324	-3.45	0.32
SITE 6B	-11.9	0.766	-2.52	0.05
SITE 7	-12.1	0.595	-1.80	0.07
SITE 8	-27.1	0.572	-4.51	0.08
SITE 9A	-10.9	0.649	-1.83	0.05
SITE 9B	-15.1	1.025	-2.35	0.11
SITE 10	-15.6	0.948	-2.76	0.11
SITE 11A	-14.9	0.574	-2.98	0.12
SITE11B	-14.2	0.563	-2.18	0.11
SITE 12	-18.5	2.510	-2.72	0.25

3.7.1. Stable isotopes

The stable isotopes of Hydrogen and Oxygen serve as appropriate tracers for groundwater movement (Thivya *et al.*, 2016). Water isotopic composition is highly dependent on environmental factors that might lead to condensation or evaporation (Fontes, 1980). In any region, groundwater mixing may result in mixed isotopic signatures as such the isotope values might be different (Hiscock and Bense, 2014). It is also important to compare local water isotope composition with local meteoric water lines, due to the changing climate conditions that affect rainfall (Abiye *et al*., 2015).

Figure 45 shows the stable isotopes data plotted with respect to the Pretoria Meteoric Water Line is $\delta D = 6.82\delta^{18}O + 10.4$ ‰. (PMWL) (IAEA-GNIP), Johannesburg Meteoric Water Line is $\delta D = 6.7\delta^{18}O + 7.2$ (JMWL) (Leketa *et al.*, 2019) and the Global Meteoric Water Line is of $\delta D = 8\delta^{18}O + 10$ ‰ (GMWL) (Craig, 1961). The 30 BH samples (referred to as BH hereon) (Table 3) were plotted in purple and the samples from the AF spring are plotted in blue.

In Figure 45 the BH plot shows an evolution pattern of water recharged after evaporation. The average δD and $\delta^{18}O$ are -16.4 ‰ and -3.69 ‰, respectively (Table 3). Most of the BH samples plotted on the MWL are below but very close to the line. As such it did not undergo significant evaporation prior to recharge. This is indicative of rapid recharge directly from precipitation. Two samples show extreme evaporation (BH2 and BH15). BH15 occurs on the banks of the Hartbeespoort Dam, as such the closest and most possible source is an open body of water prone to extreme evaporation (the Dam itself) that seeps into the Bushveld Igneous Complex aquifer through fractures. Close to all three meteoric water lines and this can be attributed to recharge directly from rainfall or rapid recharge prior to extreme evaporation (Leketa *et al*., 2019). The rapid recharge can be attributed to the fractures that are found throughout the study area (Figures 4-8).

BH2 is near one of the Brits Graben associated faults and fractures. These faults/fractures are recharged by the Hartbeespoort Dam seepage and the Crocodile River. The recharge of aquifers from surface water bodies is not exclusively in the Hartbeespoort Dam region. It can be observed close to the Sterkfontein caves using discharge measurements. Abiye *et al.* (2015) estimated seepage of mine water in the dolomites to be between 0.78 m^3/s in winter and 0.92 m^3/s in the summer season. However, the discharge stations on the Johannesburg Dome suggested streams as gaining, which might be due to the dominance of interflow over baseflow. The Hartbeespoort Dam was estimated to be losing 14 172 232 m^3 of water, however, not all this water is believed to be lost through fractures (Davis 2017). BH16, BH17 and BH18 all show extreme depletion. The possible reasons for this depleted nature of these boreholes can be (1) recharge from high altitudes, (2) recharge from a rainfall event with low humidity during condensation and (3) recharge during a colder climate. In the context of these boreholes, it is possible that a combination of these factors might have resulted in the observed signatures. The altitude might be from the surrounding quartzite ridges (Daspoort quartzites), combined with heavy rainfall and colder conditions, the possibility of extreme depletion is high. Looking at the relationship between BH16, BH17 and BH18, a CO_2-exchange reaction could be possible as a result of the presence of dolomites. The possible reasons why there could be this exchange is (1) stored CO_2 in pore spaces, (2) stored CO_2 in fractures (Serno *et al*., 2017) or (3) plants can result in the evolution of groundwater carbon (Leketa *et al.*, 2018). Option two and three are the plausible explanations, considering that we are dealing with fractured aquifers and have grasses and shrubs in most parts of the study area

For the Albert's Farm spring the average δD and $\delta^{18}O$ are -15.2 ‰ and -3.57 ‰, respectively. The Albert's Farm spring data represents isotopic signatures over multiple seasons for a single source. Considering that the Albert's Farm spring samples come from one source, the signatures are highly variable. However, most of these samples plot near and parallel to the meteoric water lines. This is attributed to water that recharged directly from precipitation through the prominent fractures in the study area. The parallel nature to the MWL is suggested to be water that has spent a short and insignificant period of time on the surface prior to recharge, allowing for low intensity evaporation to

occur (Hiscock and Bense, 2014; Thivya *et al*., 2016). The recharge for the aquifer feeding the Albert's Farm spring occurred via preferential flow through the fractures which was then followed by piston groundwater flow (Leketa *et al*., 2019). Nyebelele (2017) suggested that the source of recharge for the Albert's Farm spring is both regional and local, on the basis that the spring was affected by rainfall episodes that increased discharge (higher discharge during the rainy months than in dry months). It was also noted that the spring had some samples that showed increased evaporation prior to recharge. This can be attributed to water within the shallow fractures being prone to evaporation prior to the piston flow taking effect.

The dolomite springs have an average composition of δD and $\delta^{18}O$ -28.1 ‰ and -5.03 ‰, respectively. The composition of the dolomites shows a relatively depleted signature compared to the other groundwater samples in the study area. Nonetheless, the samples are clustered together, and all plots on the MWL's suggestive of rapid recharge directly from precipitation. The rapid recharge can be attributed to the cavities in the dolomites (Leketa *et al*., 2019) and the fractures that dominate the study area. The depletion could further suggest recharge that occurred at (1) colder climatic conditions, (2) recharge that occurred at higher elevation, or (3) rainfall event(s) that had low humidity in the vapor during condensation and/or heavy rainfall.

The stable isotope data measured from the DWS boreholes contain average values for δD and $\delta^{18}O$ at -17.0 ‰ and -2.89 ‰, respectively. All these samples plot below and parallel to the meteoric water lines. This represents rapid recharge, with some time spent on surface or in the open fractures prior to the recharge.

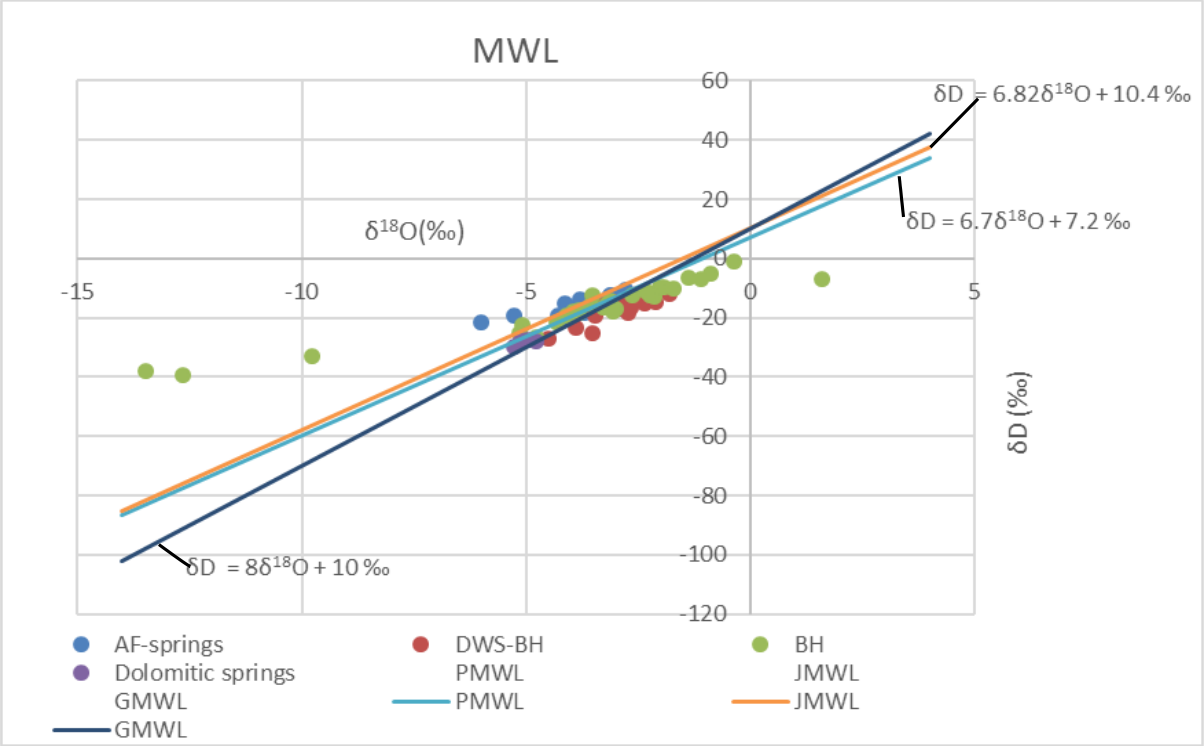


Figure 45. The stable isotope plot for the groundwater samples in the UCRB, with respect to the GMWL, PMWL and JMWL.

There are 6 clusters in the study area (Figure 46), their average compositions are summarised in table 4. Cluster one is made of BH22, BH20, BH28 and BH29. The average composition for cluster one is -15.9 ‰ and -3.68 ‰ for of δD and $\delta^{18}O$, respectively. Cluster two is made up of exclusively DWS BH's with an average value of -17.0 ‰ and -2.89 ‰ for δD and $\delta^{18}O$, respectively. Cluster three is made of BH27 and BH30. Their average composition for δD and $\delta^{18}O$ is -20.2 ‰ and -4.16 ‰, respectively. Cluster 4 is made up of BH1, BH2, BH3, BH4, BH14, BH15, BH16, BH17, BH18 and BH26. The average δD and $\delta^{18}O$ value is -21.1 ‰ and -5.29 ‰, respectively. Cluster 5 is made of BH5, BH6, BH7, BH8, BH9a and BH9b. The average δD and $\delta^{18}O$ value is -9.1 ‰ and -1.76 ‰, respectively. Cluster 6 is made up of BH10 and BH11. Their average values are -13.6 ‰ and -2.36 ‰ for δD and $\delta^{18}O$, respectively. Based on Figure 47 Clusters 2, 5 and 6 show an evaporation effect. They also plot directly below the meteoric water line suggesting that all the samples in these three clusters have undergone predominantly the evaporation process prior to recharge, in various degrees. In the case of cluster 5 and 6 the occurrence of surface water bodies in the form of rivers and dams can favour evaporation, however, the low severity of this evaporation pattern suggests that the fractures in these clusters are competent as far as permeability and porosity is concerned. Clusters 1 and 3 both plot slightly above all the meteoric water lines. This suggests that the samples in these clusters have been predominantly influenced by recharge directly from rainfall. Cluster 4 represents the upstream part of the Hartbeespoort

dam shows a pattern that is associated with recharge at colder climates, higher elevations and heavy rainfall events.

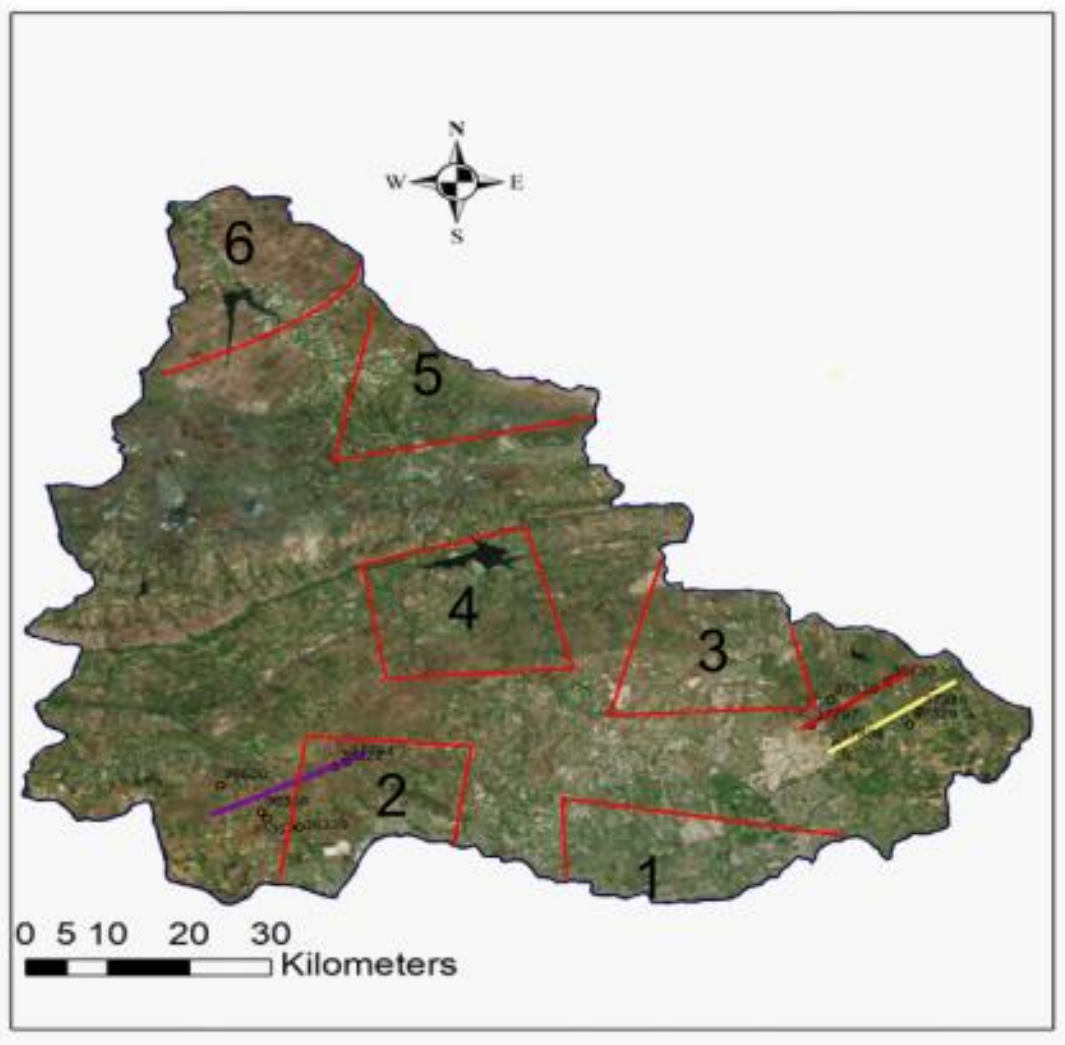


Figure 46. Clusters of BH's are based on mean isotope similarity. The red-boxes represent these clusters and are numbered for reference purposes.

Table 4. The average stable isotopic composition for the different clusters shown in Figure 46.

Clusters	δ^2H ‰	$\pm^2H$ StDev ‰	$\delta\ ^{18}O$ ‰	$\pm\ ^{18}O$ StDev ‰
C1	-15.9	0.78	-3.68	0.08
C2	-20.2	0.51	-4.16	0.05
C3	-12.7	1.07	-2.63	0.14
C4	-21.1	0.22	-5.29	0.05
C5	-9.1	0.78	-1.76	0.15
C6	-13.6	1.86	-2.36	0.26

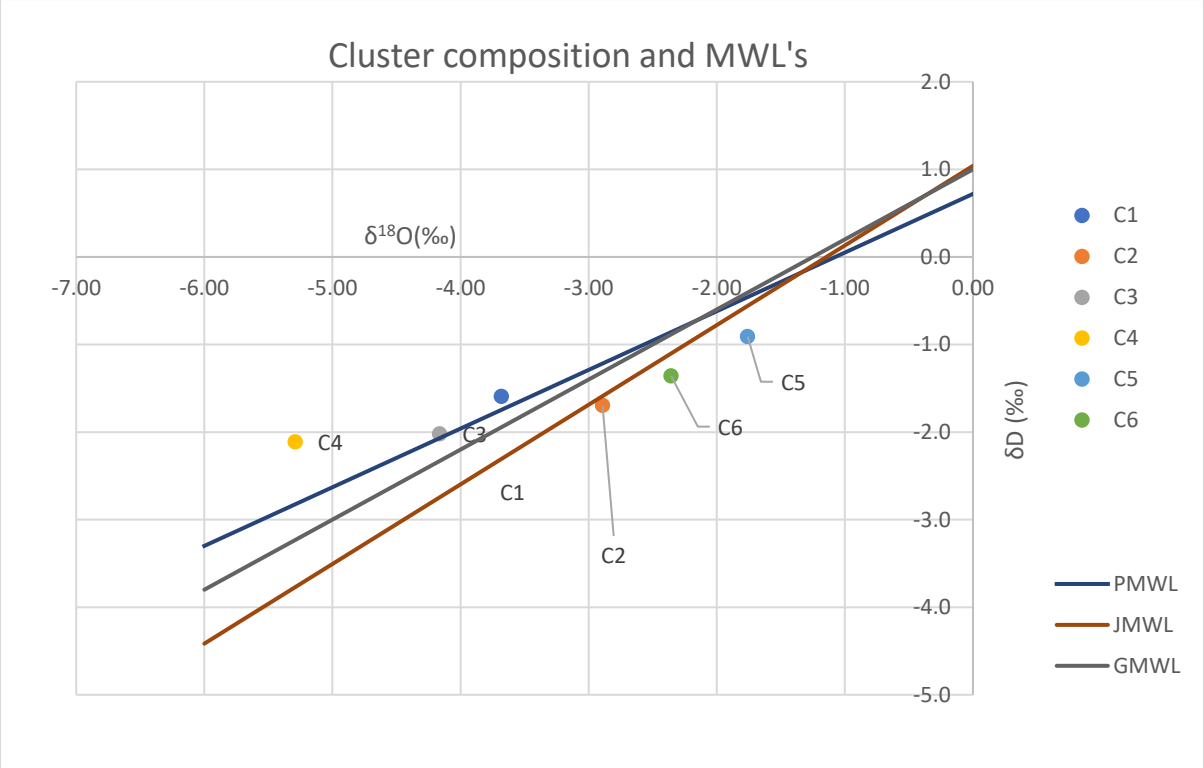


Figure 47. Average isotope values of the clusters. Plotted with the PMWL, GMWL and JMWL.

3.7.2. Tritium

Due to the radioactive nature of tritium, it can be used to estimate residence time of groundwater inside the aquifer (Poreda *et al*., 1988; Solomon and Sudicky, 1991; Hiscock and Bense, 2014). The half-life of tritium is 12.43 years and tends to be much more useful when used together with the tritiogenic helium-3 (^{3}He), for residence time determination (Poreda *et* al., 1988; Ozyurt, 2008; Hiscock and Bense, 2014, Moser *et al.* 1989). The amount of ^{3}H in water is expressed in tritium units. Tritium Units (TU) represent a ratio of one tritium unit to 10^{8} hydrogen atoms (Michel, 2004; Hiscock and Bense, 2014). To acquire the residence time, the tritium units must be converted to time using equation 1:

There are nine boreholes that were sampled for ^{3}H in the study area and those are BH 22 to BH 30. Table 5 contains the calculated residence times. An example of the residence calculation for BH 22 is also shown below. All the samples have tritium value lower than that of current rainfall of 5.6 TU (Abiye *et* al., 2015). The highest residence time being 40 years and the lowest being 9 years. The average transit time in the study area is 18 years, the rest of the results are shown in table 5.

A plot of the δ^{18}O stable isotope and tritium (Figure 48) can help in establishing groundwater mixing process (Thiyva *et al*., 2016). There is a possibility of mixing in BH 22 and BH 28 (Figure 3), and this could be due to interconnected fractures resulting similar circulation depth and path, and possibly comparable recharge time. Whereas, BH 29 shares a similar δ^{18}O signature with the two boreholes

mentioned above but with different tritium signature. BH 30 and BH 22 plot next to each other, however, the distance between the two boreholes is large. BH 25, BH 26 and BH 27 have similar residence times and $\delta^{18}O$ signatures but are not in immediate spatial proximity to each other, therefore, their connection could be due to regional structures. In particular, the NW-SE trending lineaments that the BH's are situated on. The tritium ages vary significantly with no apparent age similarities except for the BH's that are right next to each other (BH 22 and BH 28). BH 29 is significantly close to BH 22 and BH 29 but the residence time is significantly different with a residence time gap of about 22 years. BH 22 and BH 28 do show mixing signatures (Figure 45). The flow between these BHs can be towards the south, with the travel time between BH 22 and BH 28 being faster due to better fracture connections, and less permeable fractures between BH 28 and BH 29 resulting in the longer residence time. The faster flow is reflected in the recession coefficient of the Albert's Farm spring, which suggests fast flowing groundwater via the fracture network.

Looking at the relative locations of BH 22, BH 25, BH 26 and BH 27, their relationship in Figure 45 shows that there is some component of mixing between the four samples. The inter-connection of BH 22, BH 25, BH 26 and BH 27 could be due to more regional fractures and lineaments that allow for deeper groundwater circulation. It is paramount to consider that the residence time given by environmental tracers in fractured media might not be accurate (Cook *et al.*, 2005). Davisson *et al.* (1999) further explains that in regional systems geochemical and isotopic data does not provide residence time and source interpretation information accurately. This is due to (1) multiple recharge end member mixing which complicates hydraulic age determination (2) the change in isotopic compositions is governed by temperature of water (Davisson *et al*., 1999).

Table 5: showing the tritium data for the nine sampled boreholes.

Sample ID	Tritium (TU)	$\delta\ ^{18}O$ ‰	Mean residence time (years)	Sample date
BH22	1.9 ± 0.3	-3.55 ± 0.05	19	April 2017
BH23	1.5 ± 0.3	-2.62 ± 0.27	24	April 2017
BH24	1.2 ± 0.3	-5.08 ± 0.36	28	April 2017
BH25	3.4 ± 0.4	-4.32 ± 0.05	9	April 2017
BH26	3.1 ± 0.3	-3.27 ± 0.08	11	April 2017
BH27	2.6 ± 0.3	-3.18 ± 0.08	14	April 2017
BH28	1.8 ± 0.3	-3.83 ± 0.11	20	April 2017
BH29	0.5 ± 0.2	-3.83 ± 0.17	43	April 2017
BH30	0.6 ± 0.2	-5.15 ± 0.03	40	April 2017

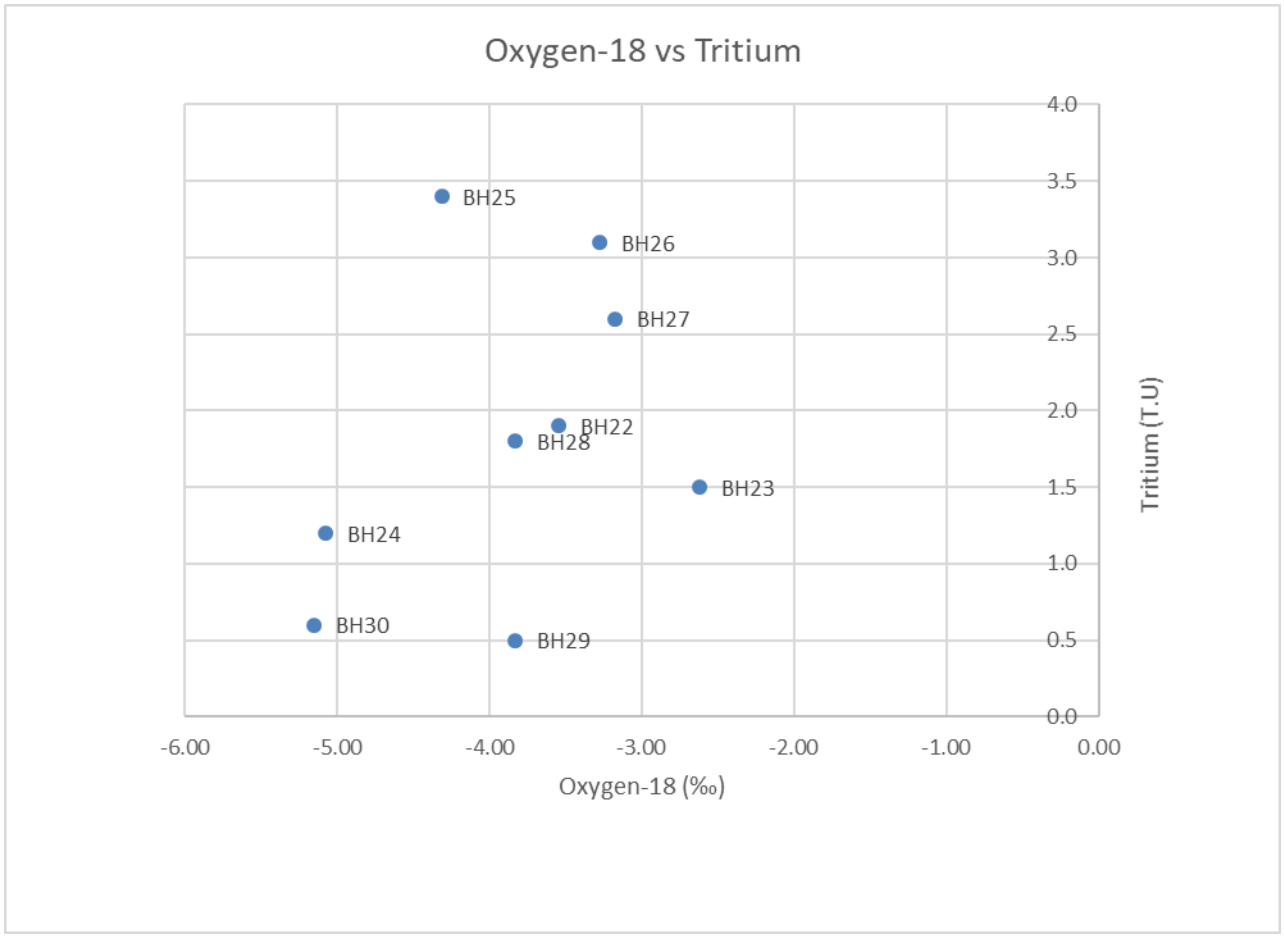


Figure 48. $\delta^{18}O$ versus tritium for the 9 boreholes with tritium measurements. Al, boreholes plot slightly below -2.00 ‰ and above -6.00 ‰.

4. Conclusions

This project was designed to study the role of geological structures on the hydrogeology of the UCRB. The study utilized magnetic data, lithological logs, environmental isotopes and visual analysis of lineaments using satellite image and hydrologic datasets.

The study area is made up of crystalline rocks, therefore, most of the groundwater occurrence is controlled by structures. The structures display conjugate sets that trend in a NW-SE and NE-SW direction, with tension release structures that trend in the E-W direction. These lineaments are associated with dykes that take advantage of the zones of weakness. These dykes have the potential to act as groundwater barriers, however, the occurrence of fractures in the area could allow for groundwater mixing. The lineament occurrences are both local and regional, suggesting that the potential for groundwater to mix throughout the study area is high.

The magnetic data highlighted high magnetic intensity lineaments that trend in the E-W direction. The E-W lineaments were found to be dolerite dykes through ground truthing. The Magnetic data failed to highlight the E-W fractures that were outlined using the ArcGIS basemap. However, the two lineaments share the same orientation of approximately 085º. Furthermore, high magnetic intensity lineaments are observed on the SE of the study area, these structures are possibly associated with the Pilanesberg dyke swarm. These dykes share their orientation with the NW-SE trending lineaments/fractures. The fractures that trend in the NW-SE direction are visible in both the magnetic and ArcGIS image analysis.

The bulk of the study area displays dendritic drainage pattern which ensues due to the occurrence of crystalline rocks that are not naturally permeable. The trellis drainage pattern on the Silverton-shales is an example of another lithological control on the occurrence and distribution of drainage patterns in the area. Fractures also form a trellis pattern near the Roodekoppies Dam and possibly affect the groundwater circulation in the area.

The recession coefficient was calculated using the Maillet equation for 4 springs. The dolomitic springs shared a similar recession coefficient which averaged 0.0004 and the quartzite had a much higher coefficient. The high value is suggestive of high hydraulic conductivity and as such interconnected fracture network. This is in line with the occurrence of the multiple fracture networks in the study area. The spring lineament analysis also revealed that the springs are exclusively controlled by the structures and lithological contacts. Suggesting that the hydrogeology of the basin is co-dependent on both lithology and structures.

Most of the groundwater samples plot on or just below but parallel to the MWL's. This is suggestive of the lack of extreme evaporation prior to recharge. This trait can be associated to the occurrence of the fractures and faults in the UCRB. Some outliers do occur. The outliers are seen in samples showing

extreme evaporation due to the proximity to the dams and streams that recharge their respective aquifers. The average residence time for the groundwater in the area is about 23 years. Most of the samples show similar tritium ages and this can be attributed to the fractures that allow for rapid groundwater circulation.

The UCRB has a combination of groundwater and surface water controls, which cannot be attributed to a single factor. The lineaments control the surface drainage, and they also control the groundwater flow properties. Based on the lineament analysis it is not possible that compartments can form and have no interaction due to lineaments that cut-across the study area. In conclusion, the lineaments are important for the occurrence, flow and characteristics of both groundwater and surface water. The springs all form along or near fractures and lithological boundaries. The springs are responsible for feeding streams during dry periods with the assistance of baseflow.

5. Reference list

Abiye, T.A., 2011. Provenance of groundwater in the crystalline aquifer of Johannesburg area, South Africa. *International Journal of Physical Sciences*, *6*(1), pp.98-111.

Abiye, T.A., Mengistu, H., Masindi, K. and Demlie, M., 2015. Surface water and groundwater interaction in the upper Crocodile River Basin, Johannesburg, South Africa: Environmental isotope approach. *South African Journal of Geology*, *118*(2), pp.109-118.

Abiye, T.A. (Editor), 2013. The use of isotope hydrology to characterize and assess water resources in South (ern) Africa. *WRC Report No. TT570/13, Pretoria. 211pp*.

Anhaeusser, C.R., 1971. The Geology and Geochemistry of the Archaean Granites and Gneisses of the Johannesburg-Pretoria Dome. *Economic Geology Research Unit, University of the Witwatersrand, No. 62, pp 37*

Amit, H., Lyakhovsky, V., Katz, A., Starinsky, A. and Burg, A., 2002. Interpretation of spring recession curves. *Groundwater*, *40*(5), pp.543-551.

Banks, D., Robins, N. and Robins, N., 2002. *An introduction to groundwater in crystalline bedrock* (p. 64). Trondheim: Norges geologiske undersøkelse.

Barnard, H.C., 2000. An explanation for the 1:500,000 Hydrogeological map of Johannesburg 2526, Department of Water Affairs and Forestry, Pretoria, South Africa, pp8.

Barton Jr, J.M., Barton, E.S. and Kröner, A., 1999. Age and isotopic evidence for the origin of the Archaean granitoid intrusives of the Johannesburg Dome, South Africa. *Journal of African Earth Sciences*, *28*(3), pp.693-702.

Boussinesq, J., 1904. Recherches the´oriques sur l'e´coulement des nappes d'eau infiltre´es dans le sol et sur les de´bits des sources. Journal de Mathe´matiques Pures et Applique´es, Paris 10, 5–78.

Boronina, A., Renard, P., Balderer, W. and Stichler, W., 2005. Application of tritium in precipitation and in groundwater of the Kouris catchment (Cyprus) for description of the regional groundwater flow. *Applied Geochemistry*, *20*(7), pp.1292-1308.

Cawthorn, G. R., Ellam, R. M., Ashwala, L. D., Webb, S. J. (2012). A clinopyroxenite intrusion from the Pilanesberg Alkaline Province, South Africa. *Precambrian Research*. 198– 199. 25– 36.

Civita, M.V., 2008. An improved method for delineating source protection zones for karst springs based on analysis of recession curve data. *Hydrogeology Journal*, *16*(5), pp.855-869.

Cook, P.G., Love, A.J., Robinson, N.I. and Simmons, C.T., 2005. Groundwater ages in fractured rock aquifers. *Journal of Hydrology*, *308*(1), pp.284-301.

Davisson, M.L., Smith, D.K., Kenneally, J. and Rose, T.P., 1999. Isotope hydrology of southern Nevada groundwater: stable isotopes and radiocarbon. *Water Resources Research*, *35*(1), pp.279-294.

Delinom, R.M., 2009. Structural geology controls on groundwater flow: Lembang Fault case study, West Java, Indonesia. *Hydrogeology journal*, *17*(4), pp.1011-1023.

Department of Water Affairs and Forestry, South Africa. 2004. Crocodile River (West) and Marico Water Management Area: Internal Strategic Perspective of the Crocodile River (West) catchment: Prepared by Goba Moahloli Keeve Steyn (Pty) Ltd, Tlou & Matji (Pty) Ltd and Golder Associates (Pty) Ltd, on behalf of the Directorate: National Water Resource Planning. DWAF Report No. 03/000/00/0303

Department of Water Affairs and Forestry, South Africa, 2006. *VAAL RIVERSYSTEM: LARGE BULK WATER SUPPLY RECONCILIATION STRATEGY: GROUNDWATER ASSESSMENT: DOLOMITE AQUIFERS.*

Emerman, S.H., 1991. Correlation of a dyke swarn in southeastern Botswana with the Pilanesberg dyke swarm, South Africa. *Journal of African Earth Sciences (and the Middle East)*, *12*(4), pp.525-531.

Goetz, A.F. and Rowan, L.C., 1981. Geologic remote sensing. *Science*, *211*(4484), pp.781-791.

Gustafson, G.U.N.N.A.R. and Krásný, J., 1994. Crystalline rock aquifers: their occurrence, use and importance. *Applied Hydrogeology*, *2*(2), pp.64-75.

Hill, M., Barker, F., Hunter, D. and Knight, R., 1996. Geochemical characteristics and origin of the Lebowa granite suite, Bushveld Complex. *International Geology Review*, *38*(3), pp.195-227.

Hilliard, P. and McCourt, S., 1995. Bedding-parallel simple shear deformation in the West Rand Group rocks on Northcliff Promontory, Johannesburg, South Africa-insight into the Late Archaean evolution of the Kaapvaal Craton. *South African Journal of Geology*, *98*(4), pp.349-355.

Hiscock, K.M. and Bense, V.F., 2014. *Hydrogeology: principles and practice*. John Wiley & Sons.

Howard, A.D., 1967. Drainage analysis in geologic interpretation: a summation. *AAPG bulletin*, *51*(11), pp.2246-2259.

Kinnaird, J.A., 2005. The Bushveld large igneous province. *Review Paper, The University of the Witwatersrand, Johannesburg, South Africa, 39pp*.

Korkmaz, N., 1990. The estimation of groundwater recharge from spring hydrographs. *Hydrological sciences journal*, *35*(2), pp.209-217.

Kovalevsky, V.S., Kruseman, G.P. and Rushton, K.R., 2004. *Groundwater studies: an international guide for hydrogeological investigations* (No. 3). Unesco.

Kresic, N. and Bonacci, O., 2010. Spring discharge hydrograph. In *Groundwater hydrology of Springs* (pp. 129-163).

Lee, S.A., Webb, S.J., Jones, M.Q.W., Durrheim, R.J. and Ganerød, M., 2013, October. A 3D potential field model of the Pilanesberg Complex shape and structure. In *13th SAGA Biennial Conference & Exhibition*.

Lee, S.A., 2016. *Geophysical investigation into the geology, geometry and geochronology of the South African Pilanesberg Complex and the Pilanesberg dyke system* (Doctoral dissertation).

Manjoro, M., 2015. Structural control of fluvial drainage in the western domain of the Cape Fold Belt, South Africa. *Journal of African Earth Sciences*, *101*, pp.350-359.

McCarthy, T. and Rubidge, B., 2005. The story of earth and life. *Struik, Cape Town*.

Michalski, A. and Britton, R., 1997. The role of bedding fractures in the hydrogeology of sedimentary bedrock—evidence from the Newark Basin, New Jersey. *Groundwater*, *35*(2), pp.318-327.

Moser, H., Wolf, M., Fritz, P., Fontes, J.C., Florkowski, T. and Payne, B.R., 1989. Deuterium, oxygen-18, and tritium in Stripa groundwater. *Geochimica et Cosmochimica Acta*, *53*(8), pp.1757-1763.

Naido, V., 2014. Hydrogeological Characterisation of Fountains East and West Compartments. MSc dissertation, University of Pretoria.

Nyebelele, S., 2017. Structural characterization of the Albert's Farm Soring, Northcliff. Honours thesis, University of the Witwatersrand.

Oosthuizen, A.C. and Van Rooy, J.L., 2015. Hazard of sinkhole formation in the Centurion CBD using the Simplified Method of Scenario Supposition. *Journal of the South African Institution of civil engineering*, *57*(2), pp.69-75.

Ozyurt, N.N., 2008. Residence time distribution in the Kirkgoz karst springs (Antalya-Turkey) as a tool for contamination vulnerability assessment. *Environmental geology*, *53*(7), pp.1571-1583.

Padilla, A., Pulido-Bosch, A. and Mangin, A., 1994. Relative importance of baseflow and quickflow from hydrographs of karst spring. *Groundwater*, *32*(2), pp.267-277.

Poreda, R.J., Cerling, T.E. and Salomon, D.K., 1988. Tritium and helium isotopes as hydrologic tracers in a shallow unconfined aquifer. *Journal of Hydrology*, *103*(1-2), pp.1-9.

Poujol, M. and Anhaeusser, C.R., 2001. The Johannesburg Dome, South Africa: new single zircon U–Pb isotopic evidence for early Archaean granite–greenstone development within the central Kaapvaal Craton. *Precambrian Research*, *108*(1-2), pp.139-157.

Robarts, R.D., Ashton, P.J., Thornton, J.A., Taussig, H.J. and Sephton, L.M., 1982. Overturn in a hypertrophic, warm, monomictic impoundment (Hartbeespoort Dam, South Africa). *Hydrobiologia*, *97*(3), pp.209-224.

Robarts, R.D. and Zohary, T., 1984. Microcystis aeruginosa and underwater light attenuation in a hypertrophic lake (Hartbeespoort Dam, South Africa). *The Journal of Ecology*, pp.1001-1017.

Robb, L.J. and Meyer, F.M., 1995. The Witwatersrand Basin, South Africa: geological framework and mineralization processes. *Ore Geology Reviews*, *10*(2), pp.67-94.

Rose, T.P., Davisson, L.M. and Criss, R.E., 1996. Isotope hydrology of voluminous cold springs in fractured rock from an active volcanic region, northeastern California. *Journal of Hydrology*, 179. pp 207 – 236.

Singhal, B.B.S. and Gupta, R.P., 2010. *Applied hydrogeology of fractured rocks*. Springer Science & Business Media.

South African Committee for Stratigraphy (SACS). 1980. Stratigraphy of South Africa. Kent, L.E., (Comp.); Part 1. Lithostratigraphy of the Republic of South Africa, South West Africa/Namibia, and the Republics of Bophutatswana, Transkei and Venda. Handb. geol. Surv. S. Afr., 8, pp690.

Smith, A.J., Beukes, N.J. and Gutzmer, J., 2013. The composition and depositional environments of Mesoarchean iron formations of the West Rand Group of the Witwatersrand Supergroup, South Africa. *Economic Geology*, *108*(1), pp.111-134.

Solomon, D.K. and Sudicky, E.A., 1991. Tritium and helium 3 isotope ratios for direct estimation of spatial variations in groundwater recharge. *Water Resources Research*, *27*(9), pp.2309-2319.

Titus, R., Witthüser, K. and Walters, B., 2009. Groundwater and mining in the Bushveld Complex. In *Proceedings of the International Mine Water Conference, Pretoria, South Africa* (pp. 178-184).

Trollip, N Y G 2006. The geology of an area south of Pretoria with specific reference to dolomite stability. MSc Dissertation, University of Pretoria, 96 p

Van Schoor, M., 2002. Detection of sinkholes using 2D electrical resistivity imaging. *Journal of Applied Geophysics*, *50*(4), pp.393-399.

Vermaak, J.J.G. 2000. Geotechnical and hydrogeological characterization of residual soils in the vadose zone. Doctoral thesis submitted to the faculty of Science, University of Pretoria.

Wigmans, F.E., Holland, M. and Janse van Rensburg, H., 2013. Groundwater Resource Directed measures for Maloney's Eye Catchment. *WRC Report No. KV 319/13, Pretoria. 79pp.*

Yeh, H.F., Lin, H.I., Lee, C.H., Hsu, K.C. and Wu, C.S., 2014. Identifying seasonal groundwater recharge using environmental stable isotopes. *Water*, *6*(10), pp.2849-2861.

Zernitz, E.R., 1932. Drainage patterns and their significance. *The Journal of Geology*, *40*(6), pp.498-521.

Zondi, S., 2017. Recharge Rates and Processes In The Upper Crocodile Catchment. MSc Dissertation, University of the Witwatersrand.

Appendices A and B refer to CD